An exploratory study of Higgs-boson pair production at hadron colliders

Chih-Ting Lu
(NCTS)

Collaborators :
Prof. Kingman Cheung, Prof. Jae-Sik Lee
Dr. Jung Chang, Dr. Jubin Park
Ref : arXiv:1804.07130
JHEP 1508 (2015) 133 (arXiv:1505.00957)

Self Introduction

Education

National Tsing Hua University, Physics Department

PhD, 2011.9 - 2015.7

Thesis Topic : The properties of Higgs boson in the further LHC search

Advisor : Prof. Kingman Cheung (NTHU)

Working experience

Postdoctoral

(1) National Tsing Hua University, Physics Department, 2015.10-2018.8 (Research and Development Substitute Services[military service])

Research Interests

High Energy Physics - Phenomenology

(1) **Collider physics of exotic phenomena**, including [1] CP properties of Higgs and BSM scalar bosons, [2] Long-lived particle with displaced vertex signature and lepton jets detection.

(2) **Phenomenology of BSM models**, including [1] Supersymmetric models, [2] 2HDMs and their non-abelian gauge extensions.

(3) **Model independent way to probe Higgs properties at colliders**, including [1] Higgs self coupling, [2] Exotic production and decay modes.

(4) **Dark Matter Phenomenology**

Chih-Ting Lu

盧致廷

Contents

- 1. Motivation
- 2. Effective Lagrangian
- 3. Numerical analysis
- 4. The comprehensive signal-background analysis
- 5. Discussions and Conclusions

Contents

Motivation : Incredible Success of the Standard Model

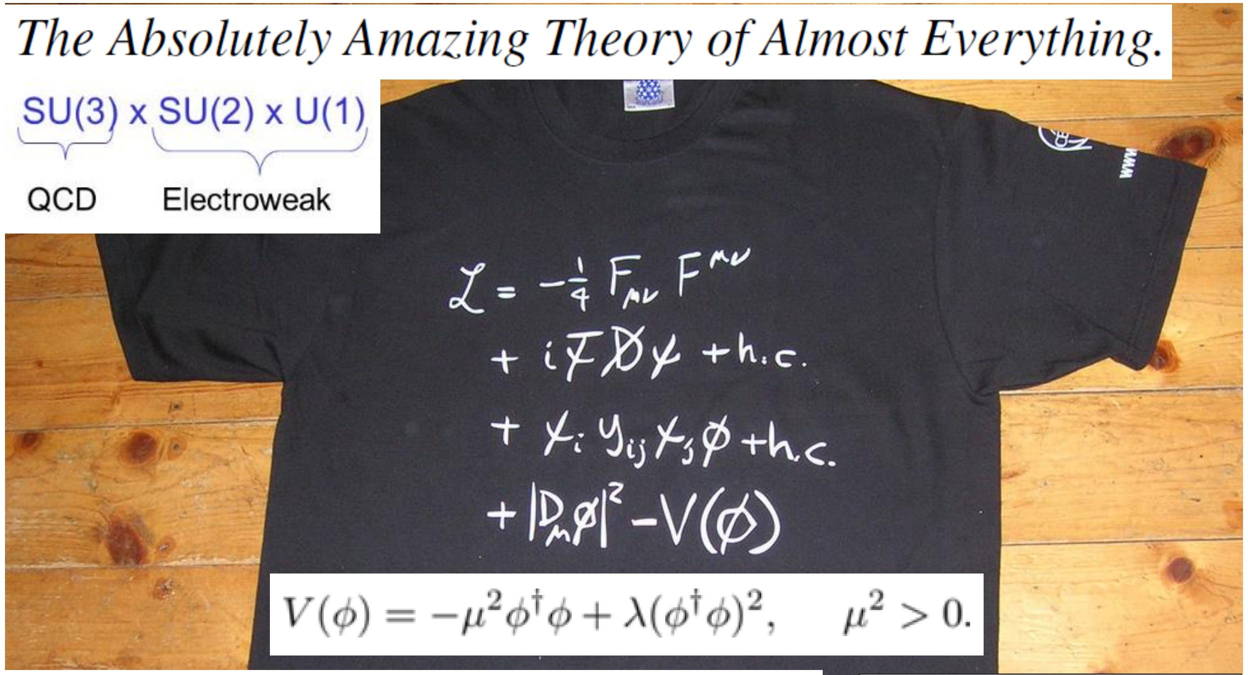

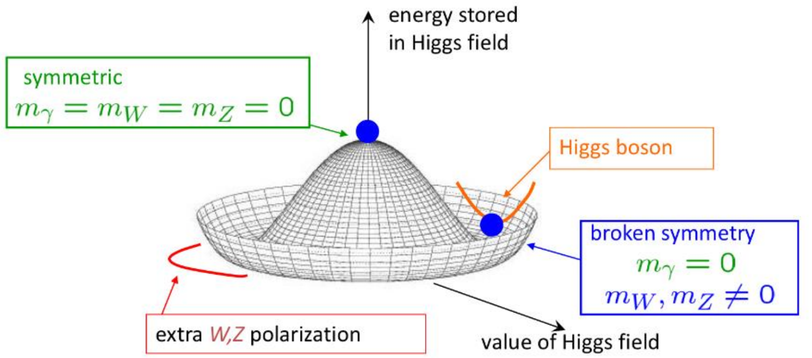

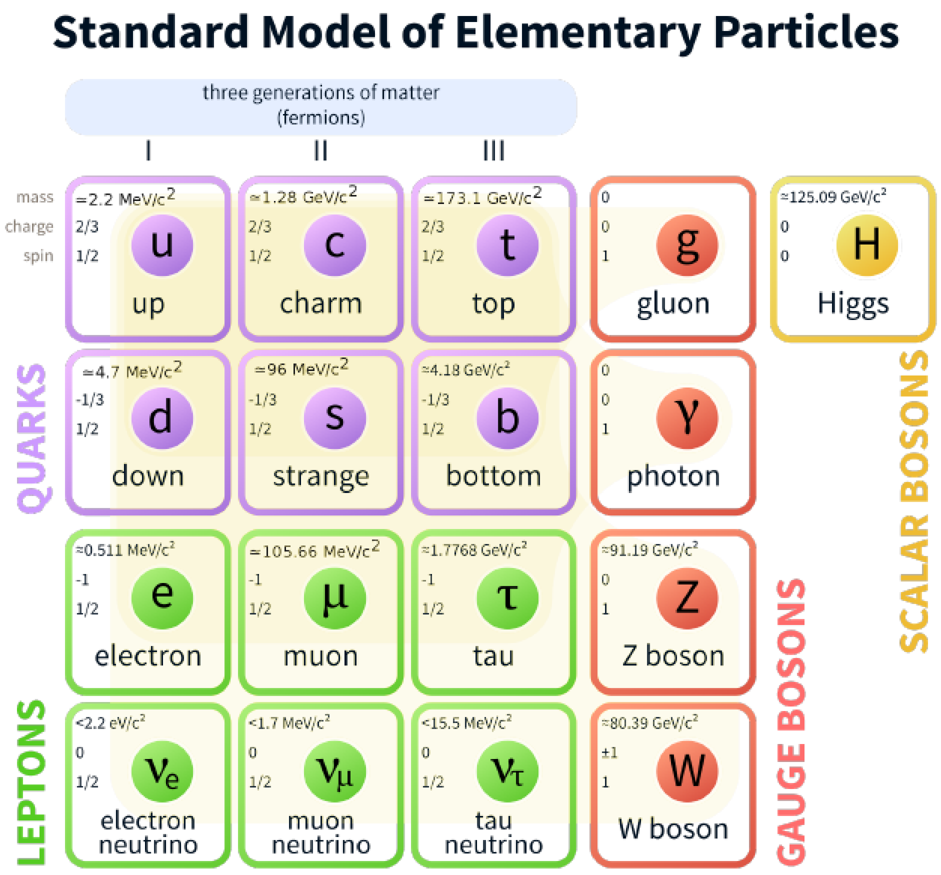

Fig. 1: Particle content of the Standard Model. Courtesy to Wikipedia.

Fermion mass hierarchy ?

Only 3 generations below electroweak scale ?

Flavor mixing structures ?

Parameters of the Standard Model			
Symbol	**Description**	**Renormalization scheme (point)**	**Value**
m_e	Electron mass		511 keV
m_μ	Muon mass		105.7 MeV
m_τ	Tau mass		1.78 GeV
m_u	Up quark mass	$\mu_{\overline{MS}}$ = 2 GeV	1.9 MeV
m_d	Down quark mass	$\mu_{\overline{MS}}$ = 2 GeV	4.4 MeV
m_s	Strange quark mass	$\mu_{\overline{MS}}$ = 2 GeV	87 MeV
m_c	Charm quark mass	$\mu_{\overline{MS}} = m_c$	1.32 GeV
m_b	Bottom quark mass	$\mu_{\overline{MS}} = m_b$	4.24 GeV
m_t	Top quark mass	On shell scheme	173.5 GeV
θ_{12}	CKM 12-mixing angle		13.1°
θ_{23}	CKM 23-mixing angle		2.4°
θ_{13}	CKM 13-mixing angle		0.2°
δ	CKM CP violation Phase		0.995
g_1 or g'	U(1) gauge coupling	$\mu_{\overline{MS}} = m_Z$	0.357
g_2 or g	SU(2) gauge coupling	$\mu_{\overline{MS}} = m_Z$	0.652
g_3 or g_s	SU(3) gauge coupling	$\mu_{\overline{MS}} = m_Z$	1.221
θ_{QCD}	QCD vacuum angle		~0
v	Higgs vacuum expectation value		246 GeV
m_H	Higgs mass		125.09 ±0.24 GeV

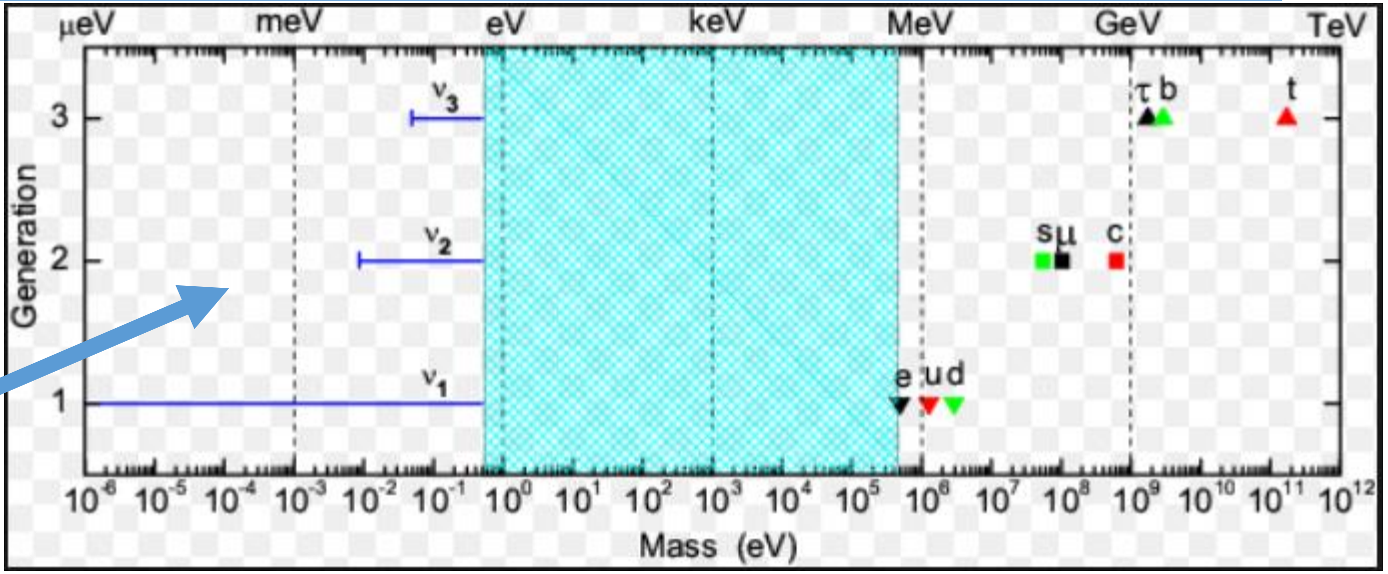

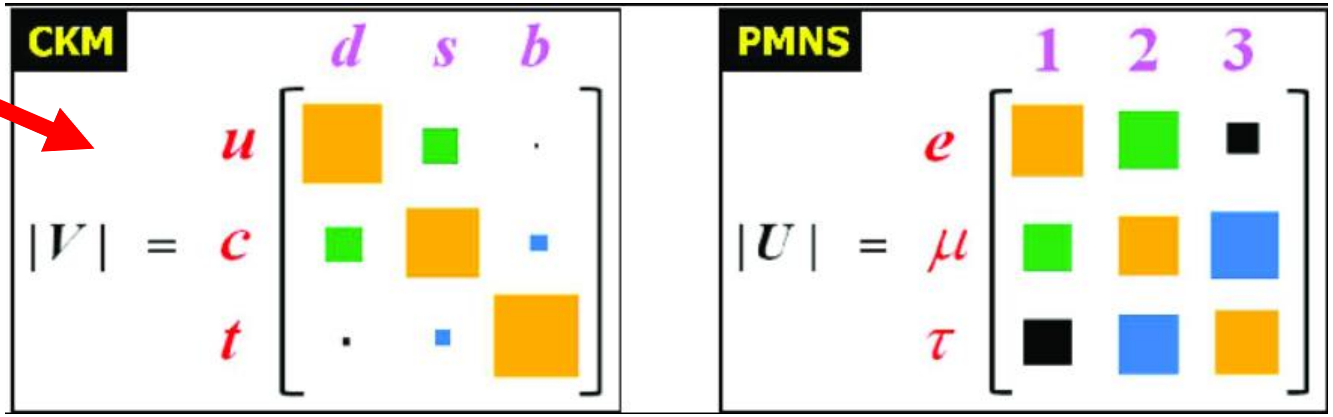

Gauge coupling unification ?

The strong CP problem ?

Parameters of the Standard Model			
Symbol	**Description**	**Renormalization scheme (point)**	**Value**
m_e	Electron mass		511 keV
m_μ	Muon mass		105.7 MeV
m_τ	Tau mass		1.78 GeV
m_u	Up quark mass	$\mu_{\overline{MS}}$ = 2 GeV	1.9 MeV
m_d	Down quark mass	$\mu_{\overline{MS}}$ = 2 GeV	4.4 MeV
m_s	Strange quark mass	$\mu_{\overline{MS}}$ = 2 GeV	87 MeV
m_c	Charm quark mass	$\mu_{\overline{MS}} = m_c$	1.32 GeV
m_b	Bottom quark mass	$\mu_{\overline{MS}} = m_b$	4.24 GeV
m_t	Top quark mass	On shell scheme	173.5 GeV
θ_{12}	CKM 12-mixing angle		13.1°
θ_{23}	CKM 23-mixing angle		2.4°
θ_{13}	CKM 13-mixing angle		0.2°
δ	CKM CP violation Phase		0.995
g_1 or g'	U(1) gauge coupling	$\mu_{\overline{MS}} = m_Z$	0.357
g_2 or g	SU(2) gauge coupling	$\mu_{\overline{MS}} = m_Z$	0.652
g_3 or g_s	SU(3) gauge coupling	$\mu_{\overline{MS}} = m_Z$	1.221
θ_{QCD}	QCD vacuum angle		~0
v	Higgs vacuum expectation value		246 GeV
m_H	Higgs mass		125.09 ±0.24 GeV

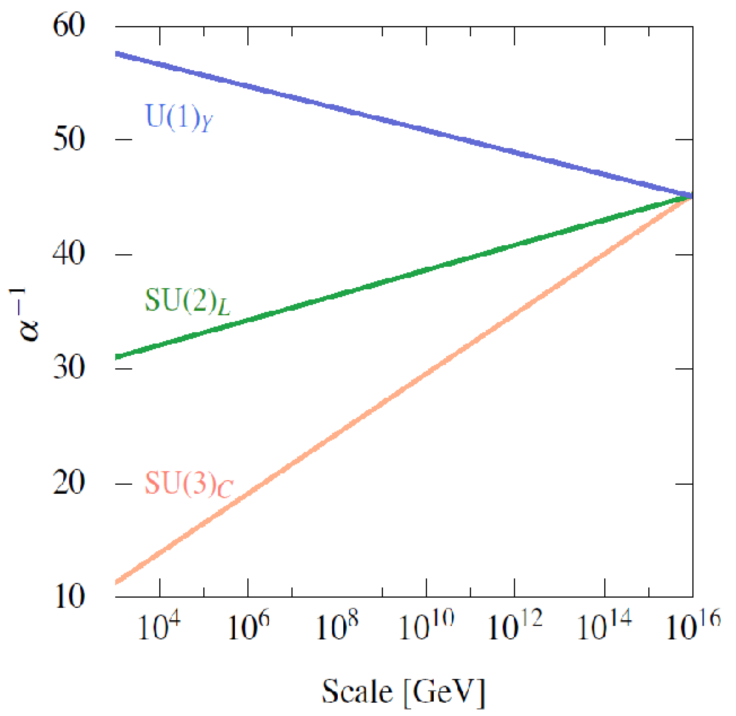

Why θ is so small?
Axions?

Metastability of Higgs field ?

Dynamical origins of the EWSB sector ?

Parameters of the Standard Model			
Symbol	Description	Renormalization scheme (point)	Value
m_e	Electron mass		511 keV
m_μ	Muon mass		105.7 MeV
m_τ	Tau mass		1.78 GeV
m_u	Up quark mass	$\mu_{\overline{MS}}$ = 2 GeV	1.9 MeV
m_d	Down quark mass	$\mu_{\overline{MS}}$ = 2 GeV	4.4 MeV
m_s	Strange quark mass	$\mu_{\overline{MS}}$ = 2 GeV	87 MeV
m_c	Charm quark mass	$\mu_{\overline{MS}} = m_c$	1.32 GeV
m_b	Bottom quark mass	$\mu_{\overline{MS}} = m_b$	4.24 GeV
m_t	Top quark mass	On shell scheme	173.5 GeV
θ_{12}	CKM 12-mixing angle		13.1°
θ_{23}	CKM 23-mixing angle		2.4°
θ_{13}	CKM 13-mixing angle		0.2°
δ	CKM CP violation Phase		0.995
g_1 or g'	U(1) gauge coupling	$\mu_{\overline{MS}} = m_Z$	0.357
g_2 or g	SU(2) gauge coupling	$\mu_{\overline{MS}} = m_Z$	0.652
g_3 or g_s	SU(3) gauge coupling	$\mu_{\overline{MS}} = m_Z$	1.221
θ_{QCD}	QCD vacuum angle		~0
v	Higgs vacuum expectation value		246 GeV
m_H	Higgs mass		125.09 ±0.24 GeV

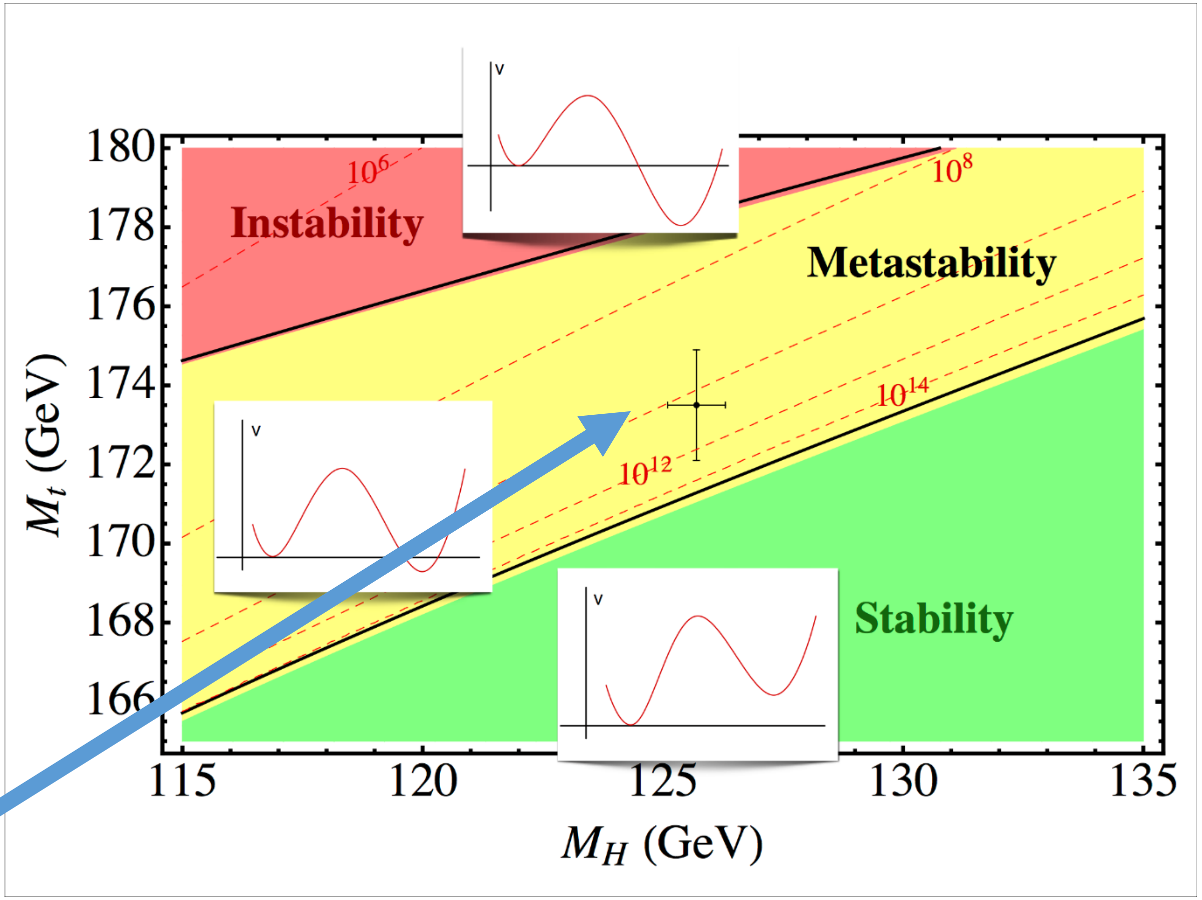

Elementary scalars or composite ones ?

Metastability of Higgs field ?

Dynamical origins of the EWSB sector ?

Is there any testable process to study the properties of the **scalar potential** at colliders ?

Self-coupling of the Higgs boson is a crucial property which depends on the dynamics of the EWSB sector.

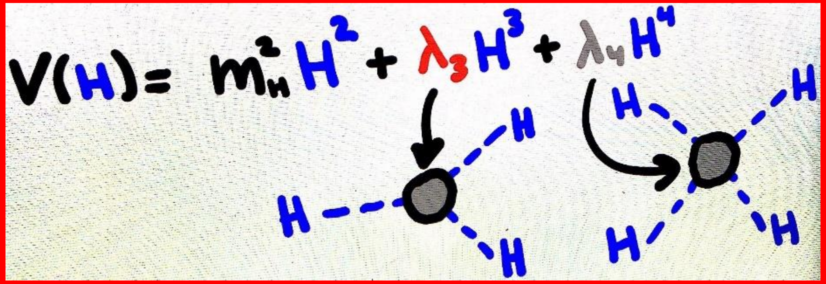

One of the probes of Higgs self-coupling is the Higgs-boson-pair production at the LHC & future hadron colliders.

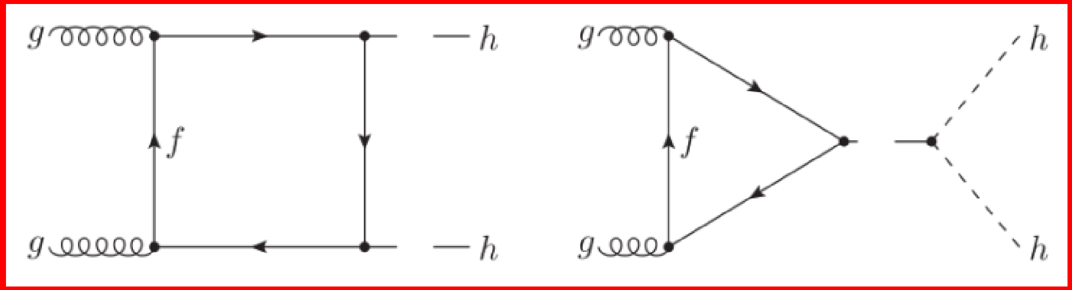

Parameters of the			
Symbol	Description		
m_e	Electron mass		
m_μ	Muon mass		
m_τ	Tau mass		
m_u	Up quark mass		
m_d	Down quark mass		
m_s	Strange quark mass		
m_c	Charm quark mass		
m_b	Bottom quark mass		
m_t	Top quark mass		
θ_{12}	CKM 12-mixing angle		
θ_{23}	CKM 23-mixing angle		
θ_{13}	CKM 13-mixing angle		
δ	CKM CP violation Phase		
g_1 or g'	U(1) gauge coupling		
g_2 or g	SU(2) gauge coupling		
g_3 or g_s	SU(3) gauge coupling	$\mu_{\overline{MS}} = m_Z$	1.221
θ_{QCD}	QCD vacuum angle		~0
v	Higgs vacuum expectation value		246 GeV
m_H	Higgs mass		125.09 ±0.24 GeV

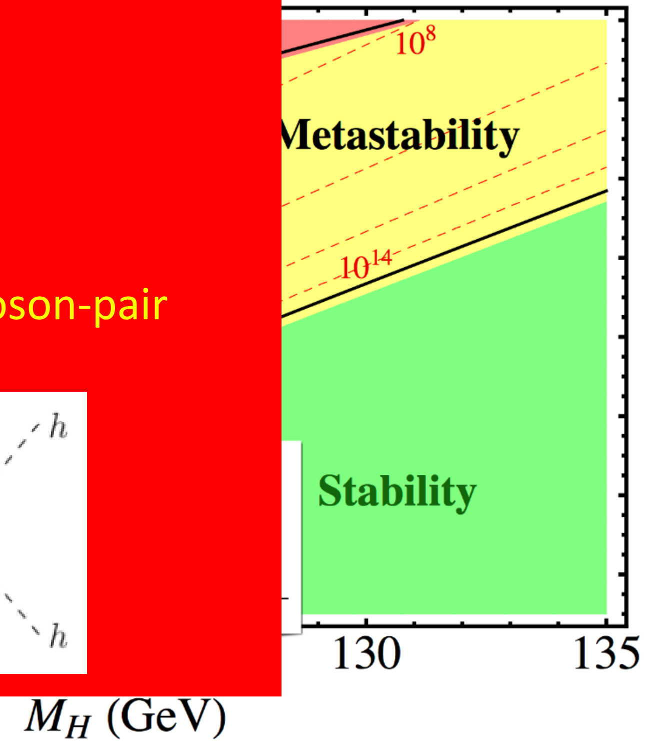

Fundamental scalars or composite ones ?

The shape of the Higgs potential & EWSB in the early universe

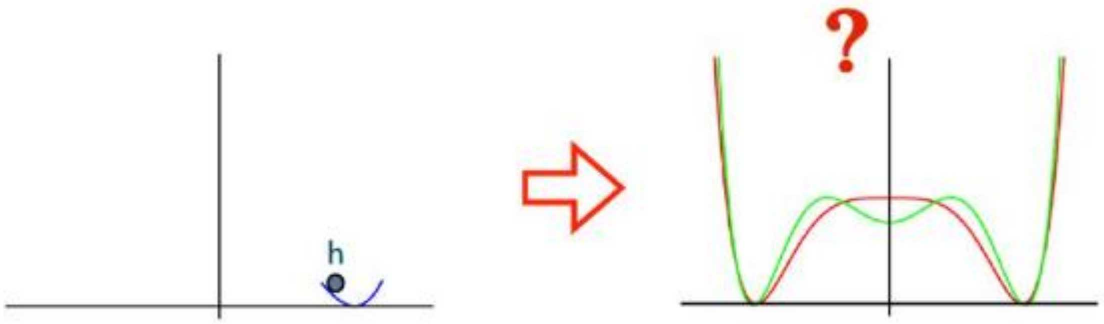

Slow 2nd order phase transition in the SM ?

VS.

Strong 1st order phase transition with a modified Higgs potential ?

EW baryogenesis

After the discovery of Higgs the next question is what is the shape of the Higgs potential. The EW phase transition is first order or second order? Strongly 1st order phase transition is motivated by the EW baryogenesis.

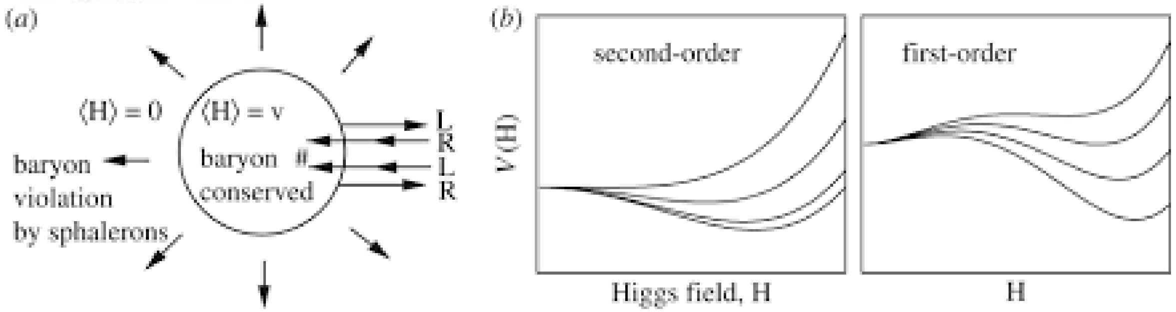

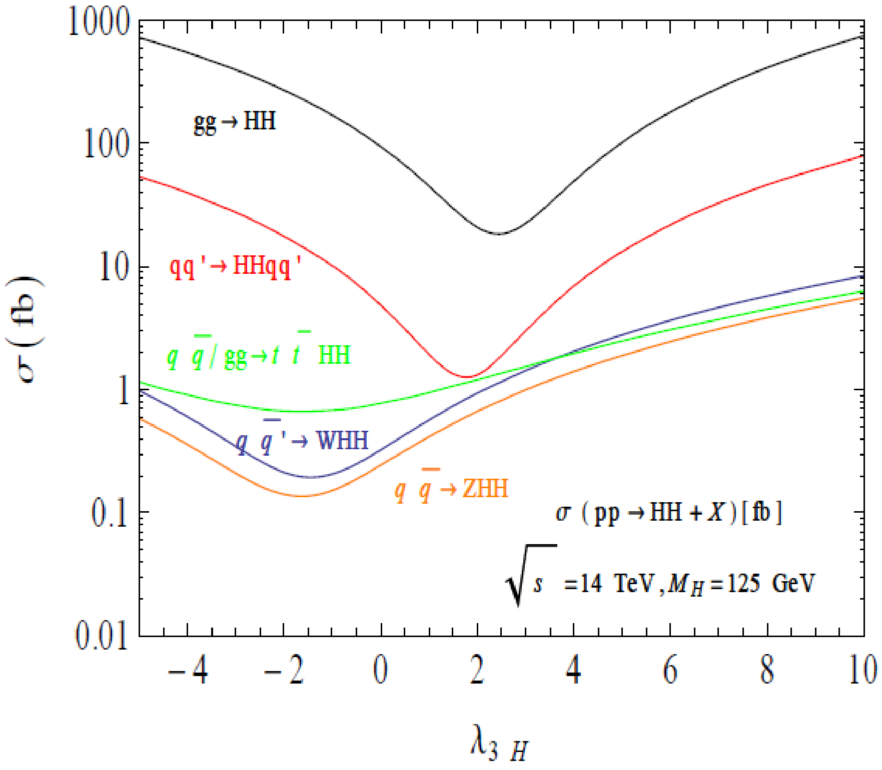

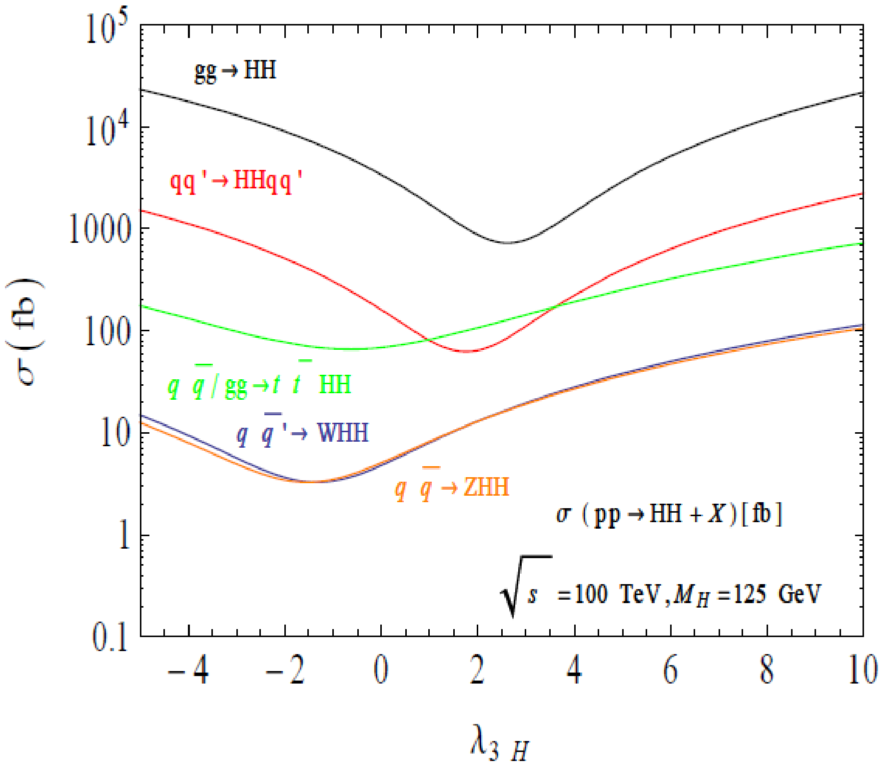

It is clear that the gluon fusion into HH gives the largest cross sections independently of λ_{3H}

From now on we shall focus on the gluon fusion mechanism for our studies !

FIG. 1. Production cross sections for various channels for HH production at $\sqrt{s} = 14$ TeV (left) and $\sqrt{s} = 100$ TeV (right). The NNPDF2.3LO PDF set is used.

arXiv:1804.07130

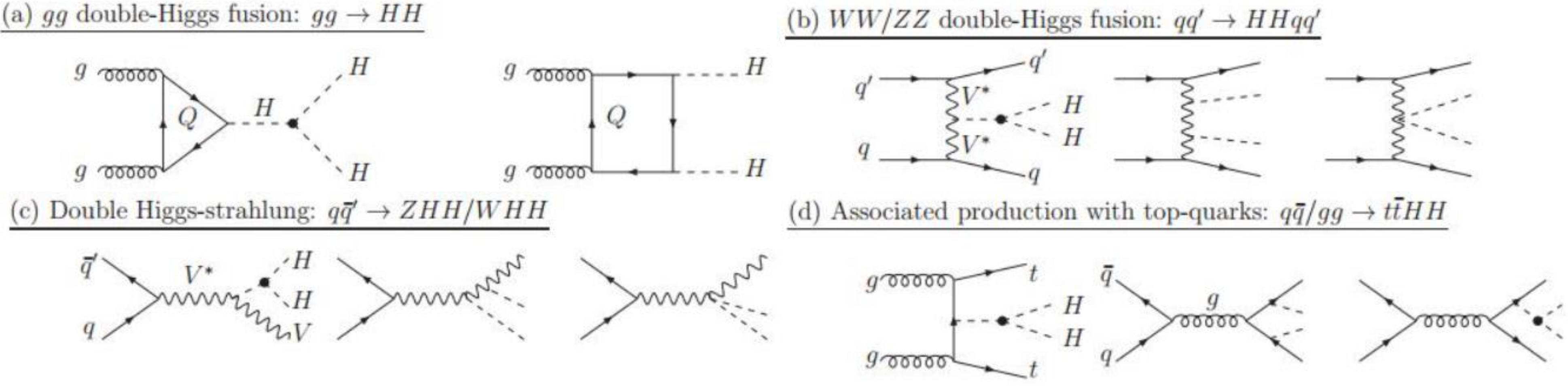

Contents

- 1. Motivation
- **2. Effective Lagrangian**
- 3. Numerical analysis
- 4. The comprehensive signal-background analysis
- 5. Discussions and Conclusions

Effective Lagrangian

JHEP08(2015)133

$$-\mathcal{L} = \frac{1}{3!}\left(\frac{3M_H^2}{v}\right)\lambda_{3H} H^3 + \frac{m_t}{v}\bar{t}\left(g_t^S + i\gamma_5 g_t^P\right)t\,H + \frac{1}{2}\frac{m_t}{v^2}\bar{t}\left(g_{tt}^S + i\gamma_5 g_{tt}^P\right)t\,H^2 .$$

trilinear coupling λ_{3H}

In the SM, $\lambda_{3H} = g_t^S = 1$ and $g_t^P = 0$ and $g_{tt}^{S,P} = 0$.

top-quark Yukawa coupling $g_t^{S,P}$

dim-5 contact-type $ttHH$ coupling $g_{tt}^{S,P}$

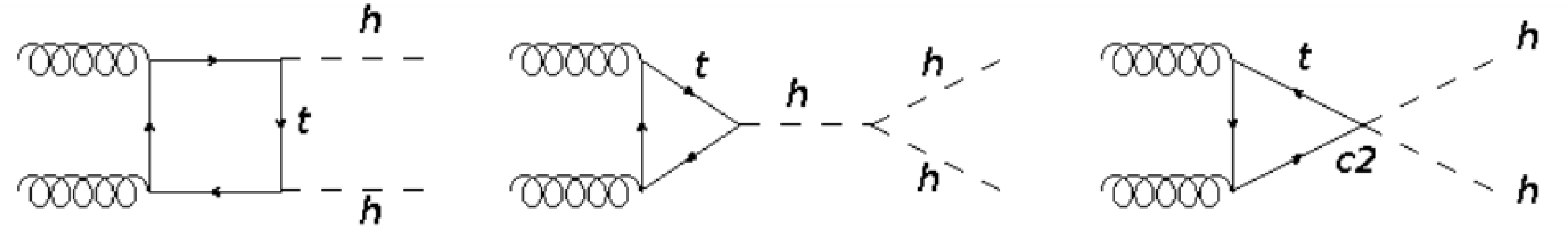

Effective Lagrangian

trilinear coupling λ_{3H}

2. Large deviation on Higgs self-coupling can shed light on Electroweak Baryogenesis, 2HDM, Composite Higgs, etc.

JHEP 1305 (2013) 066
Phys.Rev. D88 (2013) 055024

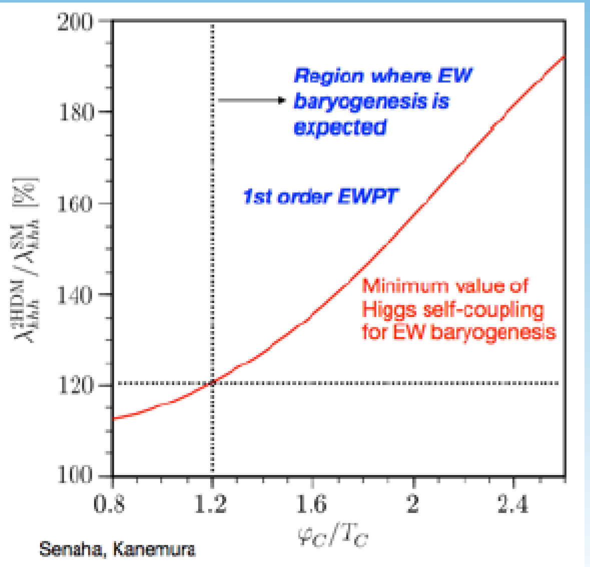

Model	$\Delta\lambda_{hhh}/\lambda^{SM}_{hhh}$
Mixed-in Singlet	-18%
Composite Higgs	tens of %
MSSM	-2%, -15%
NMSSM	-25%

Effective Lagrangian

top-quark Yukawa coupling $g_t^{S,P}$

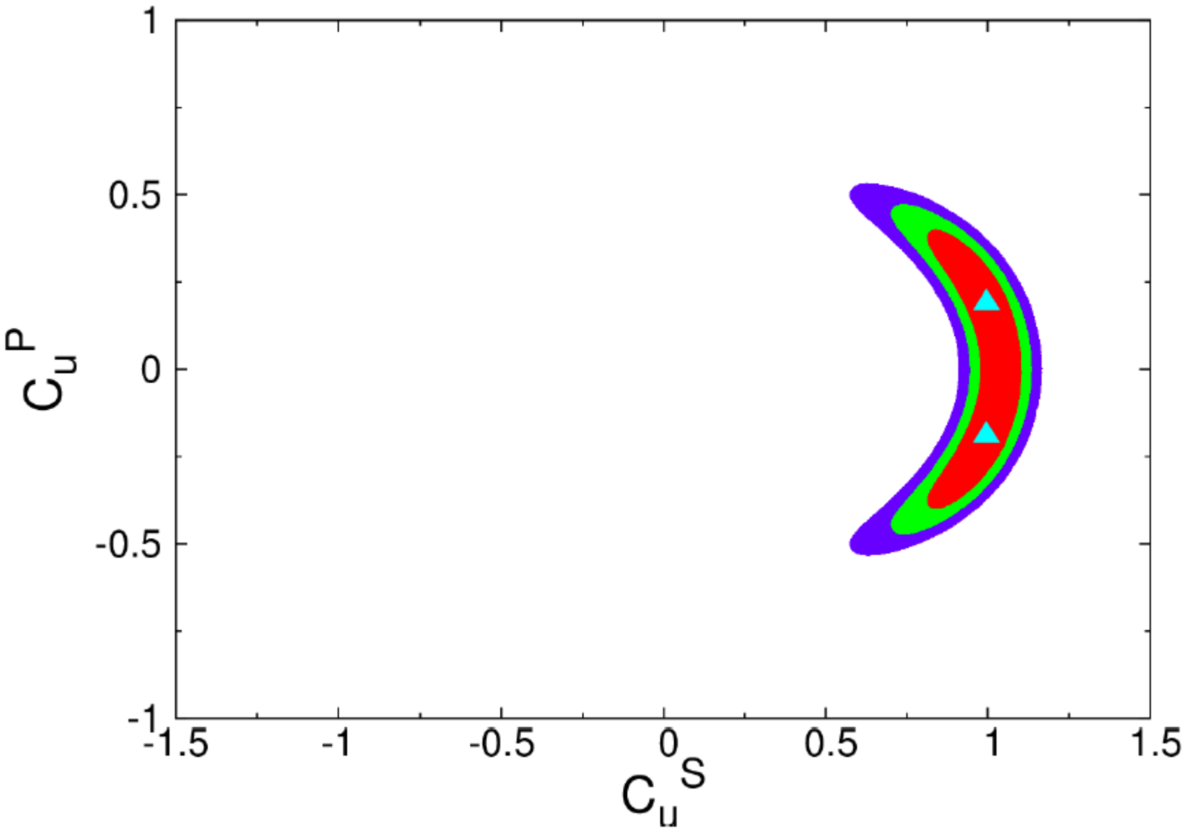

Cases	CPV2	
Parameters	Vary C_u^S, C_u^P	
C_u^S	$1.00^{+0.07}_{-0.11}$	$1.00^{+0.07}_{-0.11}$
C_d^S	1	1
C_ℓ^S	1	1
C_v	1	1
ΔS^γ	0	0
ΔS^g	0	0
$\Delta\Gamma_{\rm tot}$ (MeV)	0	0
C_u^P	$0.19^{+0.14}_{-0.52}$	$-0.19^{+0.52}_{-0.14}$
ΔP^γ	0	0
ΔP^g	0	0
χ^2/dof	52.07/62	
p-value	0.812	

After ICHEP 2018

arXiv:1810.02521

Kingman Cheung, Jae Sik Lee, Po-Yan Tseng

Effective Lagrangian

$$\boxed{\text{dim-5 contact-type } ttHH \text{ coupling } g_{tt}^{S,P}}$$

Minimal Composite Higgs models [Agashe, Contino, Pomarol; Contino, Da Rold, Pomarol]

- In an effective low-energy description only the Higgs couplings to the SM fields are modified and depend on $\xi = \frac{v^2}{f^2}$ with $\xi \in [0, 1]$
  [Giudice,Grojean,Pomarol,Rattazzi]

- spinorial representation: MCHM_4
- fundamental representation: MCHM_5

JHEP 06 (2011) 020 [arXiv: 1012.1562]

New coupling: $g_{HHf\bar{f}} = \frac{m_f}{v^2}\xi$ in MCHM_4

and $g_{HHf\bar{f}} = \frac{m_f}{v^2}4\xi$ in MCHM_5

- Global symmetry $G = SO(5) \times U(1)_X$ broken down to
  - $SO(4) \times U(1)_X$ on IR-brane
  - $SU(2)_L \times U(1)_Y$ on UV-brane

Effective Lagrangian

dim-5 contact-type $ttHH$ coupling $g_{tt}^{S,P}$

In a general 2HDM we can have a diagram with a vertex $(\bar{t}_L t_R \varphi)$ and a (φHH) vertex connected by the heavy φ .
When the heavy φ is integrated out, we are left with the contact diagram $\bar{t}_L t_R HH$.

On the other hand, $\bar{t}_L t_R HH$ is a dim-5 operator, which may originate from a genuine dim-6 operator, e.g., $(\overline{Q_L} \Phi t_R)(\Phi^\dagger \Phi)$
after electroweak symmetry breaking, $\Phi = (0,\, (v+H)/\sqrt{2})^T$

JHEP08(2015)133

Effective Lagrangian

$\boxed{\text{dim-5 contact-type } ttHH \text{ coupling } g_{tt}^{S,P}}$

JHEP08(2015)133

We can examine the validity of the anomalous $ttHH$ contact coupling by projecting out the leading partial-wave coefficient for the scattering $t\bar{t} \to HH$. At high energy, the amplitude

$$i\mathcal{M}(t\bar{t} \to HH) \sim g_{tt}^S \frac{m_t\sqrt{\hat{s}}}{v^2} \,.$$

The leading partial-wave coefficient is given by

$$a_0 = \frac{1}{64\pi}\int_{-1}^{1} d(\cos\theta)P_0(\cos\theta)(i\mathcal{M}) = g_{tt}^S \frac{m_t\sqrt{\hat{s}}}{32\pi v^2} \,.$$

Requiring $|a_0| < 1/2$ for unitarity we obtain

$$\sqrt{\hat{s}} \le \frac{17.6}{g_{tt}^S}\ \text{TeV} \,.$$

Therefore, the anomalous $ttHH$ contact term can be safely applied at the LHC for $g_{tt}^S \lesssim 3 - 5$ as most of the collisions occur at $\sqrt{\hat{s}} \lesssim$ a few TeV.

- The differential cross section for the process $g(p_1)g(p_2) \to H(p_3)H(p_4)$ in the SM :

$$\frac{d\hat{\sigma}(gg \to HH)}{d\hat{t}} = \frac{G_F^2 \alpha_s^2}{512(2\pi)^3} \left[\left| \lambda_{3H} g_t^S D(\hat{s}) F_\triangle^S + (g_t^S)^2 F_\Box^{SS} \right|^2 + \left| (g_t^S)^2 G_\Box^{SS} \right|^2 \right]$$

where

$$D(\hat{s}) = \frac{3M_H^2}{\hat{s} - M_H^2 + iM_H \Gamma_H}$$

- Here we extend the result to including the CP-odd top-Yukawa and the anomalous ttHH couplings :

$$\frac{d\hat{\sigma}(gg \to HH)}{d\hat{t}} = \frac{G_F^2 \alpha_s^2}{512(2\pi)^3} \left\{ \left| \left(\lambda_{3H} g_t^S D(\hat{s}) + g_{tt}^S \right) F_\triangle^S + (g_t^S)^2 F_\Box^{SS} + (g_t^P)^2 F_\Box^{PP} \right|^2 \right.$$

$$+ \left| (g_t^S)^2 G_\Box^{SS} + (g_t^P)^2 G_\Box^{PP} \right|^2$$

$$\left. + \left| \left(\lambda_{3H} g_t^P D(\hat{s}) + g_{tt}^P \right) F_\triangle^P + g_t^S g_t^P F_\Box^{SP} \right|^2 + \left| g_t^S g_t^P G_\Box^{SP} \right|^2 \right\} .$$

- In the heavy quark limit, one may have

$$F_{\triangle}^{S} = +\frac{2}{3} + \mathcal{O}(\hat{s}/m_Q^2)\,, \qquad F_{\Box}^{SS} = -\frac{2}{3} + \mathcal{O}(\hat{s}/m_Q^2)\,, \quad F_{\Box}^{PP} = +\frac{2}{3} + \mathcal{O}(\hat{s}/m_Q^2)\,,$$

$$F_{\triangle}^{P} = +1 + \mathcal{O}(\hat{s}/m_Q^2)\,, \qquad F_{\Box}^{SP} = -1 + \mathcal{O}(\hat{s}/m_Q^2)\,,$$

$$G_{\Box}^{SS} = G_{\Box}^{PP} = G_{\Box}^{SP} = \mathcal{O}(\hat{s}/m_Q^2)$$

leading to large cancellation between the triangle and box diagrams.

- The production cross section normalized to the corresponding SM cross section, with or without cuts, can be parameterized as follows :

$$\begin{aligned}\frac{\sigma(gg\to HH)}{\sigma_{\rm SM}(gg\to HH)} &= \lambda_{3H}^2\left[c_1(s)(g_t^S)^2 + d_1(s)(g_t^P)^2\right] + \lambda_{3H}\,g_t^S\left[c_2(s)(g_t^S)^2 + d_2(s)(g_t^P)^2\right]\\ &+\left[c_3(s)(g_t^S)^4 + d_3(s)(g_t^S)^2(g_t^P)^2 + d_4(s)(g_t^P)^4\right]\\ &+\lambda_{3H}\left[e_1(s)g_t^S g_{tt}^S + f_1(s)g_t^P g_{tt}^P\right] + g_{tt}^S\left[e_2(s)(g_t^S)^2 + f_2(s)(g_t^P)^2\right]\\ &+\left[e_3(s)(g_{tt}^S)^2 + f_3(s)g_t^S g_t^P g_{tt}^P + f_4(s)(g_{tt}^P)^2\right] \qquad (2.7)\end{aligned}$$

where the numerical coefficients $c_{1,2,3}(s)$, $d_{1,2,3,4}(s)$, $e_{1,2,3}(s)$, and $f_{1,2,3,4}(s)$ depend on s and experimental selection cuts. Upon our normalization, the ratio should be equal to 1 when $g_t^S = \lambda_{3H} = 1$ and $g_t^P = g_{tt}^{S,P} = 0$ or $c_1(s) + c_2(s) + c_3(s) = 1$. The coefficients $c_1(s)$ and $c_3(s)$ are for the SM contributions from the triangle and box diagrams, respectively, and the coefficient $c_2(s)$ for the interference between them.

Once we have the coefficients c_i, d_i, e_i, and f_i's, the cross sections can be easily obtained for any combinations of couplings. Our first task is to obtain the dependence of the coefficients on the collider energy $\sqrt{s}$, Higgs decay channels, experimental cuts, etc.

$\sqrt{s}$ (TeV)	$c_1(s)$ $[\lambda_{3H}^2(g_t^S)^2]$	$c_2(s)$ $[\lambda_{3H}(g_t^S)^3]$	$c_3(s)$ $[(g_t^S)^4]$	$d_1(s)$ $[\lambda_{3H}^2(g_t^P)^2]$	$d_2(s)$ $[\lambda_{3H}g_t^S(g_t^P)^2]$	$d_3(s)$ $[(g_t^S)^2(g_t^P)^2]$	$d_4(s)$ $[(g_t^P)^4]$
8	0.300	−1.439	2.139	0.942	−6.699	14.644	0.733
14	0.263	−1.310	2.047	0.820	−5.961	13.348	0.707
33	0.232	−1.193	1.961	0.713	−5.274	12.126	0.690
100	0.208	−1.108	1.900	0.635	−4.789	11.225	0.683

$\sqrt{s}$ (TeV)	$e_1(s)$ $[\lambda_{3H}g_t^S g_{tt}^S]$	$e_2(s)$ $[g_{tt}^S(g_t^S)^2]$	$e_3(s)$ $[(g_{tt}^S)^2]$	$f_1(s)$ $[\lambda_{3H}g_t^P g_{tt}^P]$	$f_2(s)$ $[g_{tt}^S(g_t^P)^2]$	$f_3(s)$ $[g_t^S g_t^P g_{tt}^P]$	$f_4(s)$ $[(g_{tt}^P)^2]$
8	1.460	−4.313	2.519	2.104	2.350	−7.761	3.065
14	1.364	−4.224	2.617	1.848	2.269	−6.886	3.769
33	1.281	−4.165	2.783	1.622	2.207	−6.033	5.635
100	1.214	−4.137	2.974	1.474	2.154	−5.342	10.568

JHEP08(2015)133

JHEP08(2015)133

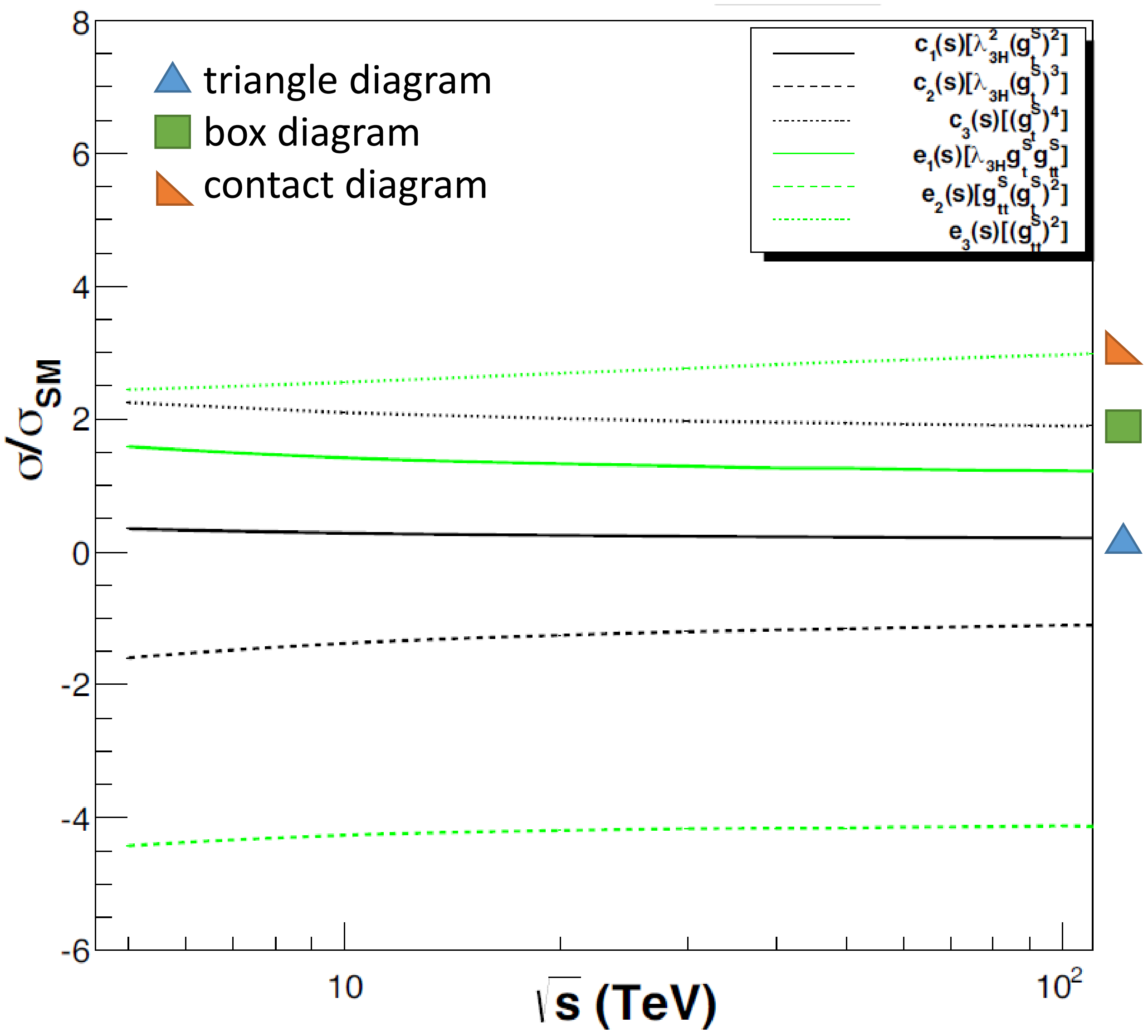

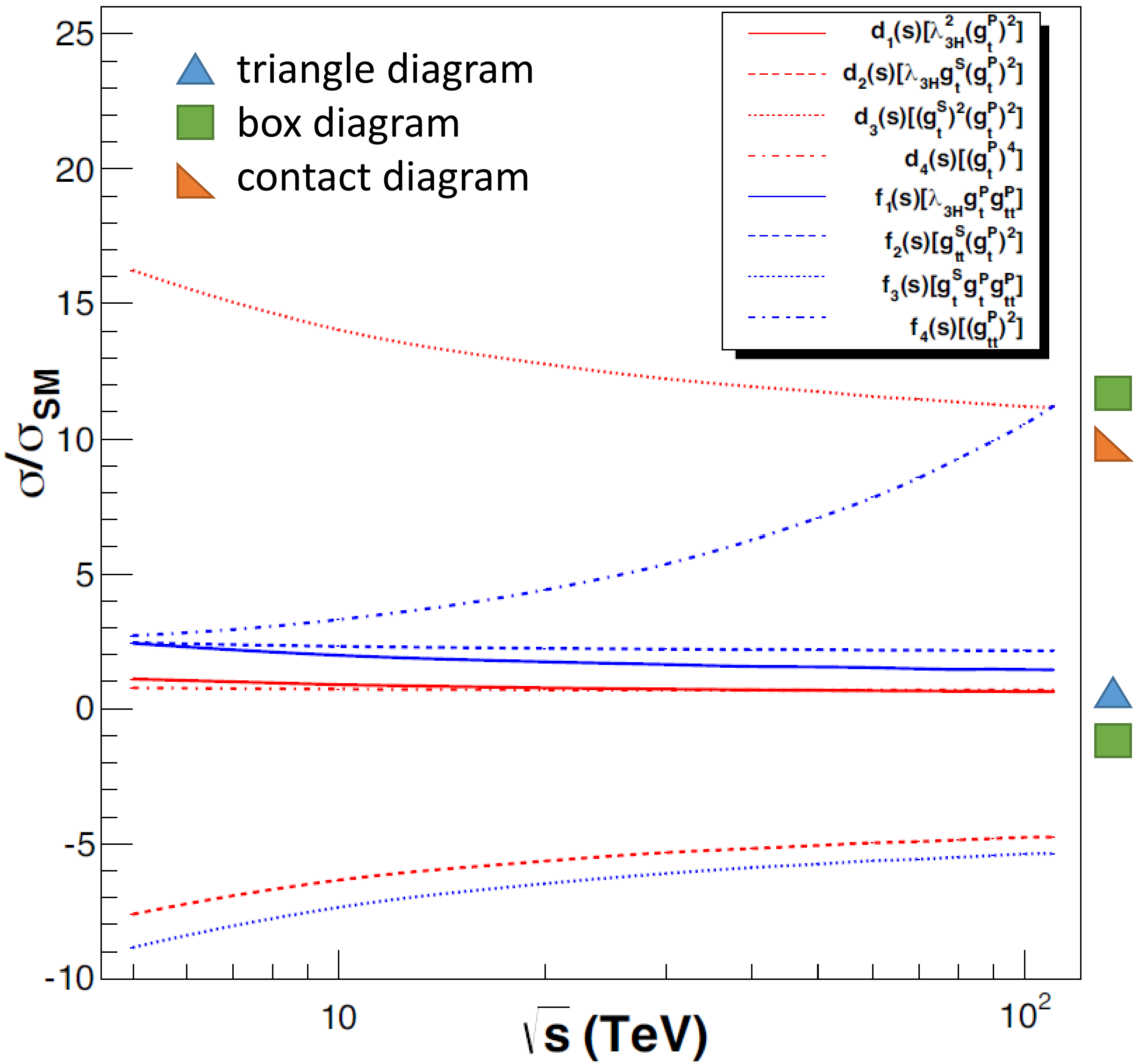

To some extent we have understood the behavior of the triangle, box, and contact diagrams with the center-of-mass energy, which is kinematically equal to the invariant mass M_{HH} of the Higgs-boson pair. One can then uses M_{HH} to enhance or reduce the relative contributions of triangle or box diagrams. The higher the M_{HH} the relatively larger proportion comes from the box and contact diagrams. Since M_{HH} correlates with the boost energy of each Higgs boson, a more energetic Higgs boson will decay into a pair of particles, which have a smaller angular separation between them than a less energetic Higgs boson. Therefore, the angular separation ΔR_{ij} between the decay products i, j is another useful kinematic variable to separate the contributions among the triangle, box, and contact diagrams.

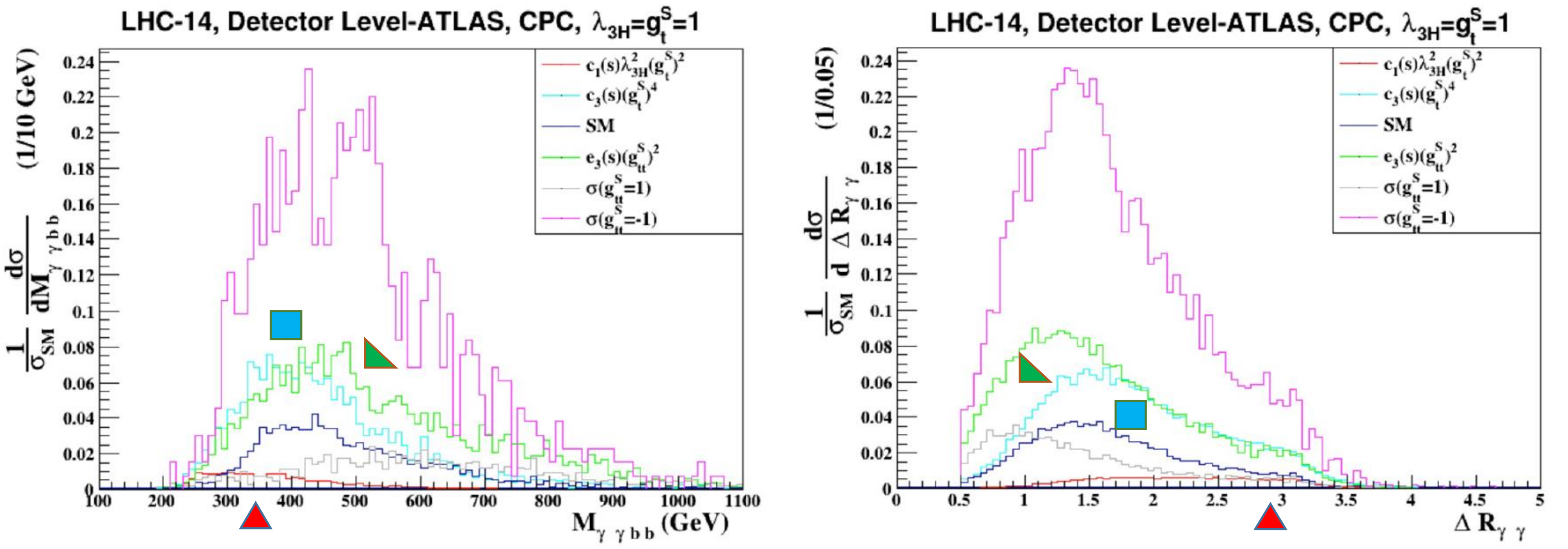

- The differential cross section for the process $g(p_1)g(p_2) \to H(p_3)H(p_4)$ in the SM :

$$\frac{d\hat{\sigma}(gg \to HH)}{d\hat{t}} = \frac{G_F^2 \alpha_s^2}{512(2\pi)^3} \left[\left| \lambda_{3H} g_t^S D(\hat{s}) F_\triangle^S + (g_t^S)^2 F_\Box^{SS} \right|^2 + \left| (g_t^S)^2 G_\Box^{SS} \right|^2 \right]$$

where

$$D(\hat{s}) = \frac{3M_H^2}{\hat{s} - M_H^2 + iM_H \Gamma_H}$$

- The triangle diagram (red line) peaks at the lower invariant mass and decreases with $M_{\gamma\gamma b\bar{b}}$, because of the s-channel Higgs propagator. The box diagram (skyblue line), on the other hand, is larger than the triangle diagram at high invariant mass.

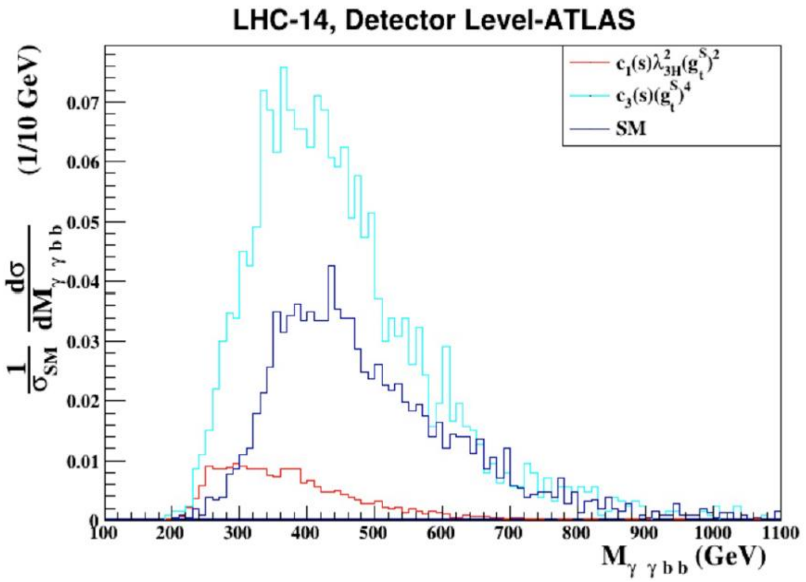

Contents

Effective Lagrangian

JHEP08(2015)133

$$-\mathcal{L} = \frac{1}{3!}\left(\frac{3M_H^2}{v}\right)\lambda_{3H} H^3 + \frac{m_t}{v}\bar{t}\left(g_t^S + i\gamma_5 g_t^P\right)t\,H + \frac{1}{2}\frac{m_t}{v^2}\bar{t}\left(g_{tt}^S + i\gamma_5 g_{tt}^P\right)t\,H^2\,.$$

trilinear coupling λ_{3H}

In the SM, $\lambda_{3H} = g_t^S = 1$ and $g_t^P = 0$ and $g_{tt}^{S,P} = 0$.

top-quark Yukawa coupling $g_t^{S,P}$

dim-5 contact-type $ttHH$ coupling $g_{tt}^{S,P}$

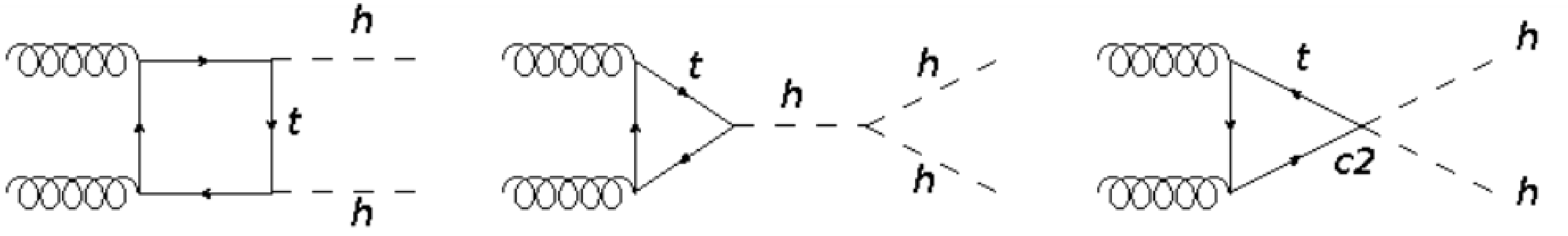

Numerical analysis : Classifications

1. **CPC1** — the top-Yukawa coupling involves only the scalar part and the scale in the anomalous contact coupling is very large — only g_t^S and λ_{3H} are relevant. The relevant coefficients are c_1, c_2, and c_3.
2. **CPC2** — the top-Yukawa and the anomalous contact couplings involve only the scalar part — g_t^S, g_{tt}^S, and λ_{3H} are relevant. The relevant coefficients are c_1, c_2, c_3, e_1, e_2 and e_3.
3. **CPV1** — the top-Yukawa coupling involves both the scalar and pseudoscalar parts — g_t^S, g_t^P, and λ_{3H} are relevant. The relevant coefficients are c_1, c_2, c_3, d_1, d_2, d_3, and d_4.
4. **CPV2** — the contact $ttHH$ coupling involves both the scalar and pseudoscalar parts — g_{tt}^S, g_{tt}^P, and λ_{3H} are relevant while the top-Yukawa coupling is kept at fixed values. In this case, all the coefficients become relevant. In one of the simplest cases with $g_t^S = 1$ and $g_t^P = 0$, for example, the relevant coefficients are c_1, c_2, c_3, e_1, e_2, e_3, and f_4.

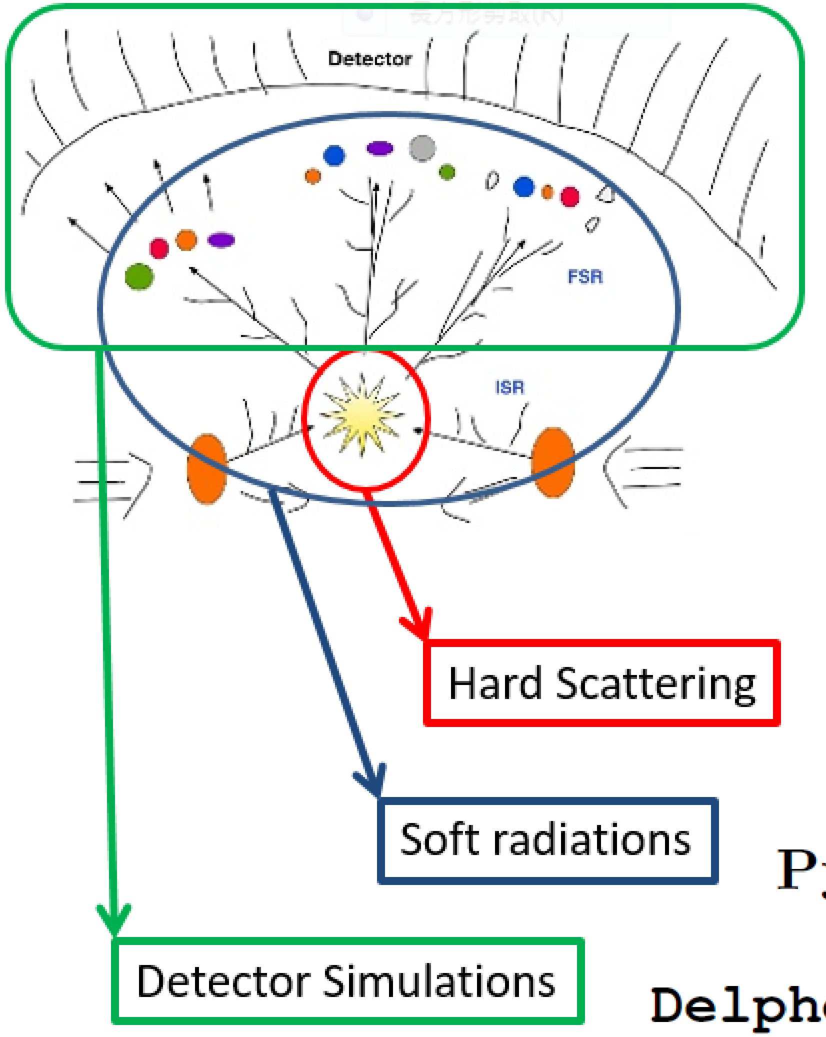

MadGraph5_aMC@NLO

Pythia8

Delphes3 & ROOT codes

$$pp \rightarrow HH \rightarrow \gamma\gamma b\bar{b}$$

The most sensitive channel because of the background suppression and signal reconstruction

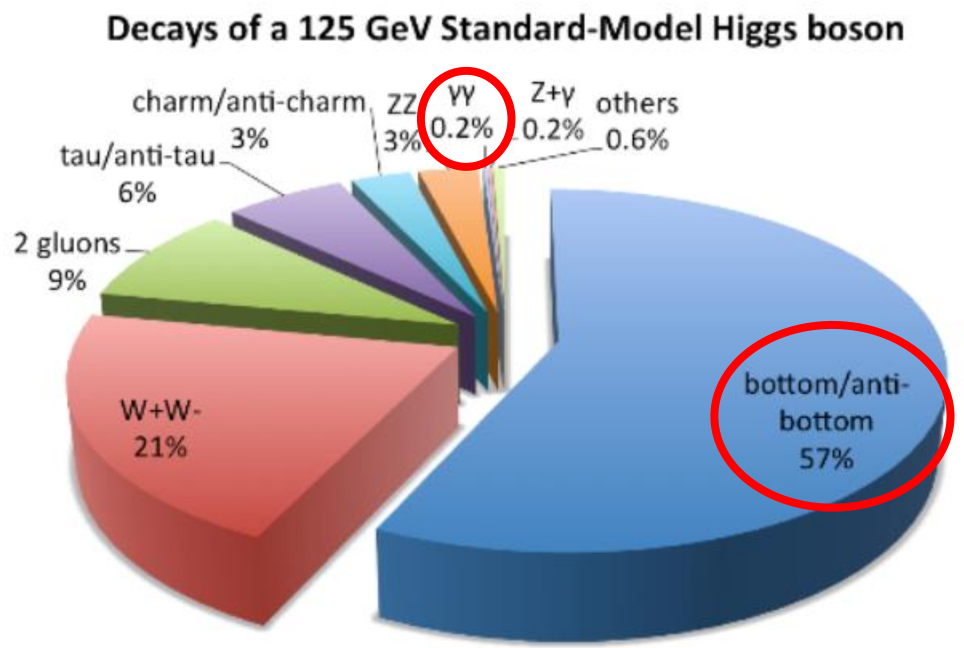

Basic cuts :

$$p_{T_\gamma} > 10\,\mathrm{GeV}, \quad p_{T_b} > 10\,\mathrm{GeV}, \quad |\eta_\gamma| < 2.5, \quad |\eta_b| < 2.5, \quad \Delta R_{\gamma\gamma} > 0.4, \quad \Delta R_{bb} > 0.4,$$
$$|M_H - M_{\gamma\gamma}| < 15\,\mathrm{GeV}, \quad |M_H - M_{bb}| < 25\,\mathrm{GeV}, \quad |M_H - M_{\tau\tau}| < 25\,\mathrm{GeV}. \qquad (4.1)$$

Numerical analysis : CPC1: g_t^S and λ_{3H}

JHEP08(2015)133

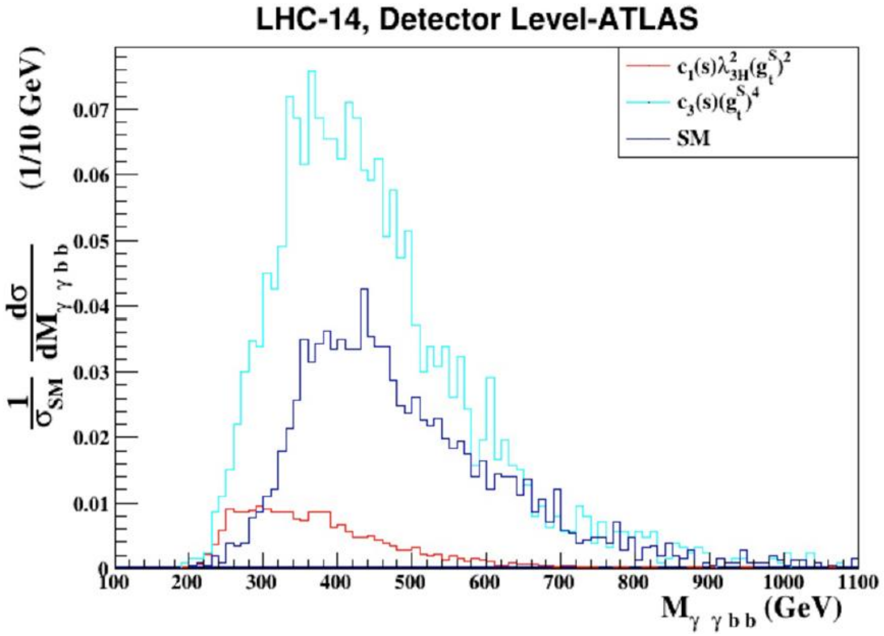

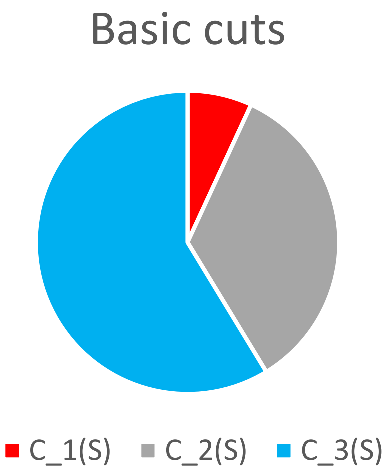

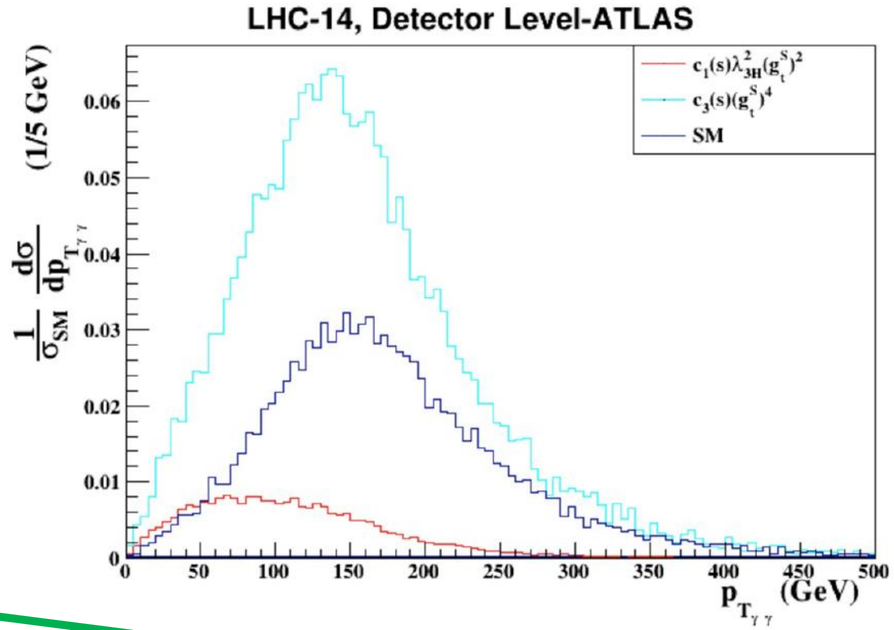

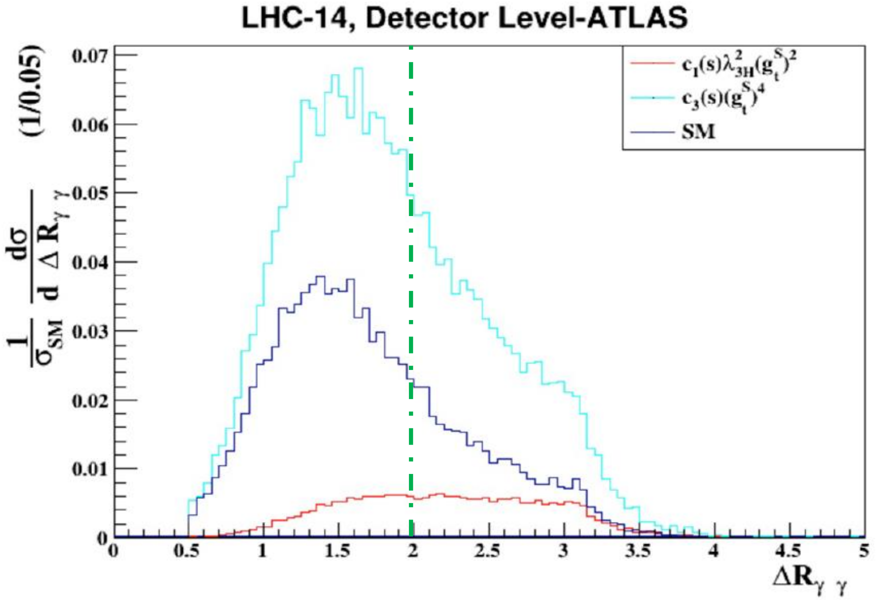

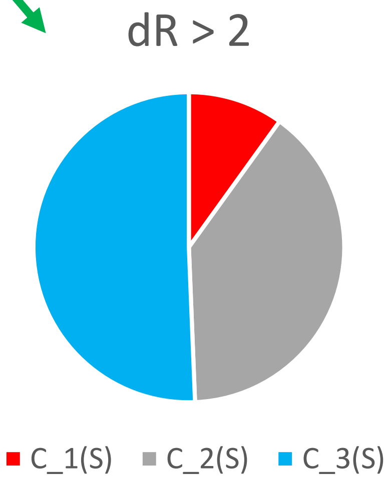

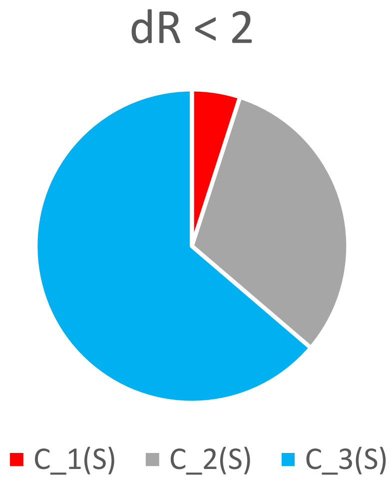

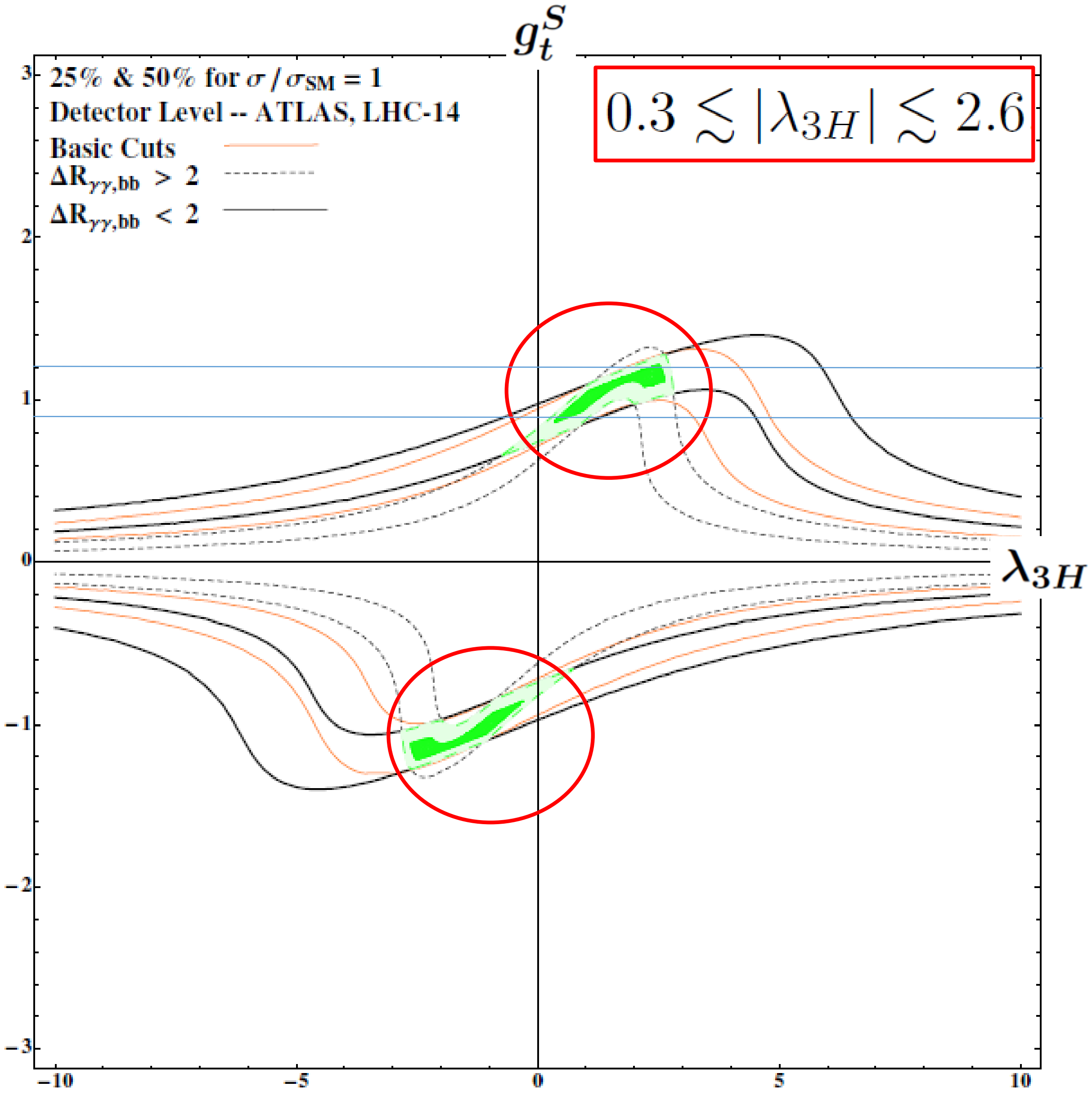

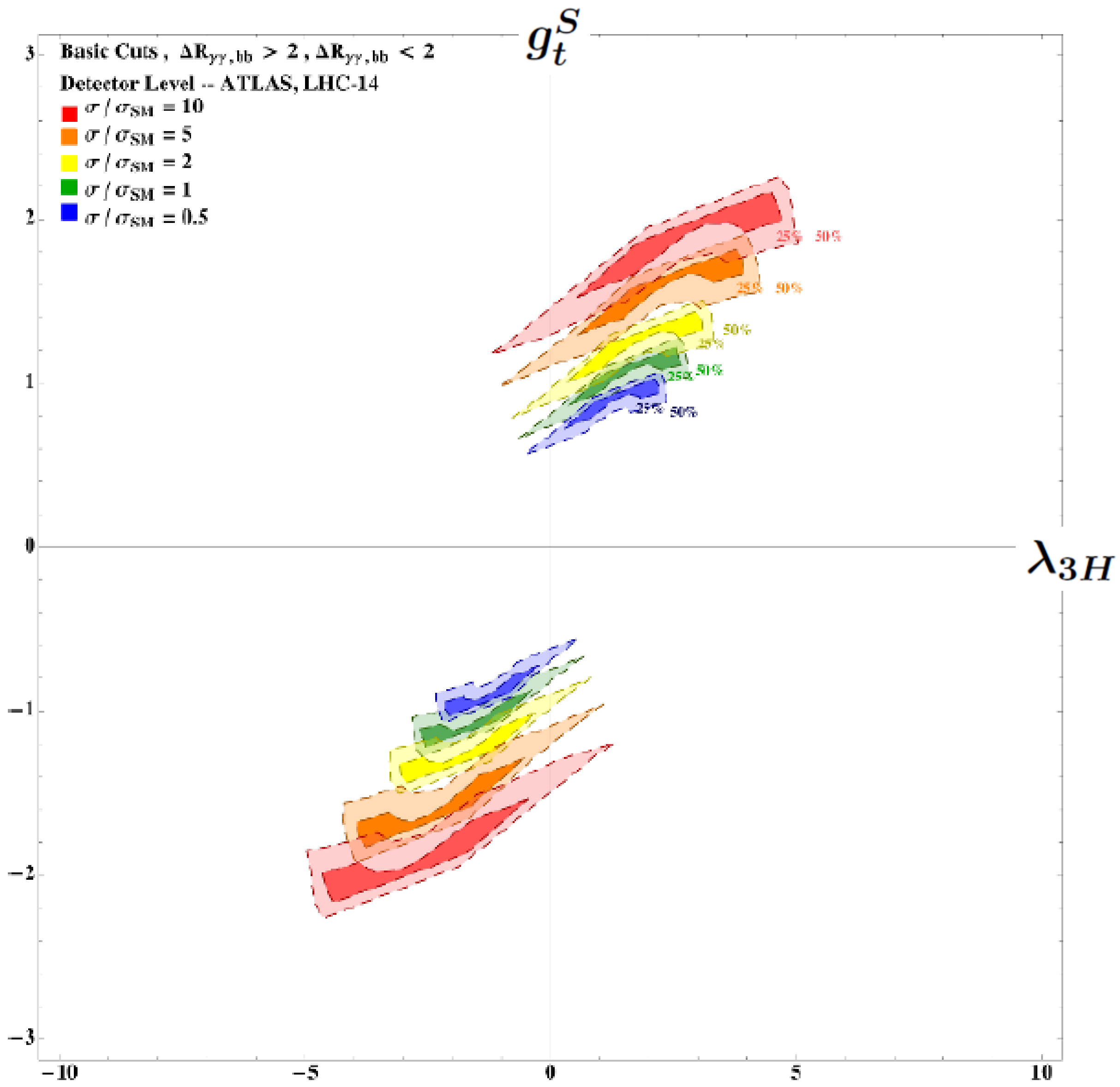

JHEP08(2015)133

We adopt an approach that the signal cross sections (after background subtraction) are measured with uncertainties of order 25-50%.

Numerical analysis : CPC2: g_t^S, λ_{3H}, and g_{tt}^S

JHEP08(2015)133

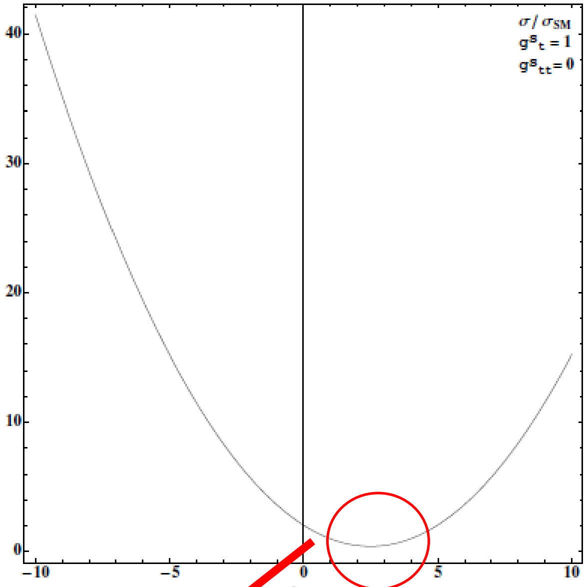

λ_{3H}

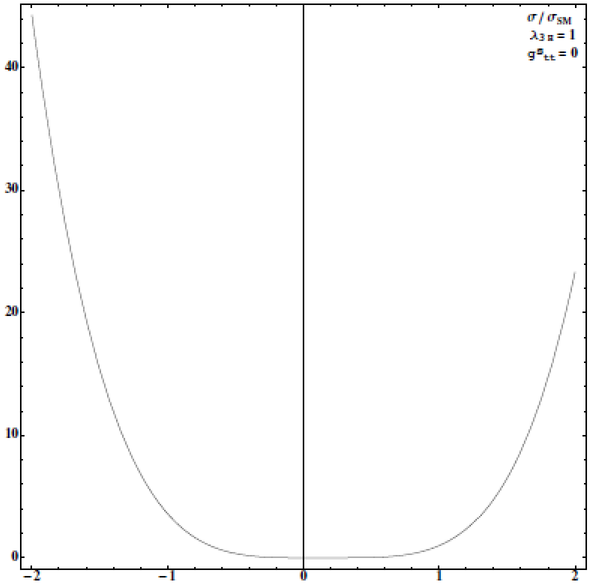

g_t^S

$\lambda_{3H} \approx 2.5$

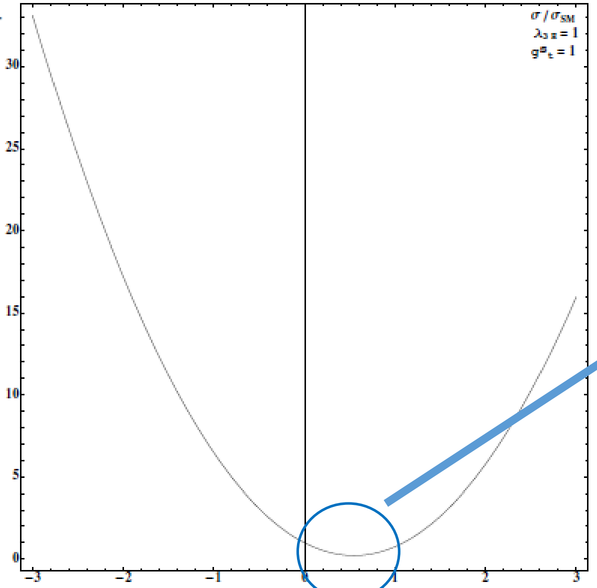

g_{tt}^S

$g_{tt}^S \approx 0.5$

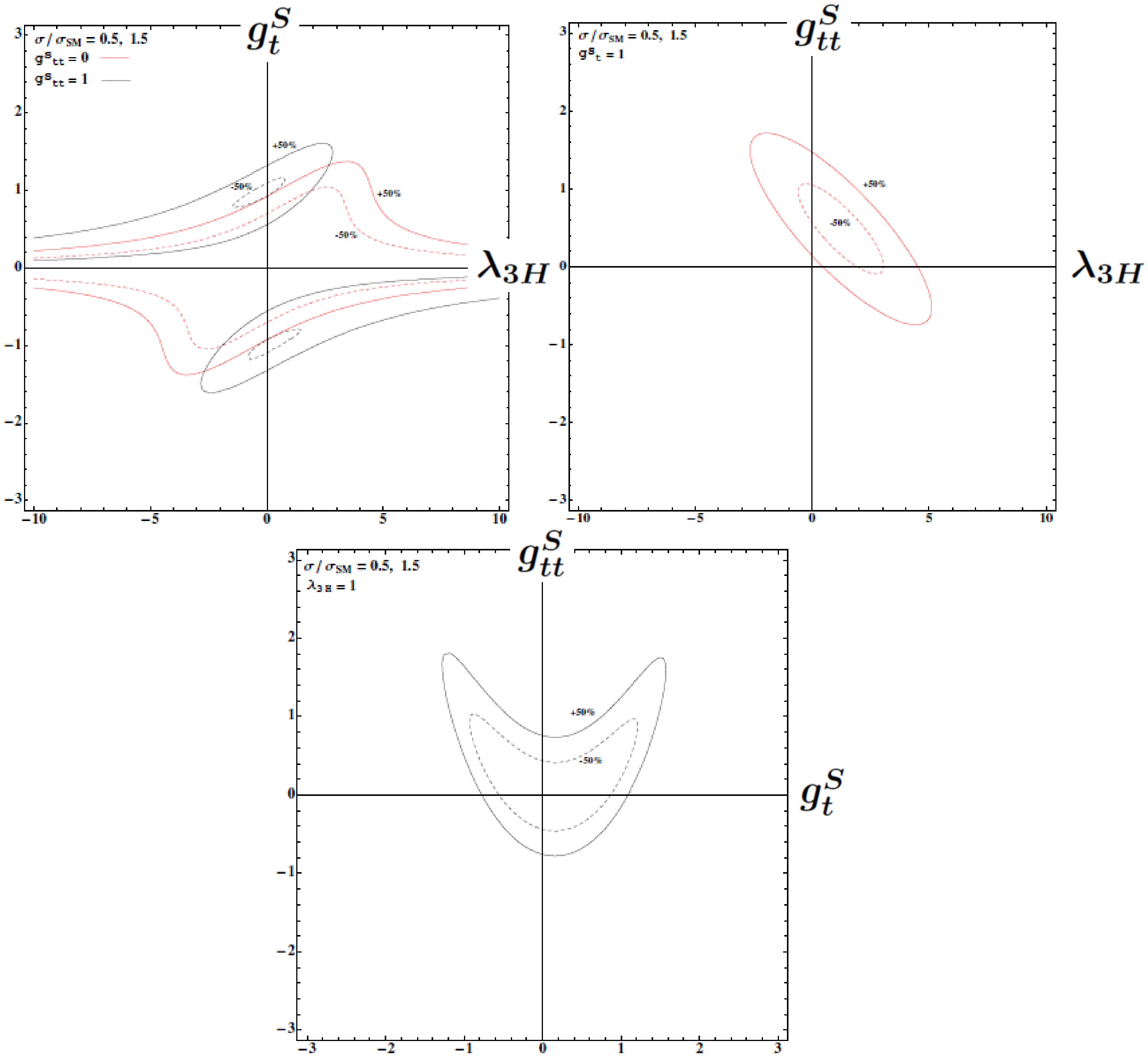

g_t^S
σ/σ_{SM} = 0.5, 1.5
g^S_{tt} = 0
g^S_{tt} = 1
+50%
-50%
λ_{3H}
g_{tt}^S
σ/σ_{SM} = 0.5, 1.5
g^S_t = 1
+50%
-50%
λ_{3H}
g_{tt}^S
σ/σ_{SM} = 0.5, 1.5
λ_{3H} = 1
+50%
-50%
g_t^S

Numerical analysis : CPC2: g_t^S, λ_{3H}, and g_{tt}^S JHEP08(2015)133

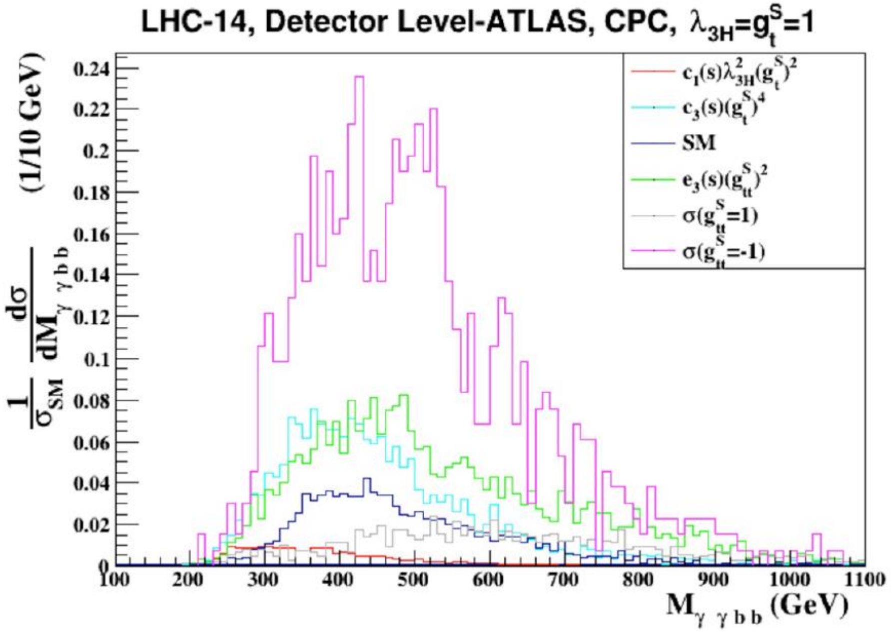

Basic cuts

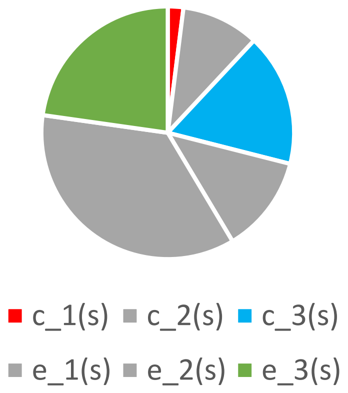

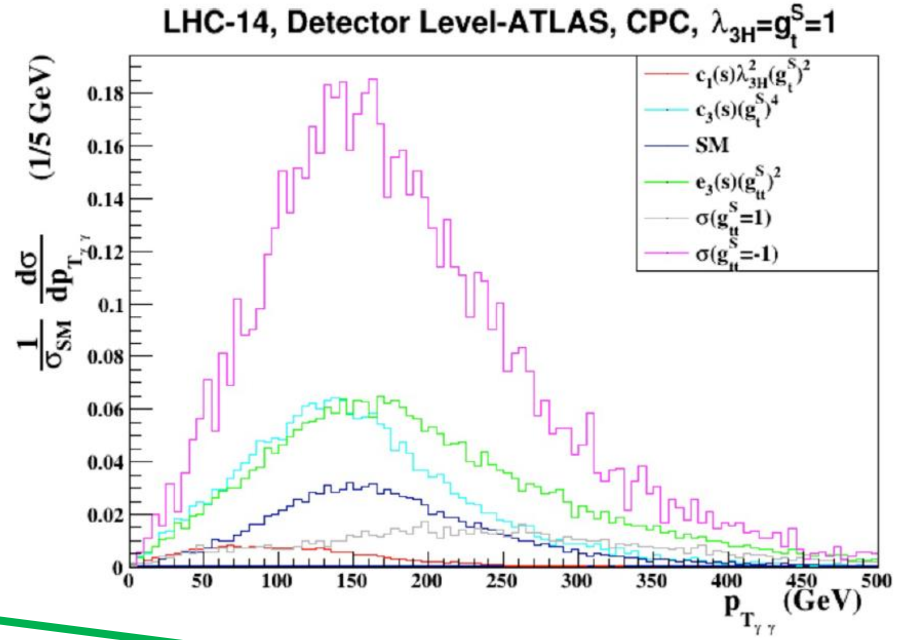

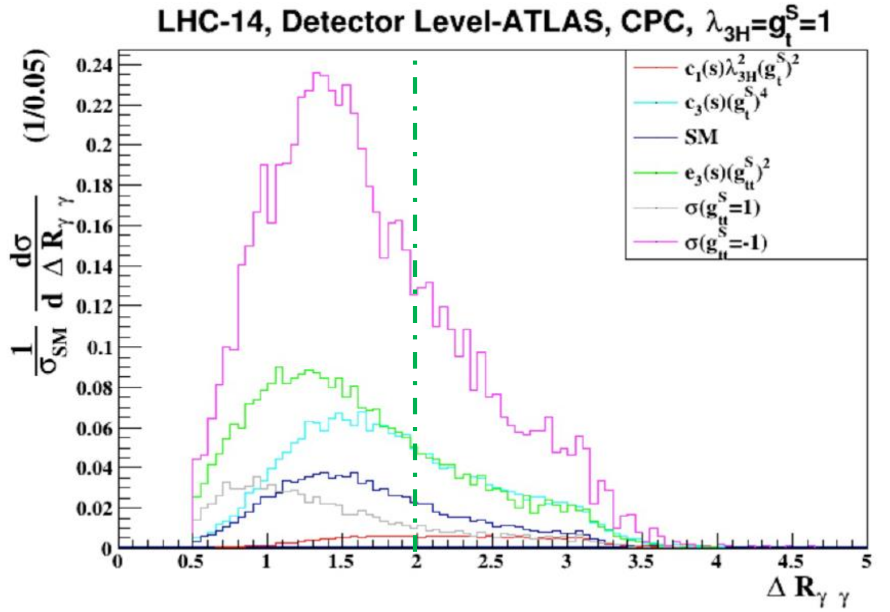

dR > 2

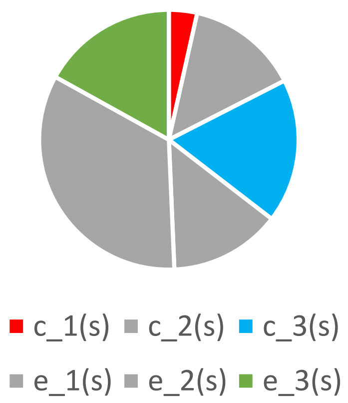

dR < 2

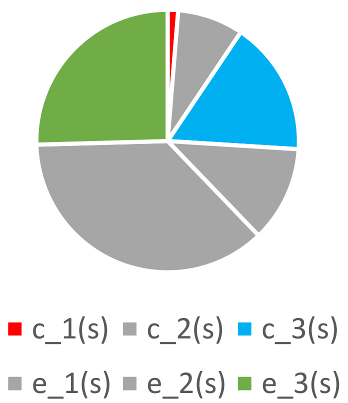

CPC2: $(\lambda_{3H}\,, g_t^S)$

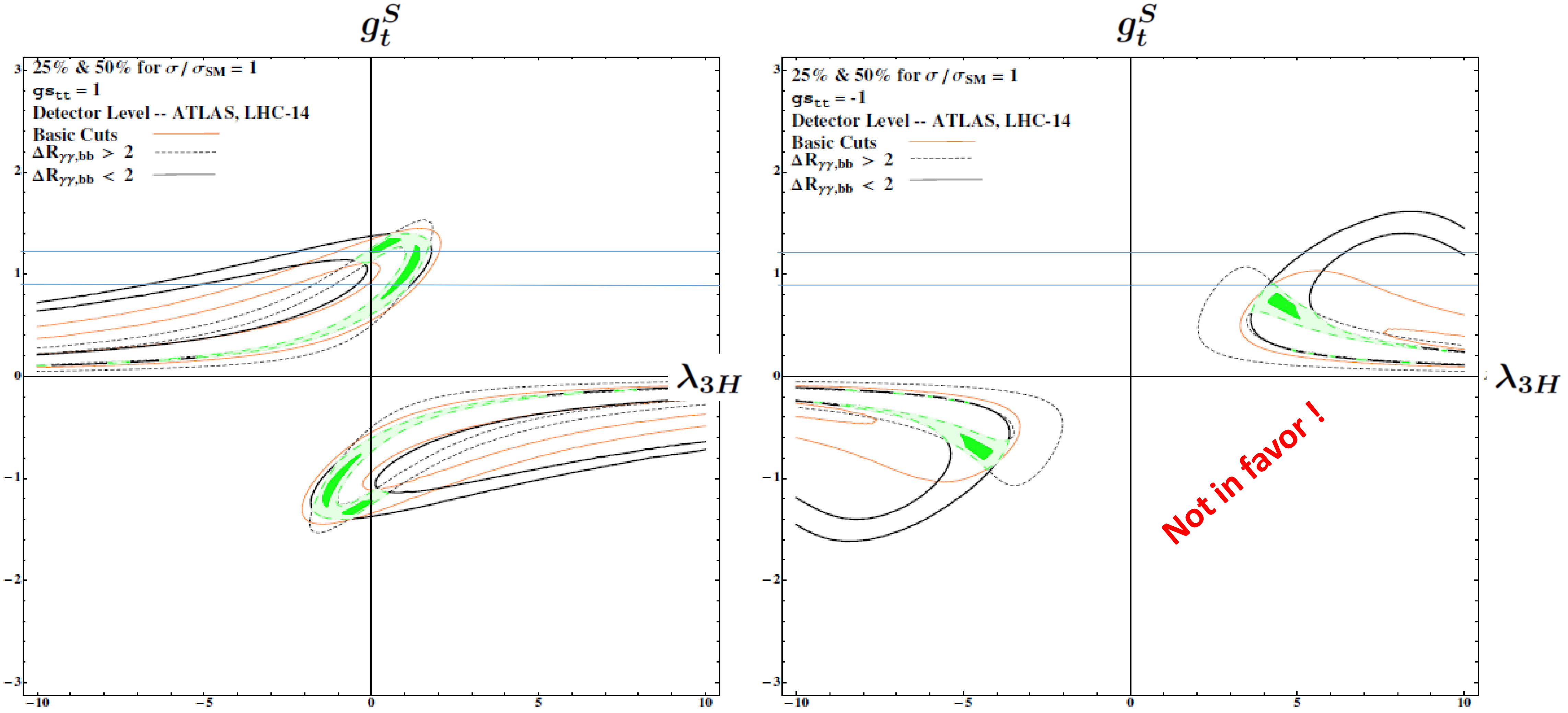

CPC2: (λ_{3H}, g^S_{tt}) & (g^S_t, g^S_{tt})

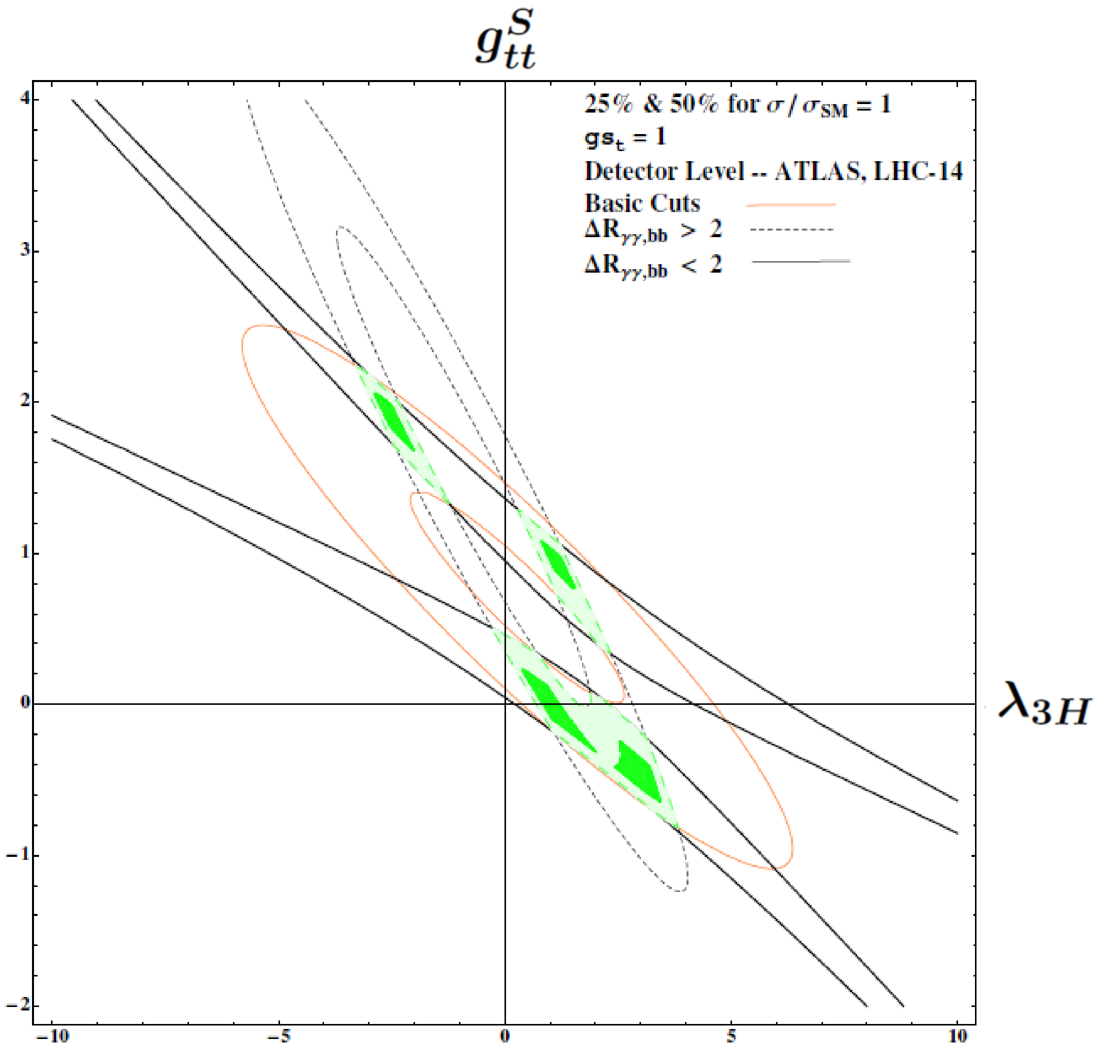

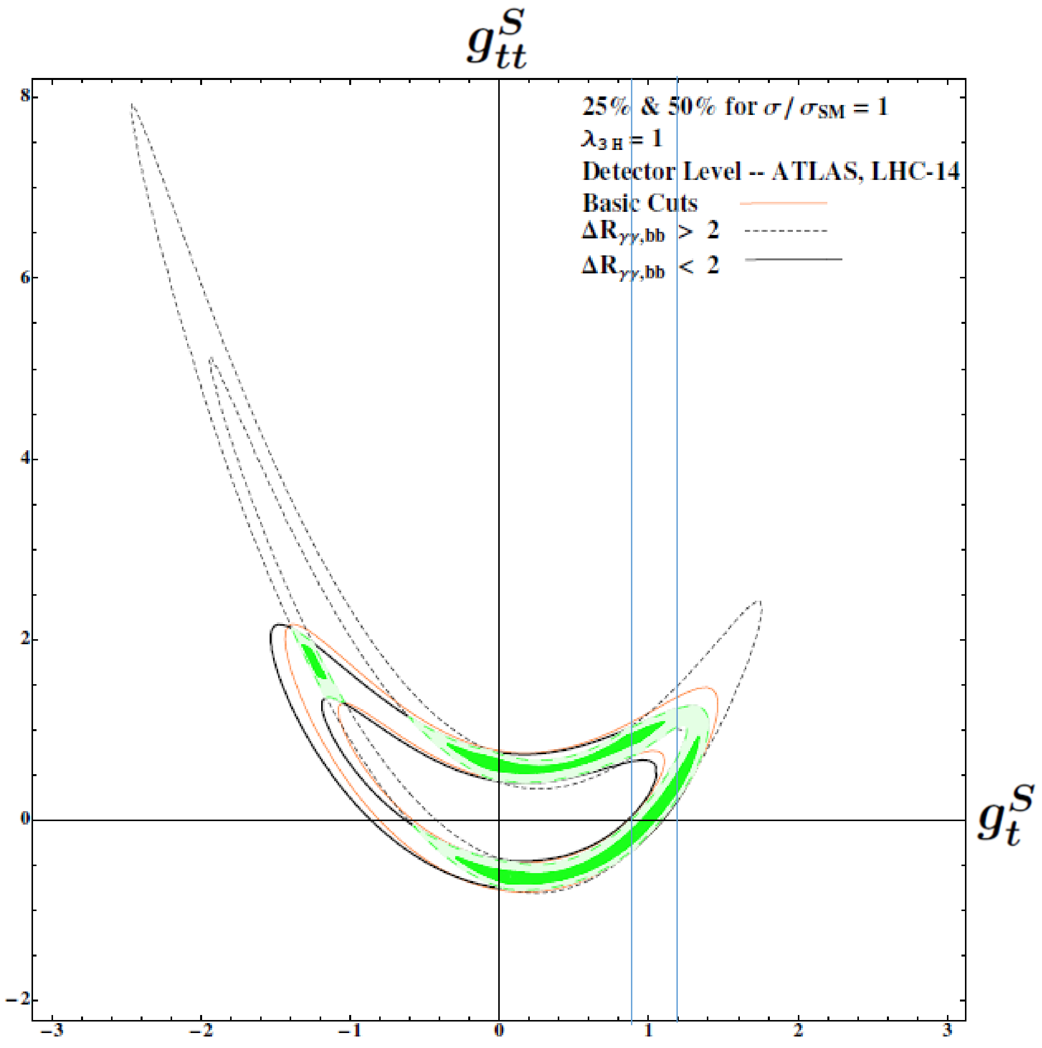

Numerical analysis : $\mathbf{CPV1}$: g_t^S, g_t^P, and λ_{3H}

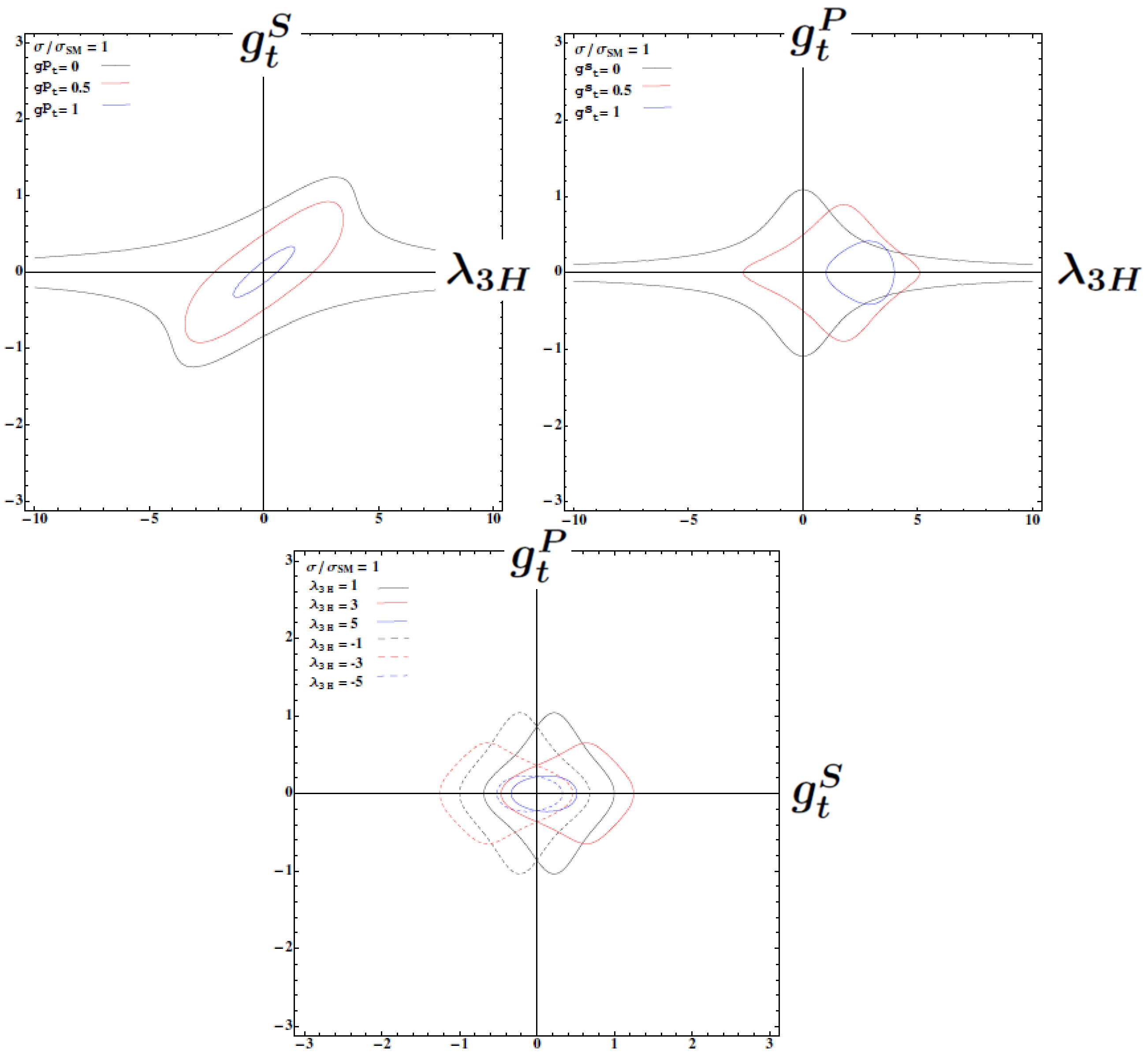

Numerical analysis : CPV1: g_t^S, g_t^P, and λ_{3H}

JHEP08(2015)133

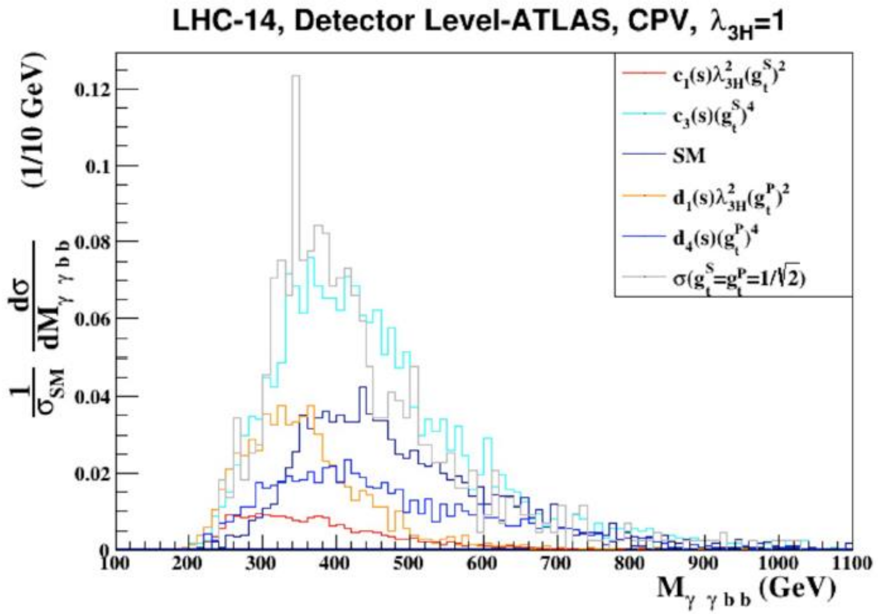

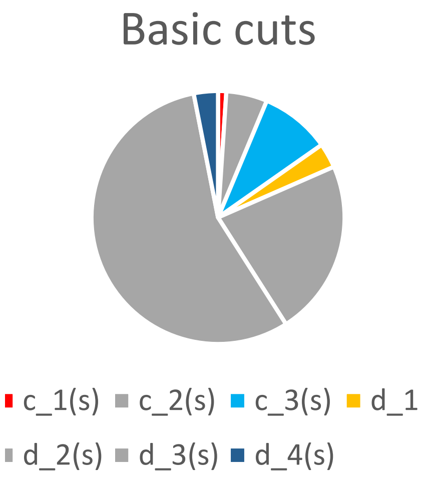

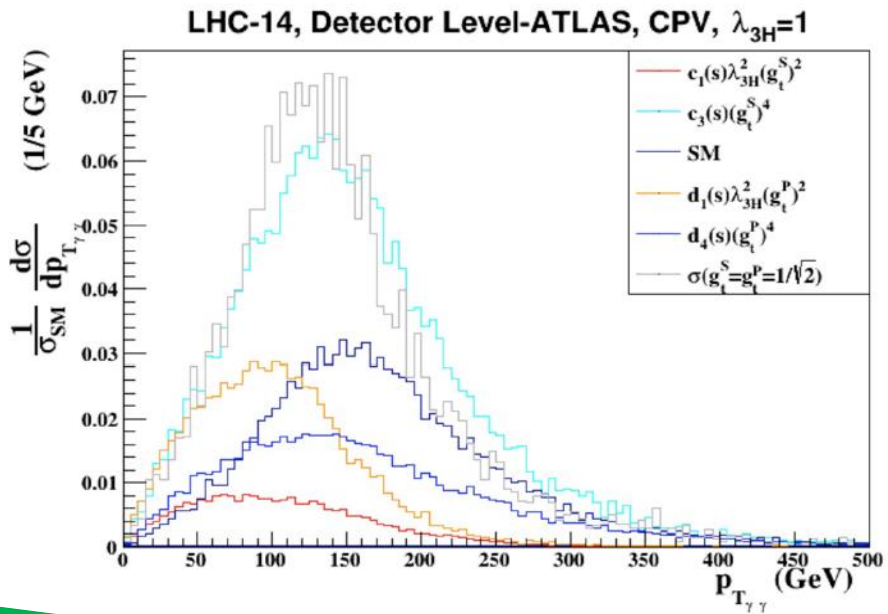

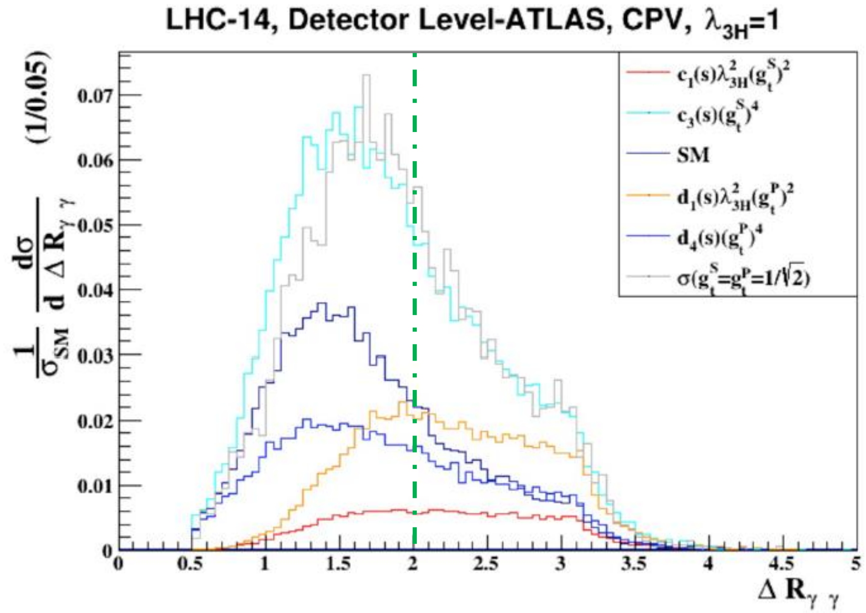

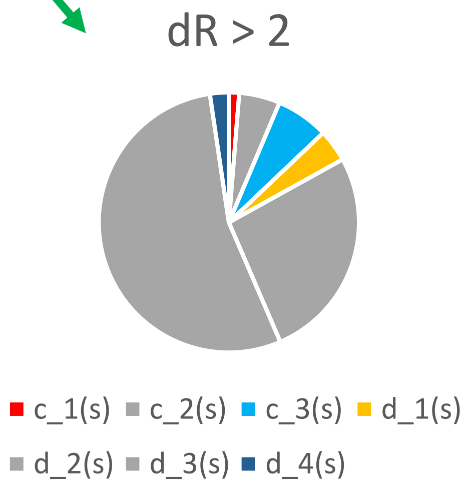

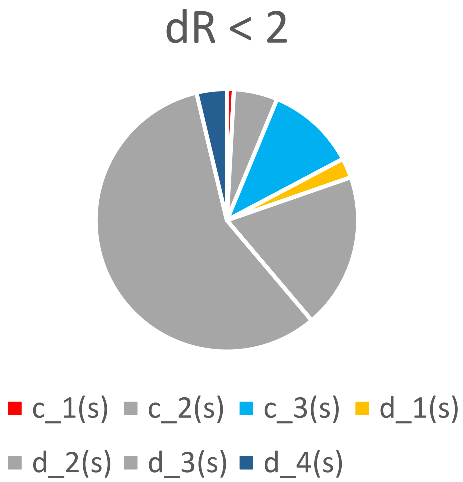

CPV1: (g_t^S, g_t^P) & (λ_{3H}, g_t^P)

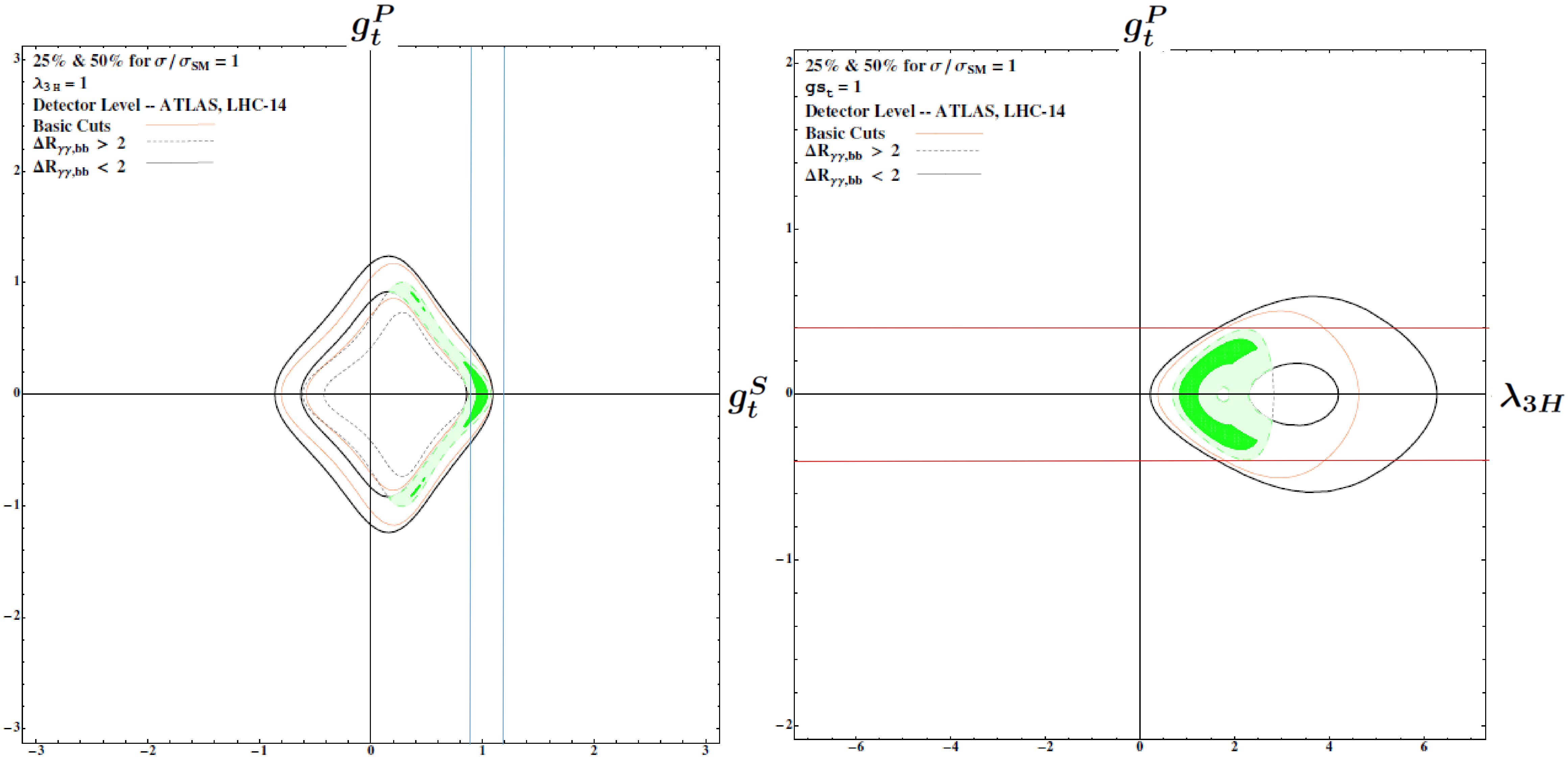

CPV1: (λ_{3H}, g_t^S)

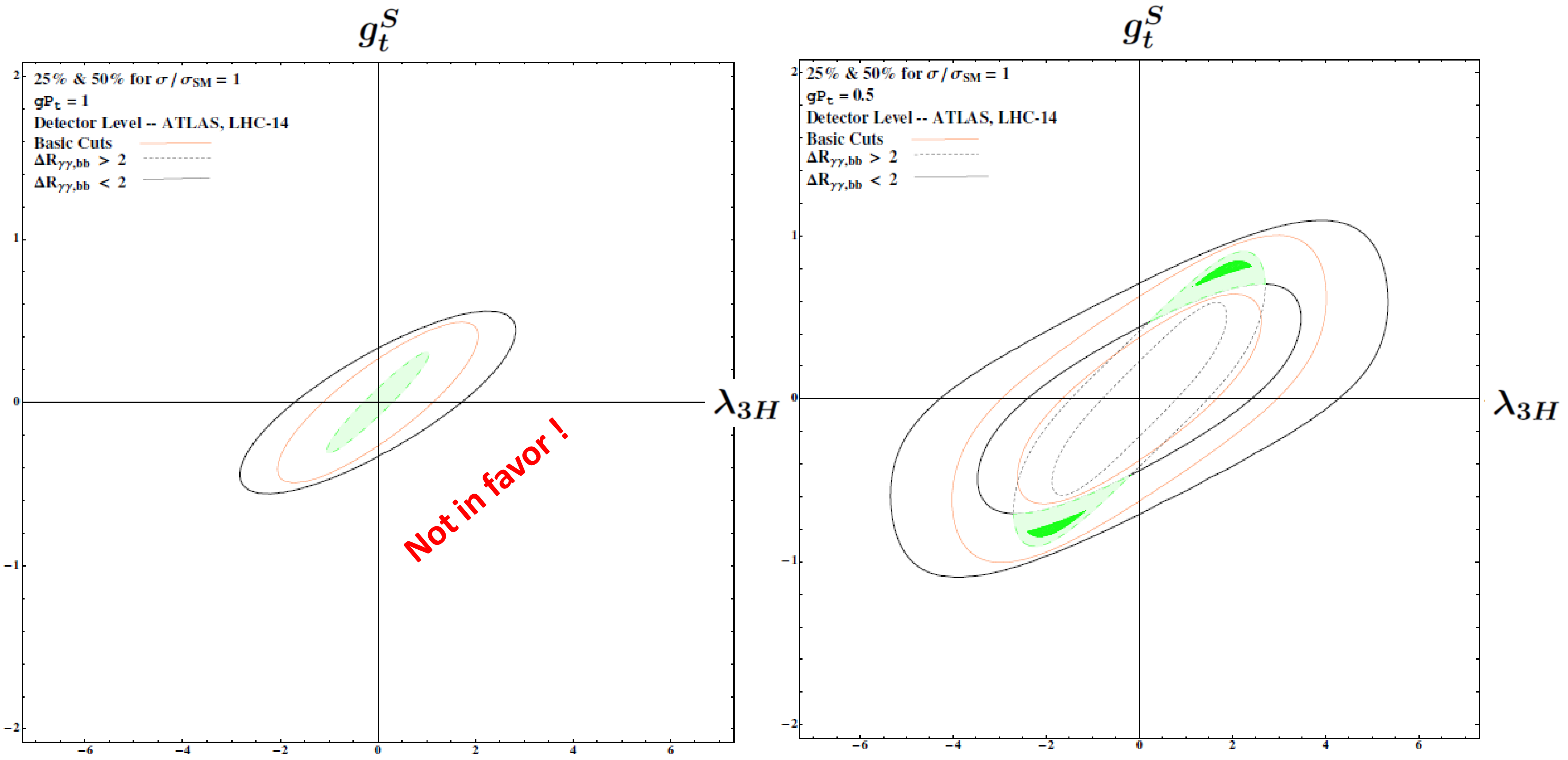

CPV2: $(g^S_{tt},\ g^P_{tt})$

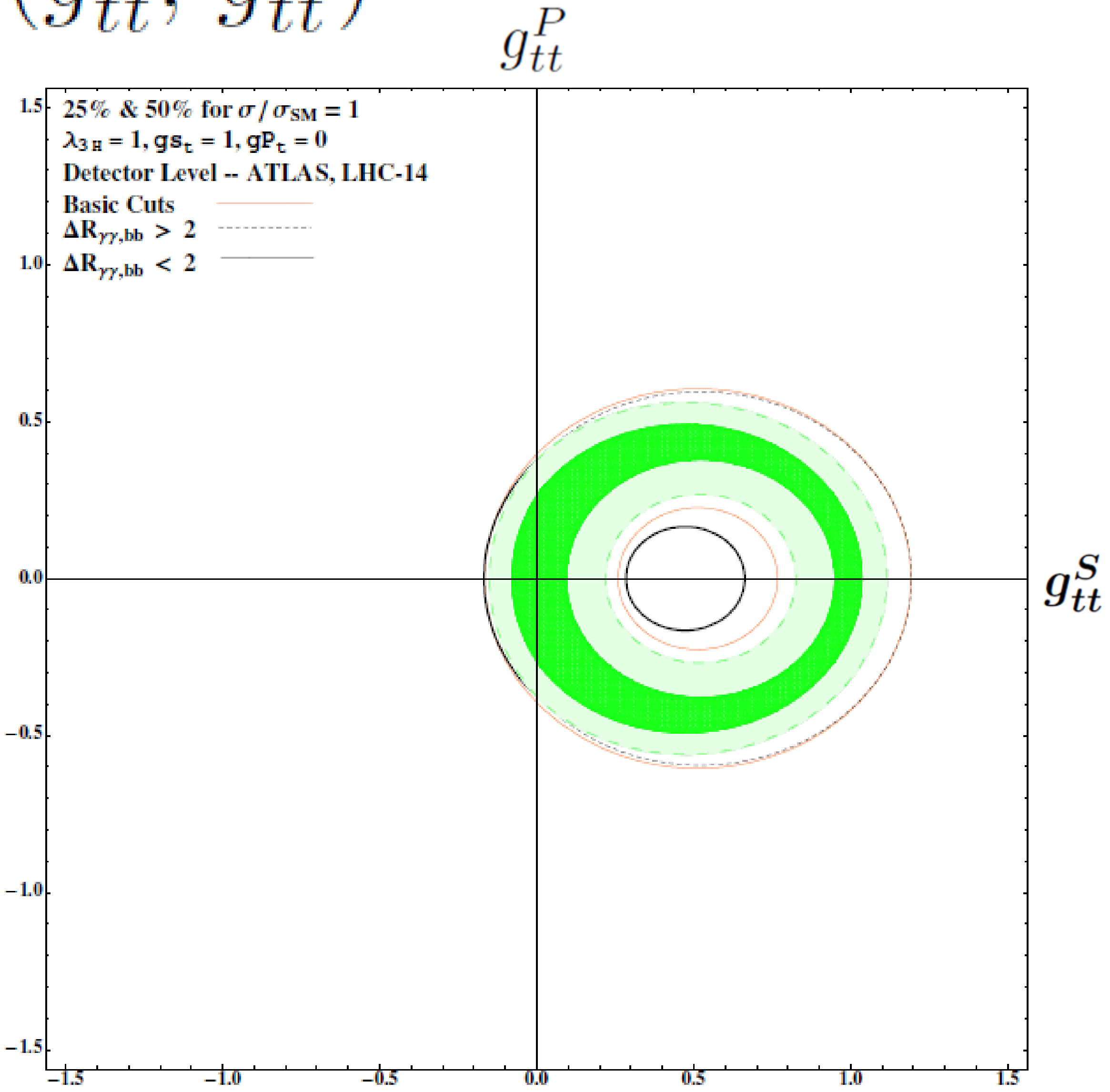

CPV2: $(\lambda_{3H},\, g_{tt}^{P})$ & $(\lambda_{3H},\, g_{tt}^{S})$

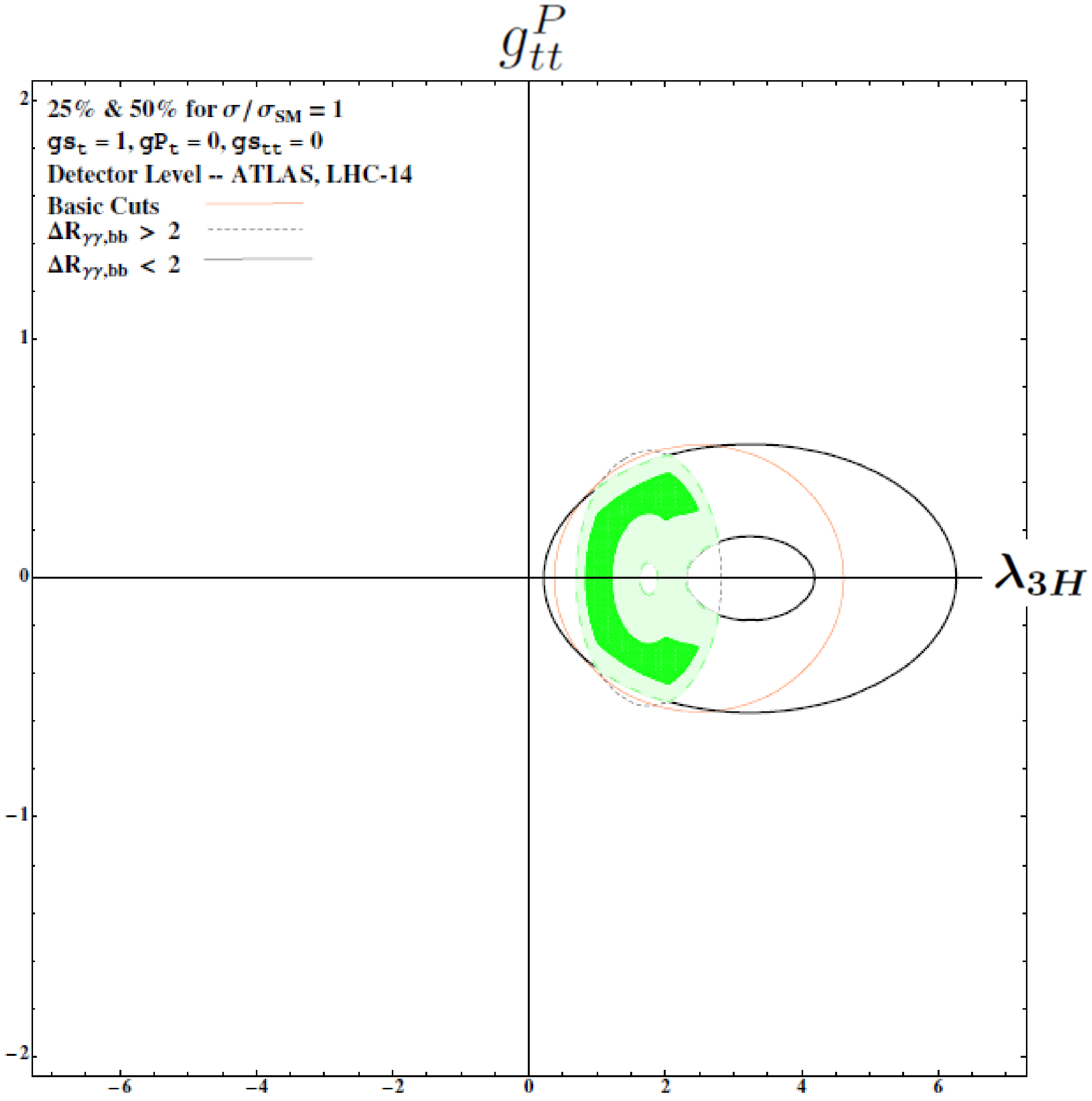

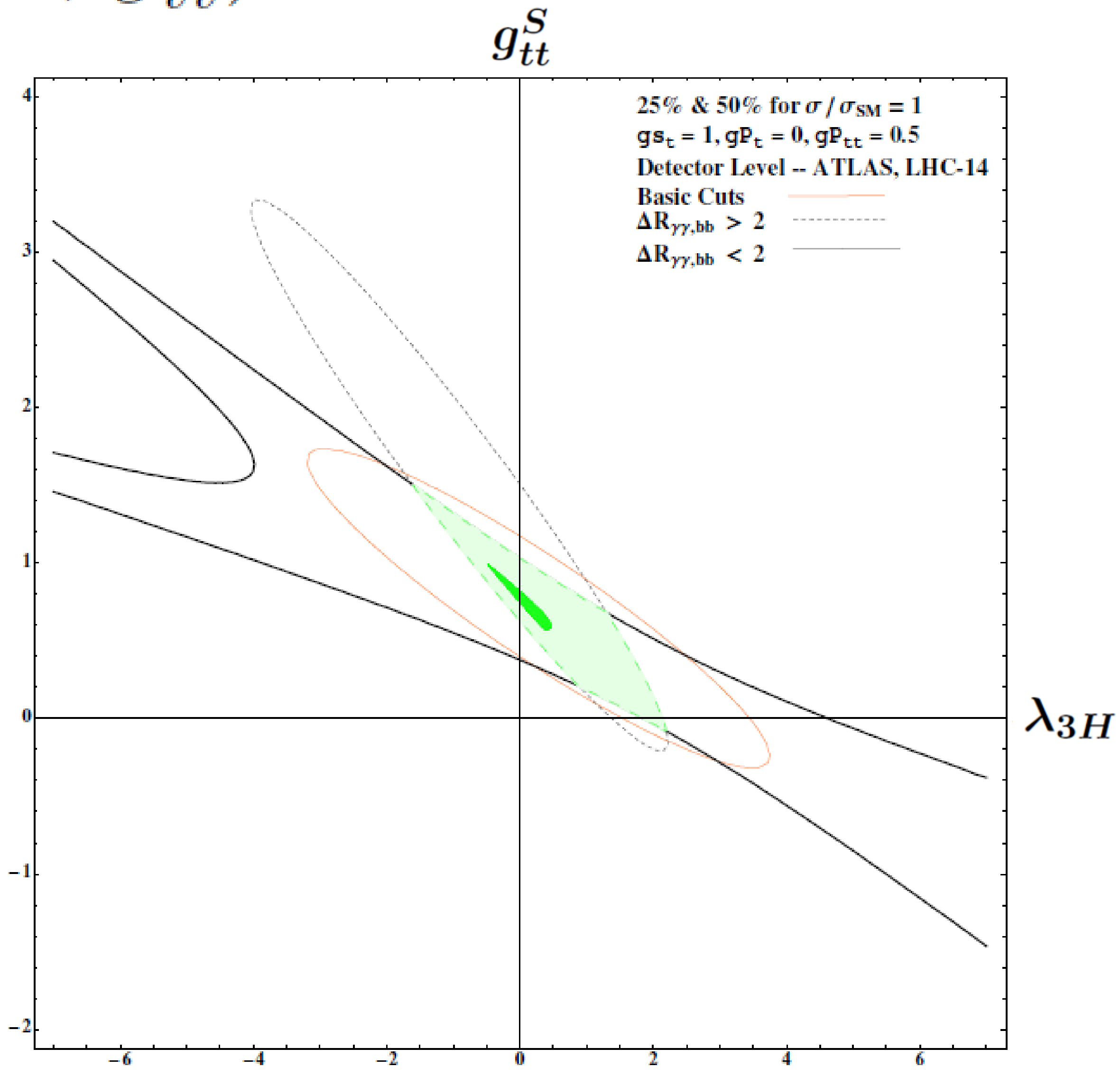

Contents

The comprehensive signal-background analysis – HL-LHC

- The backgrounds include

- single-Higgs associated production, such as ggH, $t\bar{t}H$, ZH, $b\bar{b}H$ followed by $H \to \gamma\gamma$,
- non-resonant backgrounds and jet-fake backgrounds, such as $b\bar{b}\gamma\gamma$, $c\bar{c}\gamma\gamma$, $jj\gamma\gamma$, $b\bar{b}j\gamma$, $c\bar{c}j\gamma$, $b\bar{b}jj$, and $Z\gamma\gamma \to b\bar{b}\gamma\gamma$,
- $t\bar{t}(\geq 1$ lepton) and $t\bar{t}\gamma(\geq 1$ lepton) backgrounds .

barrel region ($|\eta| < 1.37$)

Sequence	Event Selection Criteria at the HL-LHC
1	Di-photon trigger condition, ≥ 2 isolated photons with $P_T > 25$ GeV, $|\eta| < 2.5$
2	≥ 2 isolated photons with $P_T > 30$ GeV, $|\eta| < 1.37$ or $1.52 < |\eta| < 2.37$, $\Delta R_{j\gamma} > 0.4$
3	≥ 2 jets identified as b-jets with leading(subleading) $P_T > 40(30)$ GeV, $|\eta| < 2.4$
4	Events are required to contain ≤ 5 jets with $P_T > 30$ GeV within $|\eta| < 2.5$
5	No isolated leptons with $P_T > 25$ GeV, $|\eta| < 2.5$
6	$0.4 < \Delta R_{b\bar{b}} < 2.0$, $0.4 < \Delta R_{\gamma\gamma} < 2.0$
7	$122 < M_{\gamma\gamma}/\mathrm{GeV} < 128$ and $100 < M_{b\bar{b}}/\mathrm{GeV} < 150$
8	$P_T^{\gamma\gamma} > 80$ GeV, $P_T^{b\bar{b}} > 80$ GeV

arXiv:1804.07130

The comprehensive signal-background analysis – HL-LHC

Box diagram dominant

arXiv:1804.07130

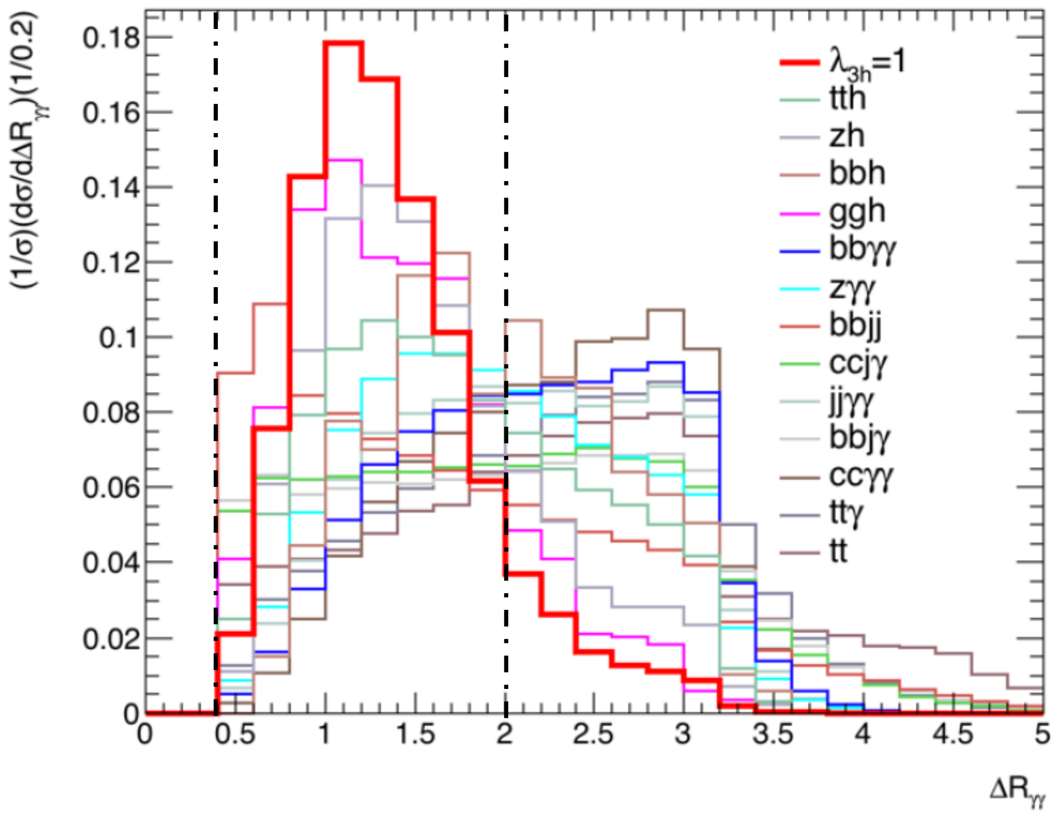

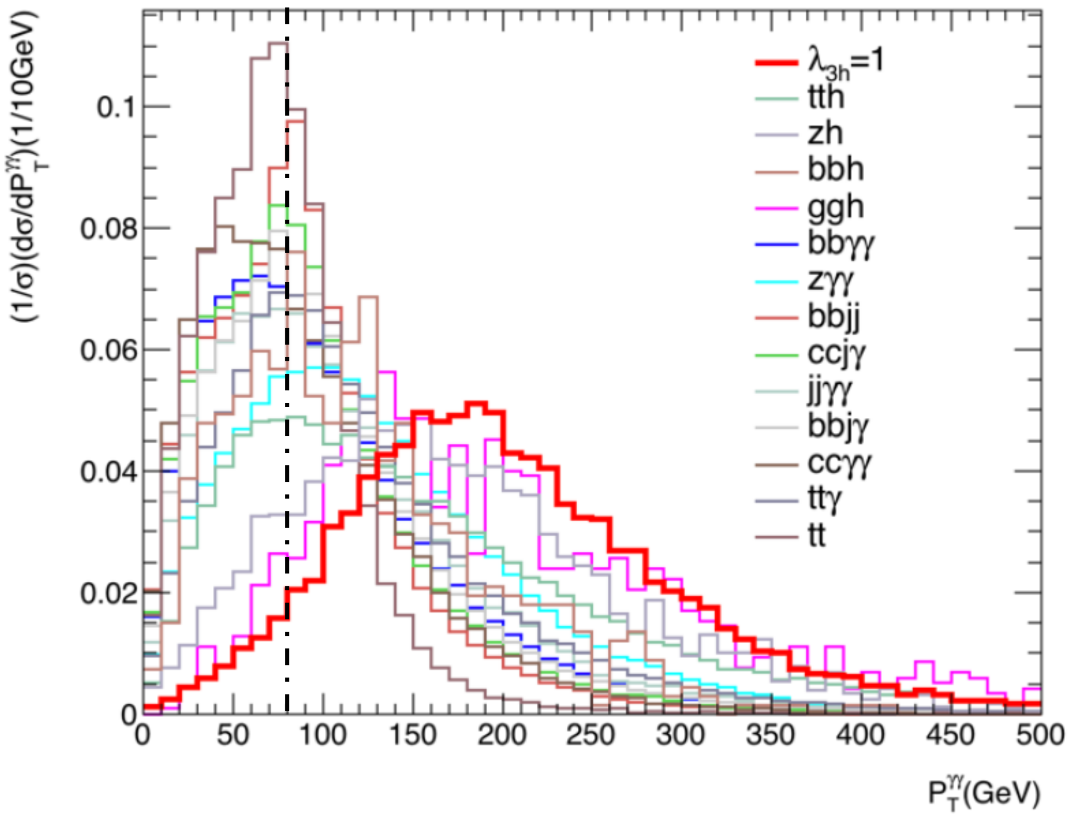

$$0.4 < \Delta R_{\gamma\gamma} < 2.0$$

$$P_T^{\gamma\gamma} > 80 \text{ GeV}$$

The comprehensive signal-background analysis – HL-LHC

Expected yields (3000 fb^{-1}) Samples	Total	Barrel-barrel	Other (End-cap)	Ratio (O/B)	# of Gen. Events
$H(b\bar{b})H(\gamma\gamma)$, $\lambda_{3H}=-4$	77.14 ± 0.94	57.03 ± 0.75	20.11 ± 0.34	0.35 ± 0.01	3×10^5
$H(b\bar{b})H(\gamma\gamma)$, $\lambda_{3H}=0$	19.50 ± 0.20	14.33 ± 0.16	5.17 ± 0.13	0.36 ± 0.01	3×10^5
$H(b\bar{b})H(\gamma\gamma)$, $\lambda_{3H}=1$	11.42 ± 0.082	8.53 ± 0.092	2.89 ± 0.048	0.34 ± 0.01	3×10^5
$H(b\bar{b})H(\gamma\gamma)$, $\lambda_{3H}=2$	6.82 ± 0.05	5.14 ± 0.04	1.68 ± 0.03	0.33 ± 0.01	3×10^5
$H(b\bar{b})H(\gamma\gamma)$, $\lambda_{3H}=6$	11.03 ± 0.21	7.91 ± 0.23	3.12 ± 0.10	0.39 ± 0.02	3×10^5
$H(b\bar{b})H(\gamma\gamma)$, $\lambda_{3H}=10$	57.46 ± 1.01	41.94 ± 0.60	15.52 ± 0.62	0.37 ± 0.02	3×10^5
$gg\,H(\gamma\gamma)$	6.60 ± 0.69	4.50 ± 0.71	2.10 ± 0.30	0.47 ± 0.10	6×10^6
$t\bar{t}H(\gamma\gamma)$	13.21 ± 0.23	9.82 ± 0.19	3.39 ± 0.17	0.35 ± 0.02	10^6
$Z\,H(\gamma\gamma)$	3.62 ± 0.16	2.44 ± 0.16	1.18 ± 0.08	0.48 ± 0.05	10^6
$b\bar{b}H(\gamma\gamma)$	0.15 ± 0.024	0.11 ± 0.027	0.04 ± 0.014	0.40 ± 0.16	10^6
$b\bar{b}\gamma\gamma$	18.86 ± 0.9	11.15 ± 0.7	7.71 ± 0.5	0.69 ± 0.06	1.1×10^7
$c\bar{c}\gamma\gamma$	7.53 ± 1.06	4.79 ± 1.10	2.74 ± 0.81	0.57 ± 0.21	10^7
$jj\gamma\gamma$	3.34 ± 0.46	1.59 ± 0.31	1.75 ± 0.32	1.10 ± 0.29	10^7
$b\bar{b}j\gamma$	18.77 ± 1.00	10.40 ± 0.83	8.37 ± 0.63	0.80 ± 0.09	10^7
$c\bar{c}j\gamma$	5.52 ± 1.4	3.94 ± 1.0	1.58 ± 0.6	0.40 ± 0.18	10^7
$b\bar{b}jj$	5.54 ± 0.5	3.81 ± 0.3	1.73 ± 0.2	0.45 ± 0.06	5×10^6
$Z(b\bar{b})\gamma\gamma$	0.90 ± 0.03	0.54 ± 0.02	0.36 ± 0.02	0.67 ± 0.04	10^7
$t\bar{t}$ (≥ 1 leptons)	4.98 ± 0.23	3.04 ± 0.12	1.94 ± 0.21	0.64 ± 0.07	10^7
$t\bar{t}\gamma$ (≥ 1 leptons)	3.61 ± 0.21	2.29 ± 0.15	1.32 ± 0.15	0.58 ± 0.08	10^7
Total Background	92.63 ± 2.5	58.42 ± 2.0	34.21 ± 1.4	0.59 ± 0.03	
Significance Z	1.163	1.090	0.487		
Combined significance		1.194			

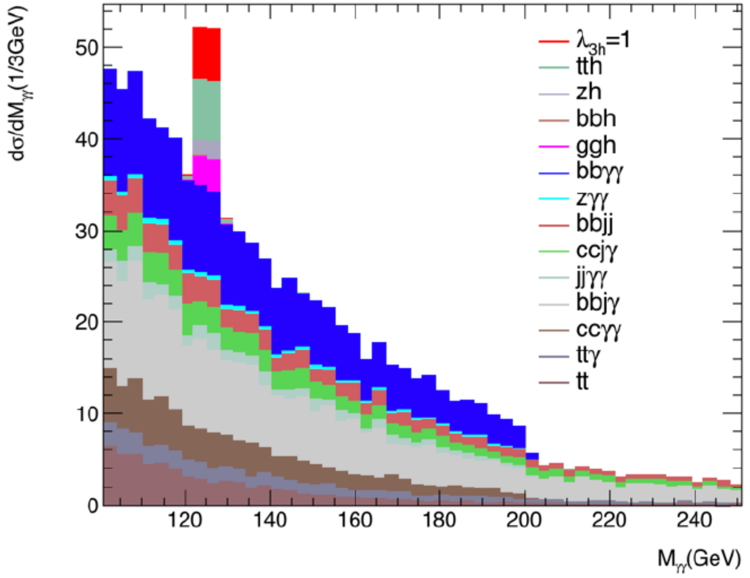

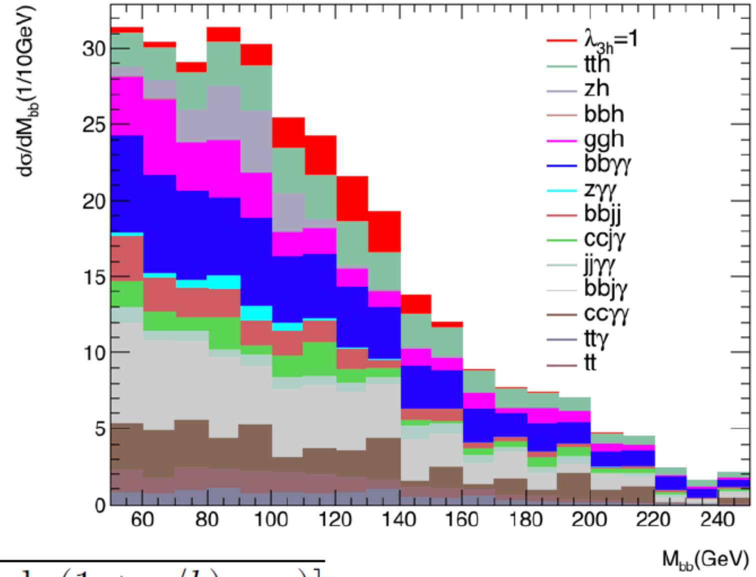

$$Z = \sqrt{2 \cdot [((s+b) \cdot \ln(1+s/b) - s)]}$$

The comprehensive signal-background analysis – HL-LHC

arXiv:1804.07130

$$Z = \sqrt{2 \cdot [((s+b) \cdot \ln(1+s/b) - s)]}$$

95% CL sensitivity

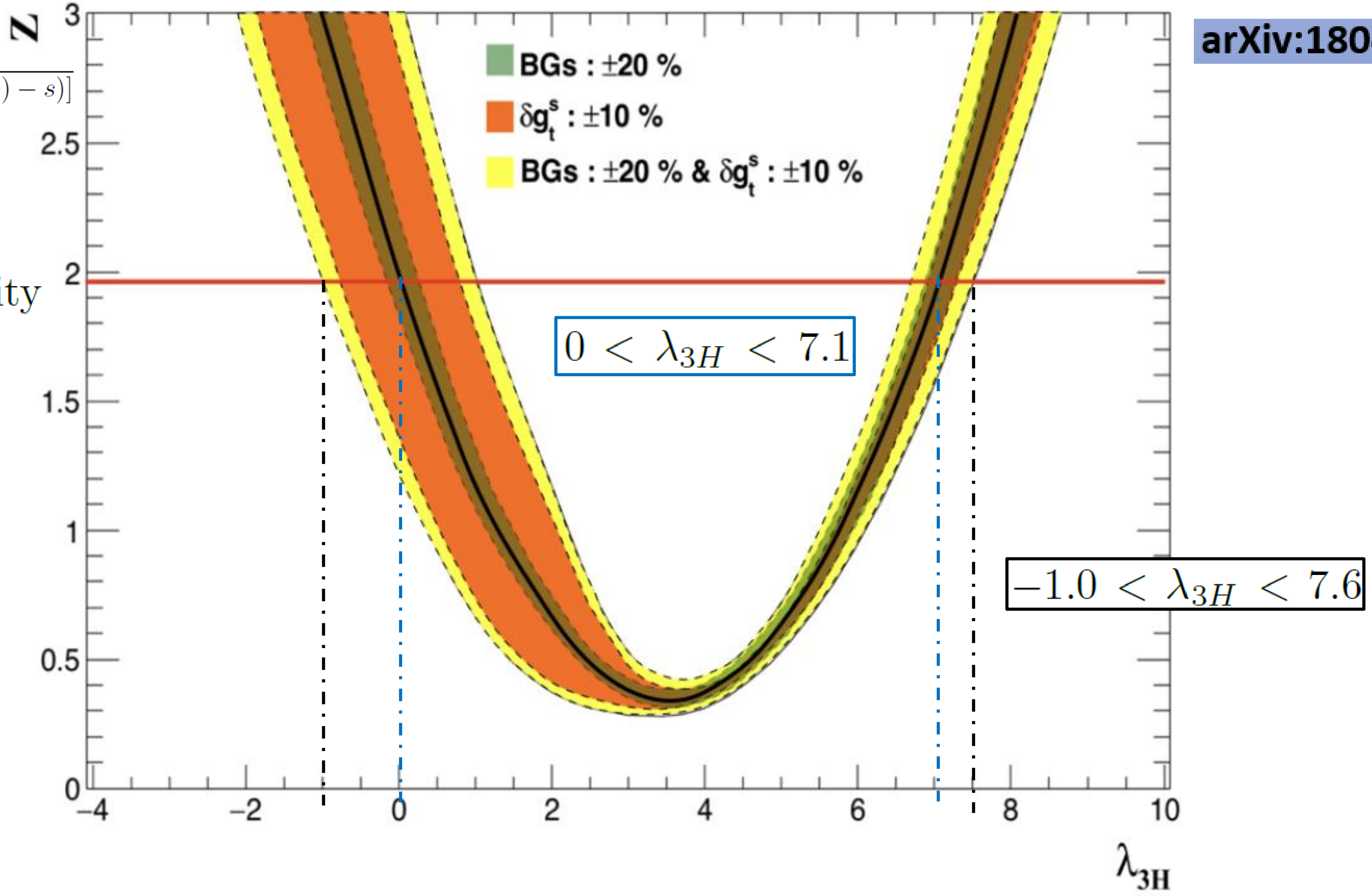

The comprehensive signal-background analysis – HL-LHC

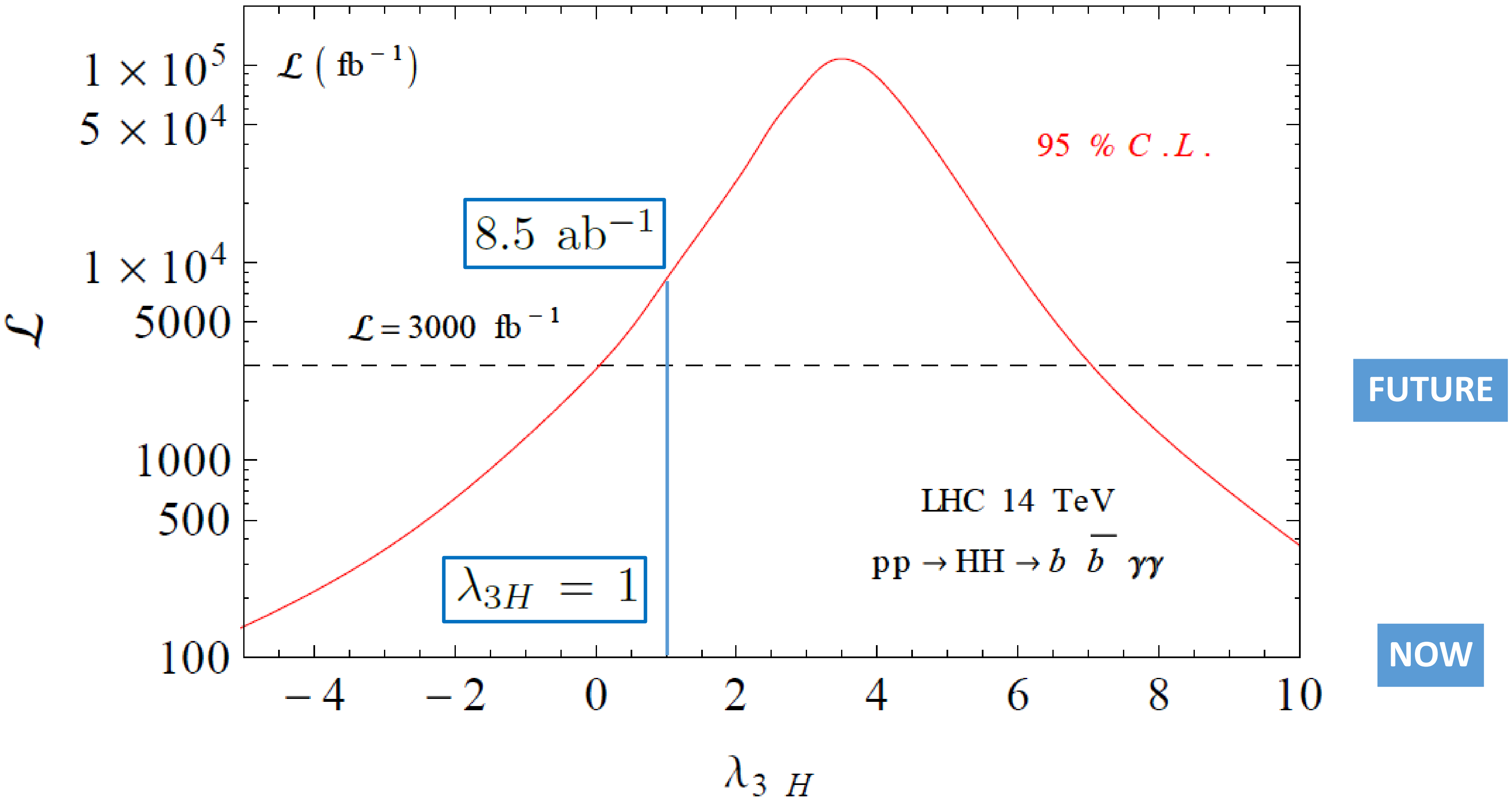

FIG. 7. **HL-LHC**: Required luminosity for 95% CL sensitivity at the 14 TeV HL-LHC versus λ_{3H}. Here we assume that the top-Yukawa coupling takes the SM value.

arXiv:1804.07130

The comprehensive signal-background analysis – HL-100 TeV Collider

- The backgrounds include

arXiv:1804.07130

- single-Higgs associated production, such as ggH, $t\bar{t}H$, ZH, $b\bar{b}H$ followed by $H \to \gamma\gamma$,
- non-resonant backgrounds and jet-fake backgrounds, such as $b\bar{b}\gamma\gamma$, $c\bar{c}\gamma\gamma$, $jj\gamma\gamma$, $b\bar{b}j\gamma$, $c\bar{c}j\gamma$, $b\bar{b}jj$, and $Z\gamma\gamma \to b\bar{b}\gamma\gamma$,
- $t\bar{t}(\geq 1$ lepton) and $t\bar{t}\gamma(\geq 1$ lepton) backgrounds .

Sequence	Event Selection Criteria at the HL-100 TeV hadron collider
1	Di-photon trigger condition, ≥ 2 isolated photons with $P_T > 30$ GeV, $\lvert\eta\rvert < 5$
2	≥ 2 isolated photons with $P_T > 40$ GeV, $\lvert\eta\rvert < 3$, $\Delta R_{j\gamma} > 0.4$
3	≥ 2 jets identified as b-jets with leading(subleading) $P_T > 50(40)$ GeV, $\lvert\eta\rvert < 3$
4	Events are required to contain ≤ 5 jets with $P_T > 40$ GeV within $\lvert\eta\rvert < 5$
5	No isolated leptons with $P_T > 40$ GeV, $\lvert\eta\rvert < 3$
6	$0.4 < \Delta R_{b\bar{b}} < 3.0$, $0.4 < \Delta R_{\gamma\gamma} < 3.0$
7	$122.5 < M_{\gamma\gamma}/\mathrm{GeV} < 127.5$ and $90 < M_{b\bar{b}}/\mathrm{GeV} < 150$
8	$P_T^{\gamma\gamma} > 100$ GeV, $P_T^{b\bar{b}} > 100$ GeV

The comprehensive signal-background analysis – HL-100 TeV Collider

Expected yields (3000 fb^{-1}) Samples	Total	Barrel-barrel	Other (End-cap)	Ratio (O/B)	# of Gen. Events
$H(b\bar{b})\,H(\gamma\gamma)$, $\lambda_{3H}=-4$	5604.46 ± 63.36	4257.36 ± 57.90	1347.10 ± 23.22	0.32 ± 0.007	3×10^5
$H(b\bar{b})\,H(\gamma\gamma)$, $\lambda_{3H}=0$	1513.56 ± 14.81	1163.04 ± 14.09	350.52 ± 3.57	0.30 ± 0.005	3×10^5
$H(b\bar{b})\,H(\gamma\gamma)$, $\lambda_{3H}=1$	941.37 ± 7.65	723.86 ± 6.64	217.51 ± 3.66	0.30 ± 0.006	3×10^5
$H(b\bar{b})\,H(\gamma\gamma)$, $\lambda_{3H}=2$	557.36 ± 1.93	431.45 ± 1.87	125.91 ± 1.21	0.29 ± 0.003	3×10^5
$H(b\bar{b})\,H(\gamma\gamma)$, $\lambda_{3H}=6$	753.18 ± 6.02	566.18 ± 5.59	187.00 ± 5.33	0.33 ± 0.010	3×10^5
$H(b\bar{b})\,H(\gamma\gamma)$, $\lambda_{3H}=10$	3838.33 ± 36.82	2924.25 ± 32.11	914.08 ± 28.01	0.31 ± 0.010	3×10^5
$gg\,H(\gamma\gamma)$	890.47 ± 72.91	742.97 ± 58.43	147.50 ± 20.51	0.20 ± 0.03	10^6
$t\bar{t}\,H(\gamma\gamma)$	868.73 ± 8.53	659.33 ± 12.94	209.40 ± 7.04	0.32 ± 0.01	9.63×10^5
$Z\,H(\gamma\gamma)$	168.86 ± 5.91	122.91 ± 4.68	45.95 ± 1.69	0.37 ± 0.02	10^6
$b\bar{b}\,H(\gamma\gamma)$	9.82 ± 0.59	7.00 ± 0.58	2.82 ± 0.25	0.40 ± 0.05	10^6
$b\bar{b}\gamma\gamma$	770.42 ± 23.48	514.96 ± 20.81	255.46 ± 15.10	0.50 ± 0.04	1.1×10^7
$c\bar{c}\gamma\gamma$	222.88 ± 40.55	111.44 ± 32.55	111.44 ± 26.92	1.00 ± 0.38	1.1×10^7
$jj\gamma\gamma$	32.28 ± 3.23	20.98 ± 3.99	11.30 ± 2.34	0.54 ± 0.15	10^7
$b\bar{b}j\gamma$	1829.13 ± 75.08	1288.34 ± 45.27	540.79 ± 49.79	0.42 ± 0.04	1.1×10^7
$c\bar{c}j\gamma$	293.81 ± 40.11	216.49 ± 36.71	77.32 ± 32.97	0.36 ± 0.16	1.1×10^7
$b\bar{b}jj$	3569.73 ± 209.93	2294.83 ± 207.69	1274.90 ± 189.68	0.56 ± 0.10	3.43×10^6
$Z(b\bar{b})\gamma\gamma$	54.87 ± 3.79	35.72 ± 3.36	19.15 ± 2.02	0.54 ± 0.08	10^6
$t\bar{t}$ (≥ 1 leptons)	59.32 ± 7.40	38.32 ± 5.79	21.00 ± 5.61	0.55 ± 0.17	1.1×10^7
$t\bar{t}\gamma$ (≥ 1 leptons)	105.68 ± 8.22	62.53 ± 5.07	43.15 ± 7.95	0.69 ± 0.14	10^6
Total Background	8876.00 ± 243.07	6115.82 ± 227.41	2760.18 ± 202.67	0.45 ± 0.04	
Significance Z	9.823	9.082	4.087		
Combined significance		9.959			

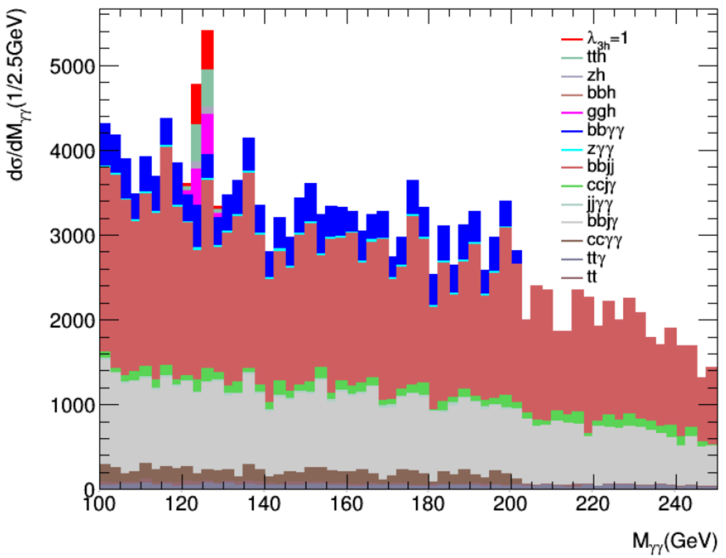

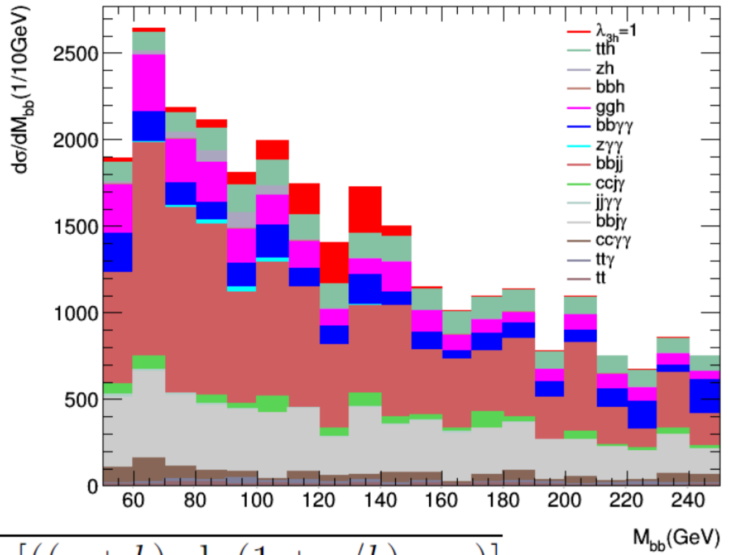

$$Z = \sqrt{2 \cdot [((s+b)\cdot \ln(1+s/b) - s)]}$$

The comprehensive signal-background analysis – HL-100 TeV Collider

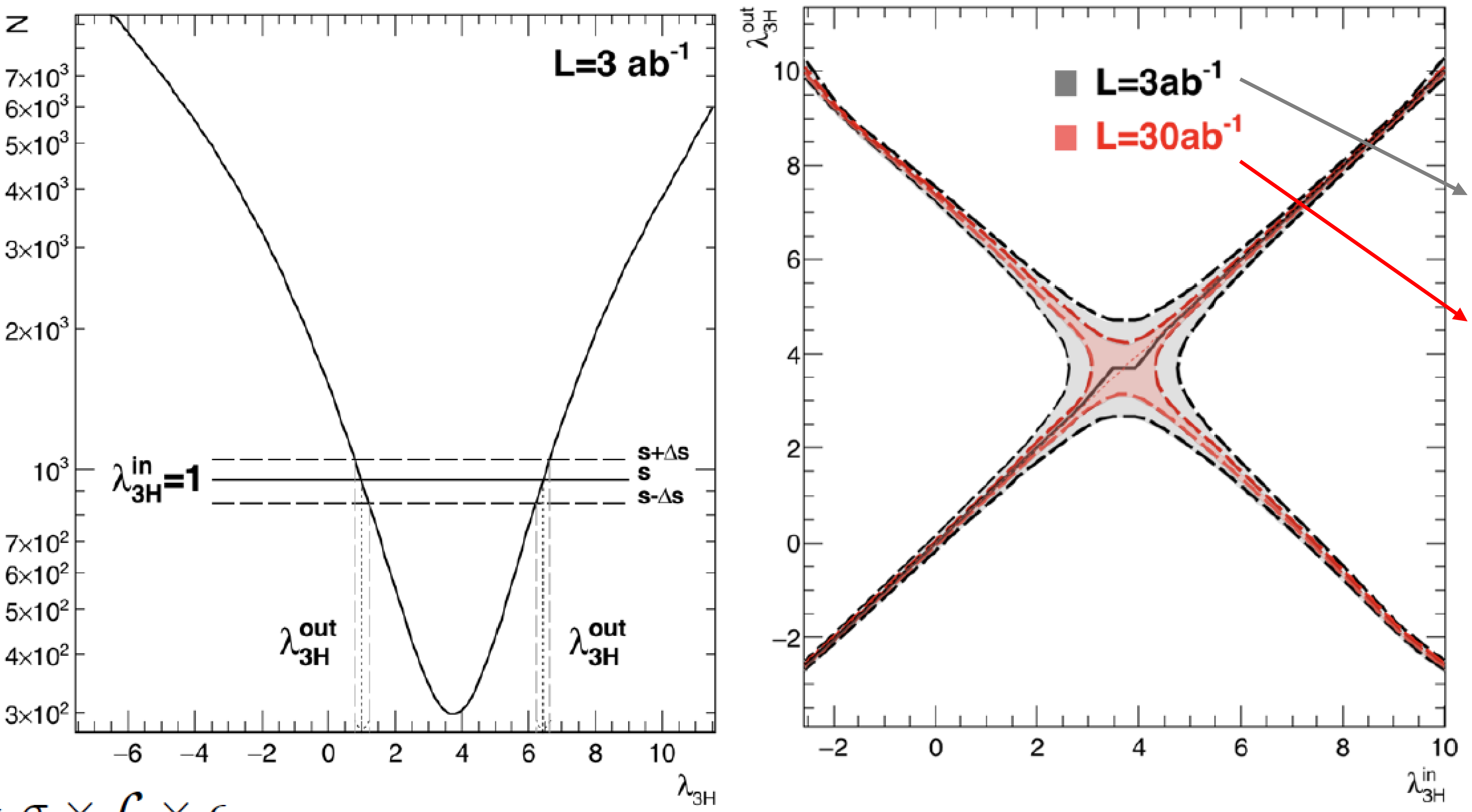

$2.6 \lesssim \lambda_{3H} \lesssim 4.8$

$3.1 \lesssim \lambda_{3H} \lesssim 4.3$

We can not pin down for 1-sigma error regions.

$$N = \sigma \times \mathcal{L} \times \epsilon$$

FIG. 9. **HL-100 TeV**: (Left) The number of signal events N versus λ_{3H} with 3 ab^{-1}. The horizontal solid line is for the number of signal events s when $\lambda_{3H}^{\rm in} = 1$ and the dashed lines for $s \pm \Delta s$ with the statistical error of $\Delta s = \sqrt{s+b}$. (Right) The 1-σ error regions versus the input values of $\lambda_{3H}^{\rm in}$ assuming 3 ab^{-1} (black) and 30 ab^{-1} (red).

arXiv:1804.07130

The comprehensive signal-background analysis – HL-100 TeV Collider

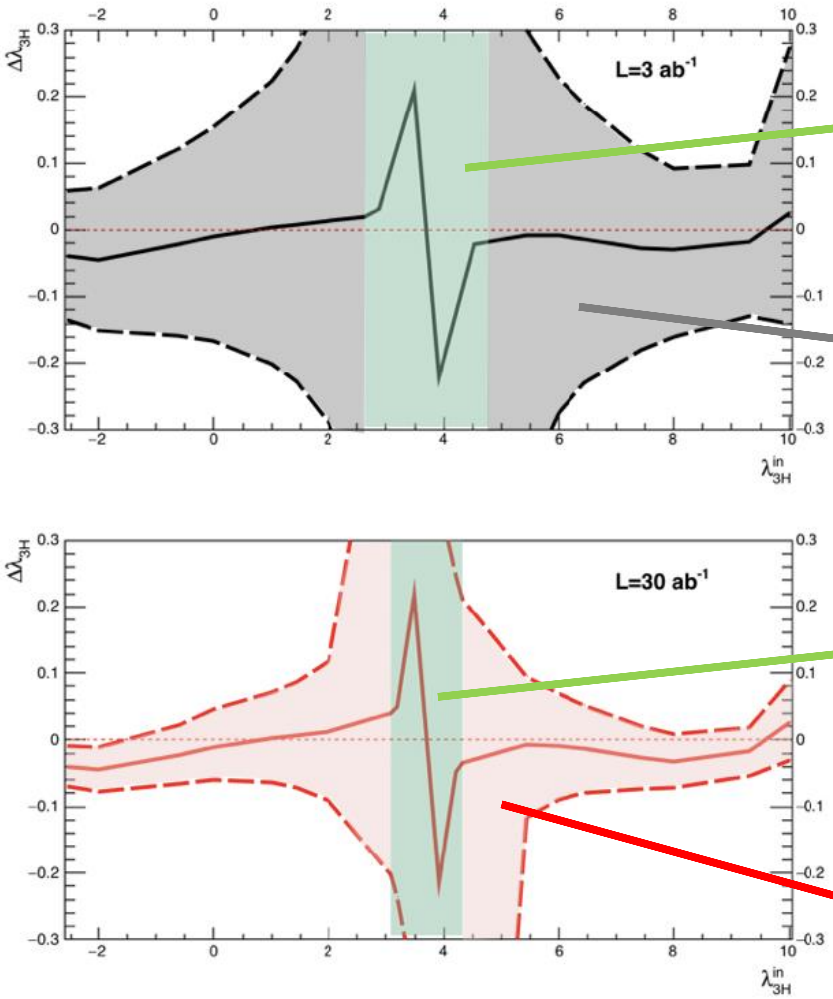

$$\Delta\lambda_{3H} = \lambda_{3H}^{\text{out}} - \lambda_{3H}^{\text{in}}$$

$|\Delta\lambda_{3H}| \leq 0.3$

$2.6 \lesssim \lambda_{3H} \lesssim 4.8$

$\lambda_{3H} \lesssim 1.6$

$\lambda_{3H} \gtrsim 5.9$

$\lambda_{3H} = 1$

$|\Delta\lambda_{3H}| \lesssim 20\ \%$

The boundaries of $|\Delta\lambda_{3H}| \leq 0.3$

$3.1 \lesssim \lambda_{3H} \lesssim 4.3$

$\lambda_{3H} \lesssim 2.4$

$\lambda_{3H} \gtrsim 5.3$

$\lambda_{3H} = 1$

$|\Delta\lambda_{3H}| \lesssim 7\ \%$

FIG. 10. **HL-100 TeV**: $\Delta\lambda_{3H} = \lambda_{3H}^{\text{out}} - \lambda_{3H}^{\text{in}}$ versus λ_{3H}^{in} along the $\lambda_{3H}^{\text{out}} = \lambda_{3H}^{\text{in}}$ line with 3 ab^{-1} (upper) and 30 ab^{-1} (lower). The lines are the same as in the right frame of Fig. 9. We consider $|\Delta\lambda_{3H}| \leq 0.3$ to find the regions in which one can pin down the λ_{3H} coupling with an absolute error smaller than 0.3.

arXiv:1804.07130

Contents

Discussions and Conclusions

- 1. One of the major goals of the HL-LHC and HL-100 TeV hadron collider is to unfold **the mystery of the EWSB mechanism**, which is related **to the origin of mass**. We have investigated the **trilinear self-coupling** of the Higgs boson in **Higgs-pair production** using the most promising channel $pp \to HH \to \gamma\gamma b\bar{b}$ with a fully comprehensive signal-background analysis.

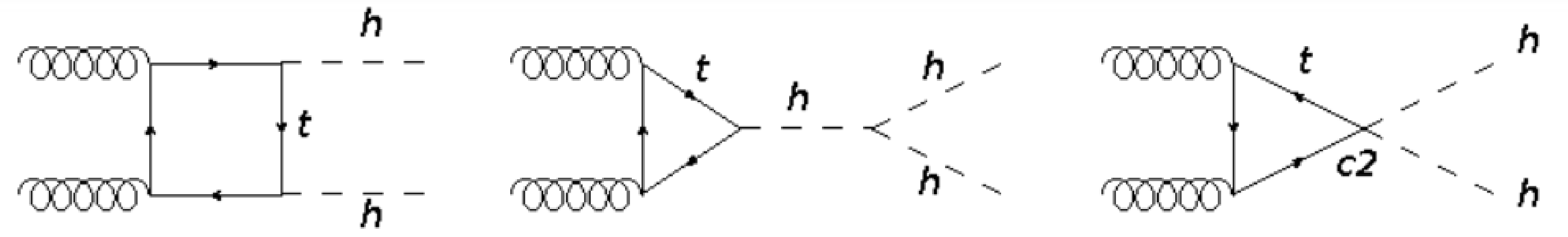

Discussions and Conclusions

- 2. We have performed an exploratory study with *heavy degrees of freedom being integrated out* and resulting in possible modifications of the top-Yukawa coupling, Higgs trilinear coupling, and a new contact ttHH coupling, as well as the potential **CP-odd** component in the Yukawa and contact couplings.

$$-\mathcal{L} = \frac{1}{3!}\left(\frac{3M_H^2}{v}\right)\lambda_{3H} H^3 + \frac{m_t}{v}\bar{t}\left(g_t^S + i\gamma_5 g_t^P\right)t\,H + \frac{1}{2}\frac{m_t}{v^2}\bar{t}\left(g_{tt}^S + i\gamma_5 g_{tt}^P\right)t\,H^2 .$$

trilinear coupling λ_{3H}

In the SM, $\lambda_{3H} = g_t^S = 1$ and $g_t^P = 0$ and $g_{tt}^{S,P} = 0$.

top-quark Yukawa coupling $g_t^{S,P}$

dim-5 contact-type $ttHH$ coupling $g_{tt}^{S,P}$

Discussions and Conclusions

- 3. We have identified useful variables — **the angular separation between the decay products of the Higgs boson** — to discriminate among the contributions from the triangle, box, and contact diagrams.

Numerical analysis : CPC2: g_t^S, λ_{3H}, and g_{tt}^S

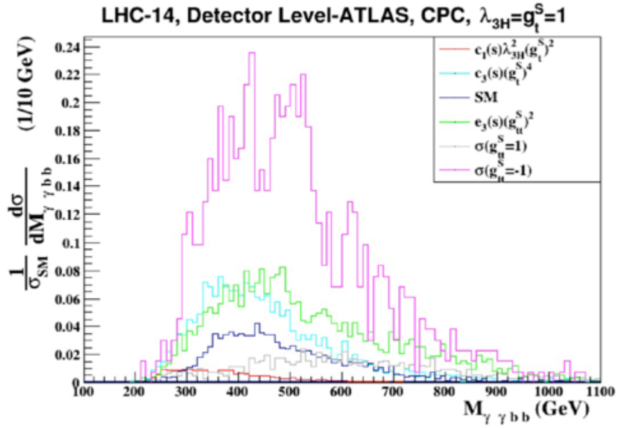

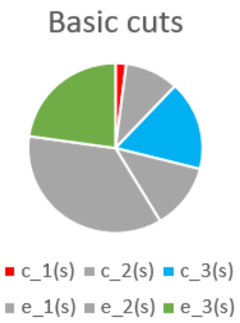

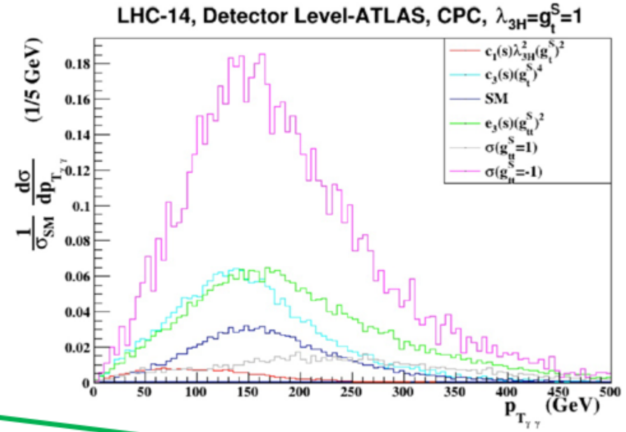

The triangle diagram, which contains an s-channel Higgs propagator, does not increase as much as the box diagram or the contact diagram with the center-of-mass energy.

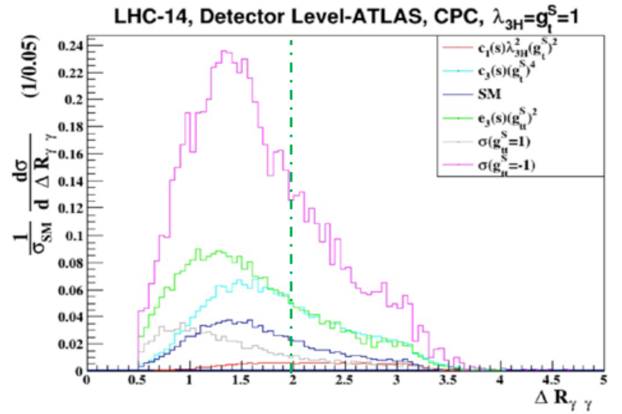

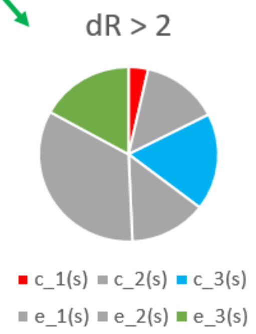

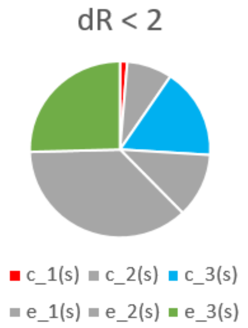

Discussions and Conclusions

Higgs boson trilinear self-coupling precision test !

The comprehensive signal-background analysis – HL-LHC

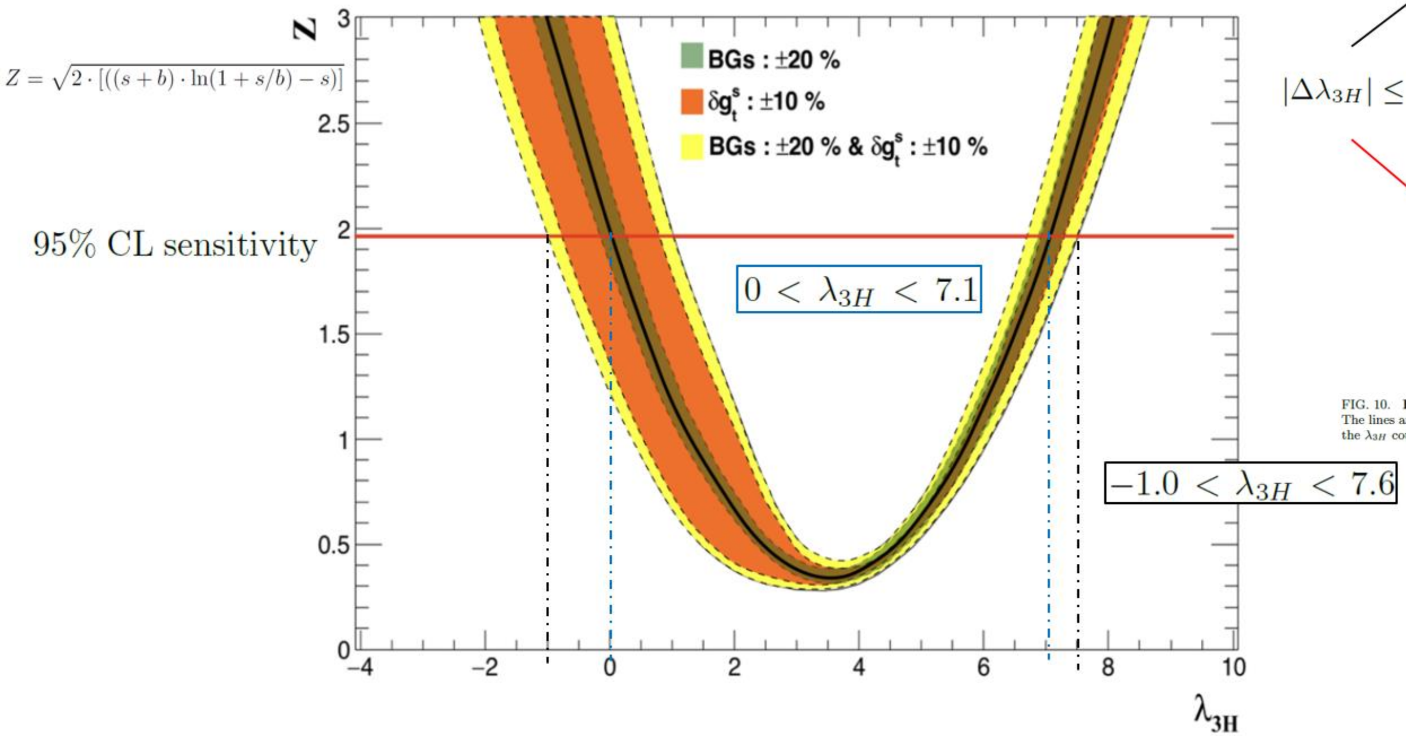

The comprehensive signal-background analysis – HL-100 TeV Collider

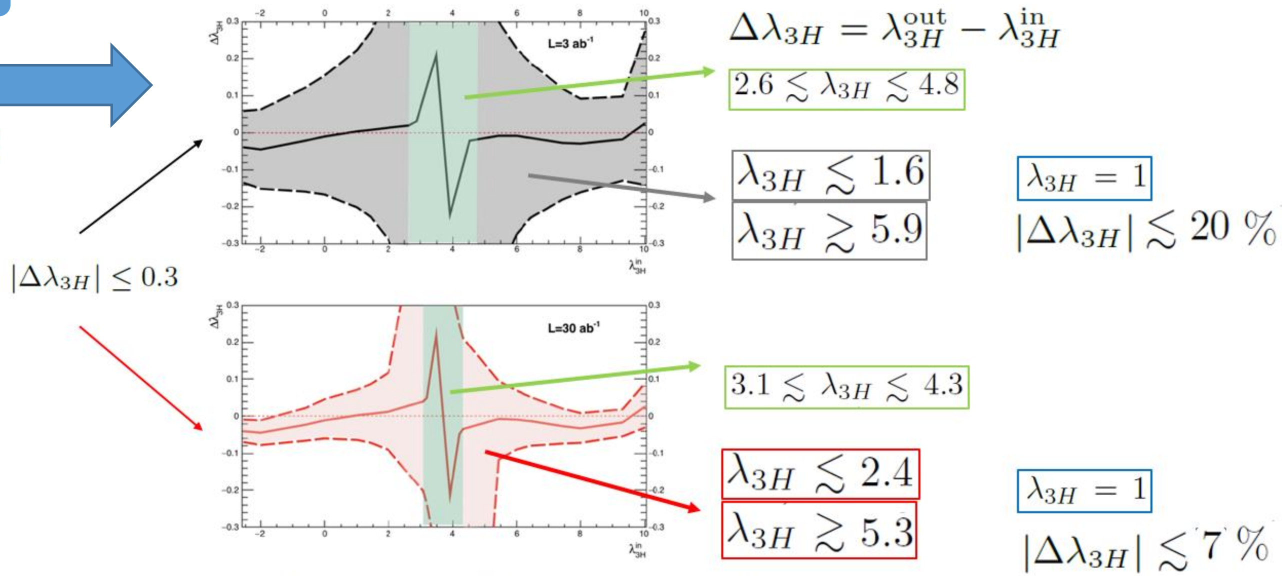

FIG. 10. **HL-100 TeV**: $\Delta\lambda_{3H} = \lambda_{3H}^{\text{out}} - \lambda_{3H}^{\text{in}}$ versus λ_{3H}^{in} along the $\lambda_{3H}^{\text{out}} = \lambda_{3H}^{\text{in}}$ line with 3 ab^{-1} (upper) and 30 ab^{-1} (lower). The lines are the same as in the right frame of Fig. 9. We consider $|\Delta\lambda_{3H}| \leq 0.3$ to find the regions in which one can pin down the λ_{3H} coupling with an absolute error smaller than 0.3.

Discussions and Conclusions

- 5. The large event samples of signal and background processes can afford **machine learning**, which is believed to give more efficient background rejection and signal retention. **(In Progress !)**

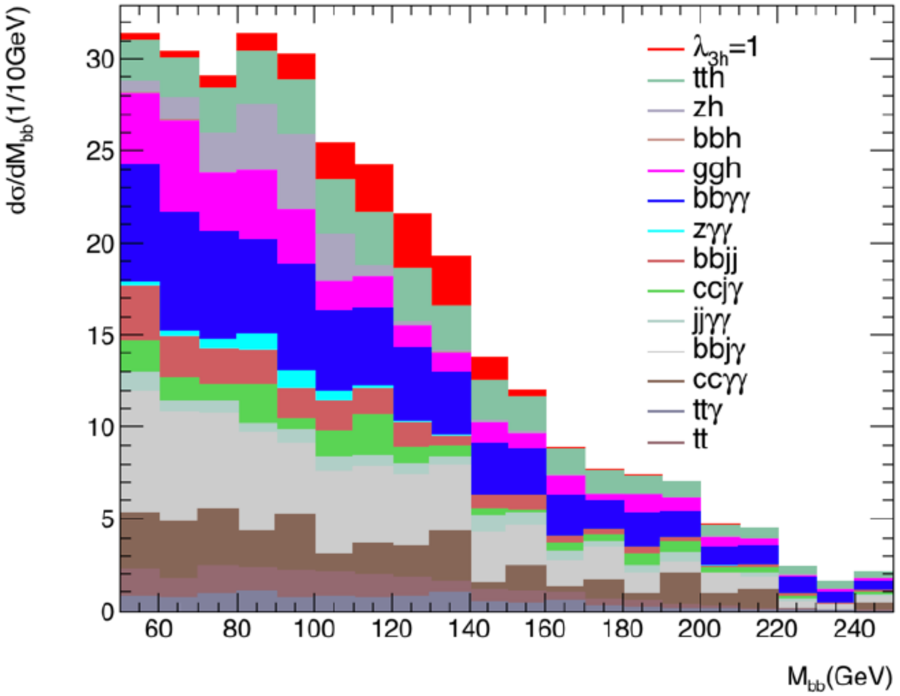

BDT cuts $Z_{Max}^{l_{3h}=1}$

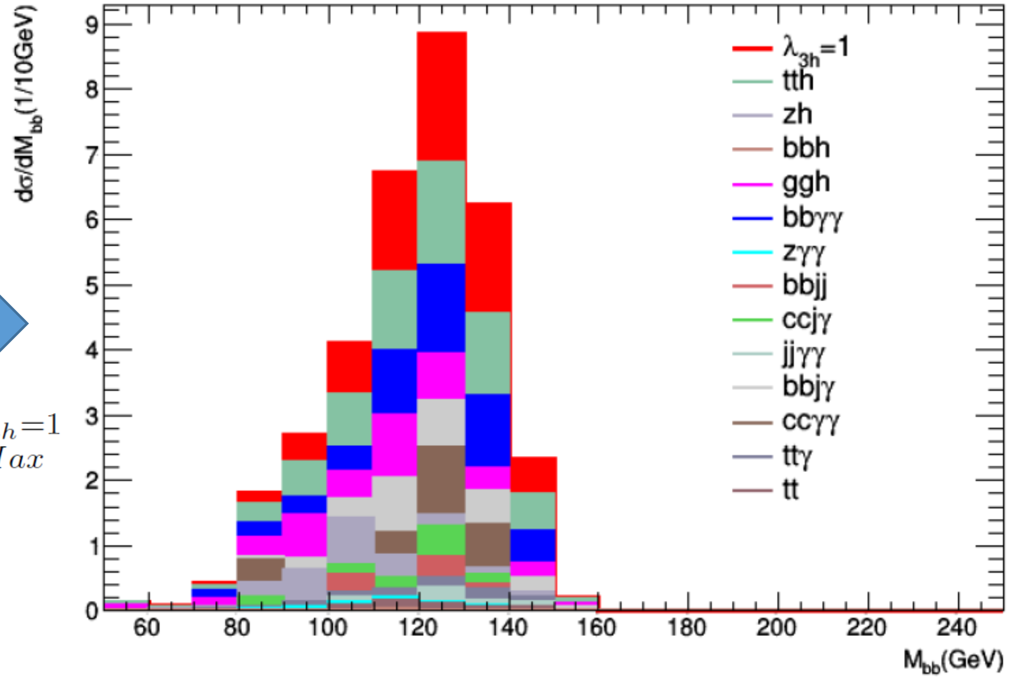

$\lambda_{3h} = 1$ **Optimised Analysis**

皆さんのご静聴に感謝いたします。

Thank you for listening！！

Thank you for your listening!!!

Back-up Slide

Measurement of the Higgs Self-coupling at the ILC

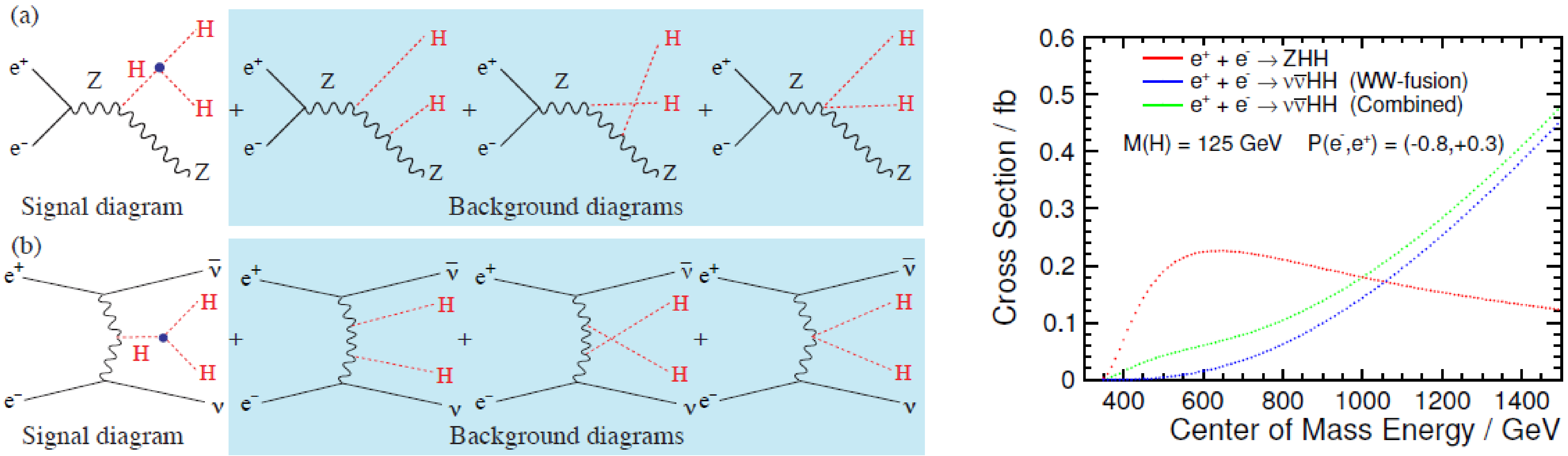

Figure 7: Diagrams of the double Higgs production processes, $e^+e^- \to ZHH$ (left a) and $e^+e^- \to \nu\bar{\nu}HH$ (left b), and their cross sections as function of $\sqrt{s}$ (right).

arXiv:1311.6528

Measurement of the Higgs Self-coupling at the ILC

$\Delta g/g$	Baseline $1000\ \mathrm{fb}^{-1}$			LumiUP $2500\ \mathrm{fb}^{-1}$		
	250 GeV	+ 500 GeV	+ 1 TeV	250 GeV	+ 500 GeV	+ 1 TeV
g_{HZZ}	1.3%	1.0%	1.0%	0.61%	0.51%	0.51%
g_{HWW}	4.8%	1.2%	1.1%	2.3%	0.58%	0.56%
g_{Hbb}	5.3%	1.6%	1.3%	2.5%	0.83%	0.66%
g_{Hcc}	6.8%	2.8%	1.8%	3.2%	1.5%	1.0%
g_{Hgg}	6.4%	2.3%	1.6%	3.0%	1.2%	0.87%
$g_{H\tau\tau}$	5.7%	2.3%	1.7%	2.7%	1.2%	0.93%
$g_{H\gamma\gamma}$	18%	8.4%	4.0%	8.2%	4.5%	2.4%
$g_{H\mu\mu}$	-	-	16%	-	-	10%
g_{Htt}	-	14%	3.1%	-	7.8%	1.9%
Γ_H	11%	5.0%	4.6%	5.4%	2.5%	2.3%
λ_{HHH}	-	83%	21%	-	46%	13%

Table 1: Expected precisions of Higgs couplings, total Higgs width, and Higgs self-coupling for both baseline and luminosity upgrade (LumiUP) scenarios, at each running stage 250 GeV, 500 GeV, and 1 TeV, where the data at earlier stages is always combined to those at the current stage.

arXiv:1311.6528

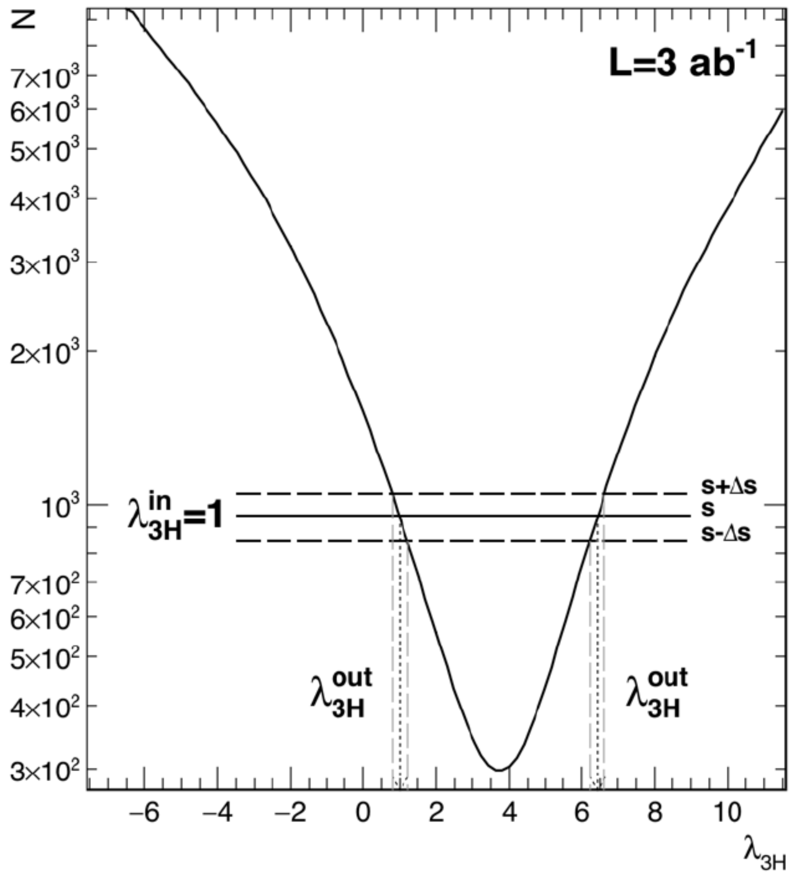

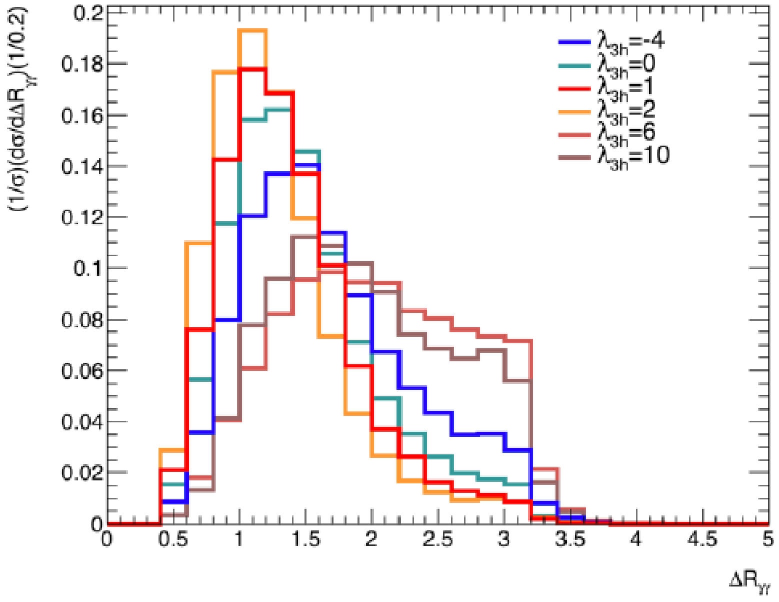

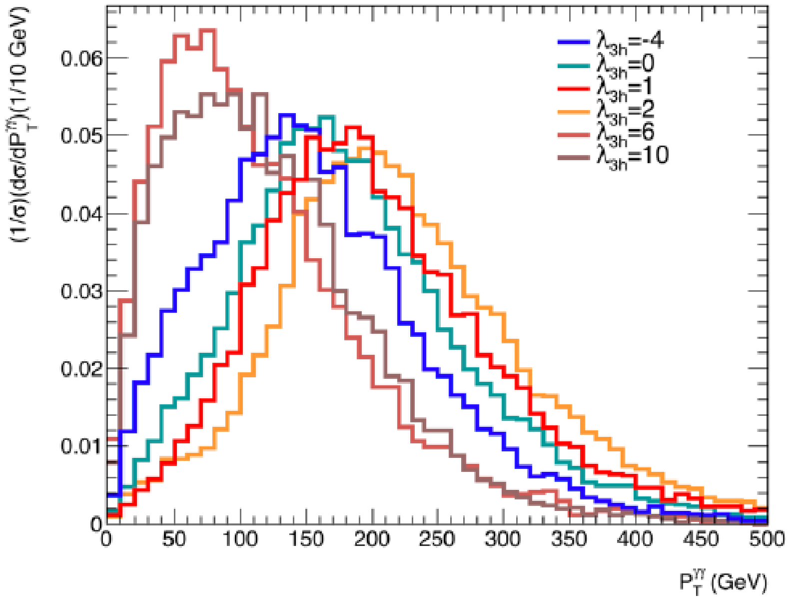

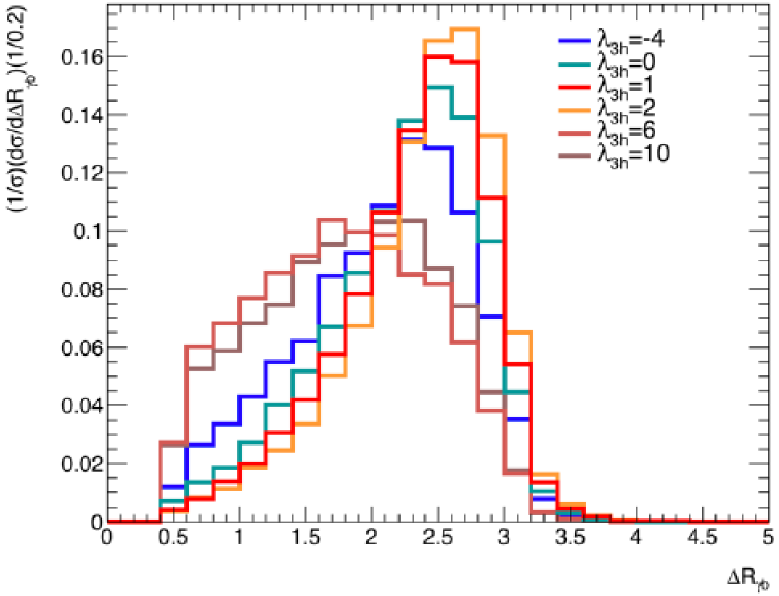

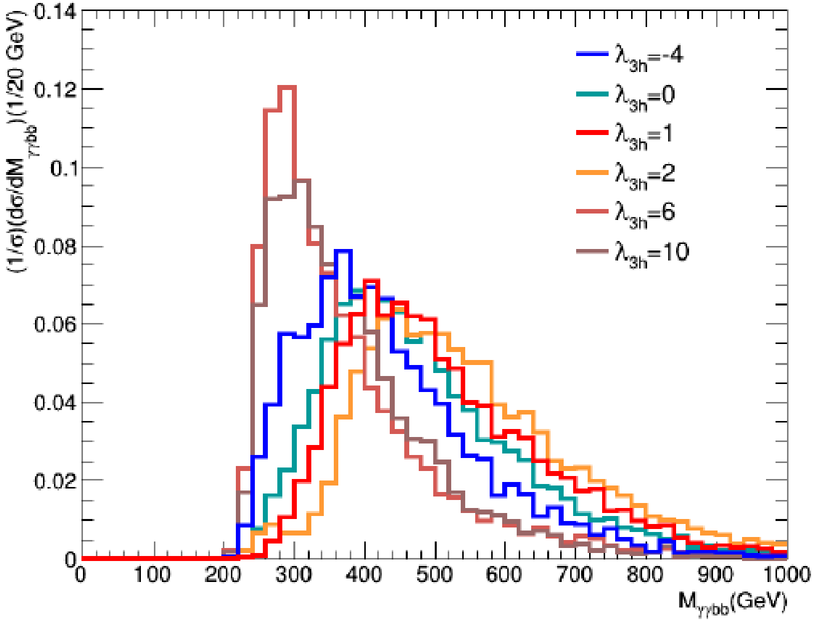

Use **machine learning analysis** to disentangle these degenerate points λ_{3H} ?

Cross sections for various HH production channels

To get a feeling for the size of the cross sections that we are considering, we show the total production cross sections for various HH production channels in Fig. 1. At 14 TeV, the SM cross sections $\sigma(gg \to HH) = 45.05$ fb [15], $\sigma(qq' \to HHqq') = 1.94$ fb [16], $\sigma(q\bar{q}(') \to VHH = 0.567(V = W^{\pm})\,/0.415(V = Z)$ fb [17], and $\sigma(gg/q\bar{q} \to t\bar{t}HH) = 0.949$ fb [16] are calculated at NNLO+NNLL, NLO, NNLO, and NLO, respectively [18]. The 100 TeV cross sections $\sigma(gg \to HH) = 1749$ fb, $\sigma(qq' \to HHqq') = 80.3$ fb, $\sigma(q\bar{q}(') \to VHH = 8.00(V = W^{\pm})\,/8.23(V = Z)$ fb, and $\sigma(gg/q\bar{q} \to t\bar{t}HH) = 82.1$ fb are calculated at the same orders as at 14 TeV [19, 20]. From Fig. 1, it is clear that the gluon fusion into HH gives the largest cross sections independently of λ_{3H} with its minimum occurring at $\lambda_{3H} \simeq 2.5$.

Monte Carlo samples

LHC

Signal					
Signal process		Generator/Parton Shower	$\sigma \cdot BR$ [fb]	Order in QCD	PDF used
$gg \to HH \to b\bar{b}\gamma\gamma$ [18]		MG5_aMC@NLO/PYTHIA8	0.119	NNLO +NNLL	NNPDF2.3LO
Backgrounds					
Background(BG)	Process	Generator/Parton Shower	$\sigma \cdot BR$ [fb]	Order in QCD	PDF used
Single-Higgs associated BG [18]	$ggH(\to \gamma\gamma)$	POWHEG − BOX/PYTHIA6	1.20×10^2	NNNLO	CT10
	$t\bar{t}H(\to \gamma\gamma)$	PYTHIA8/PYTHIA8	1.37	NLO	
	$ZH(\to \gamma\gamma)$	PYTHIA8/PYTHIA8	2.24	NLO	
	$b\bar{b}H(\to \gamma\gamma)$	PYTHIA8/PYTHIA8	1.26	NLO	
Non-resonant BG	$b\bar{b}\gamma\gamma$	MG5_aMC@NLO/PYTHIA8	1.40×10^2	LO	CTEQ6L1
	$c\bar{c}\gamma\gamma$	MG5_aMC@NLO/PYTHIA8	1.14×10^3	LO	
	$jj\gamma\gamma$	MG5_aMC@NLO/PYTHIA8	1.62×10^4	LO	
	$b\bar{b}j\gamma$	MG5_aMC@NLO/PYTHIA8	3.67×10^5	LO	
	$c\bar{c}j\gamma$	MG5_aMC@NLO/PYTHIA8	1.05×10^6	LO	
	$b\bar{b}jj$	MG5_aMC@NLO/PYTHIA8	4.34×10^8	LO	
	$Z(\to b\bar{b})\gamma\gamma$	MG5_aMC@NLO/PYTHIA8	5.17	LO	
$t\bar{t}$ and $t\bar{t}\gamma$ BG ($\geq$ 1 lepton)	$t\bar{t}$ [22]	POWHEG − BOX/PYTHIA8	5.30×10^5	NNLO +NNLL	CT10
	$t\bar{t}\gamma$ [23]	MG5_aMC@NLO/PYTHIA8	1.60×10^3	NLO	CTEQ6L1

Monte Carlo samples

100 TeV hadron collider

	Signal process	Generator/Parton Shower	$\sigma \cdot BR$ [fb]	Order in QCD	PDF used
Signal					
	$gg \to HH \to b\bar{b}\gamma\gamma$ [20]	MG5_aMC@NLO/PYTHIA8	4.62	NNLO +NNLL	NNPDF2.3LO
Backgrounds					
Background(BG)	Process	Generator/Parton Shower	$\sigma \cdot BR$ [fb]	Order in QCD	PDF used
Single-Higgs associated BG	$ggH(\to \gamma\gamma)$ [20]	POWHEG − BOX/PYTHIA8	1.82×10^3	NNNLO	CT10
	$t\bar{t}H(\to \gamma\gamma)$ [20]	PYTHIA8/PYTHIA8	7.29×10^1	NLO	
	$ZH(\to \gamma\gamma)$ [20]	PYTHIA8/PYTHIA8	2.54×10^1	NNLO	
	$b\bar{b}H(\to \gamma\gamma)$ [37]	PYTHIA8/PYTHIA8	1.96×10^1	NNLO(5FS)	
Non-resonant BG	$b\bar{b}\gamma\gamma$	MG5_aMC@NLO/PYTHIA8	4.93×10^3	LO	CTEQ6L1
	$c\bar{c}\gamma\gamma$	MG5_aMC@NLO/PYTHIA8	4.54×10^4	LO	
	$jj\gamma\gamma$	MG5_aMC@NLO/PYTHIA8	5.38×10^5	LO	
	$b\bar{b}j\gamma$	MG5_aMC@NLO/PYTHIA8	1.44×10^7	LO	
	$c\bar{c}j\gamma$	MG5_aMC@NLO/PYTHIA8	4.20×10^7	LO	
	$b\bar{b}jj$	MG5_aMC@NLO/PYTHIA8	1.60×10^{10}	LO	
	$Z(\to b\bar{b})\gamma\gamma$	MG5_aMC@NLO/PYTHIA8	9.53×10^1	LO	
$t\bar{t}$ and $t\bar{t}\gamma$ BG [20] ($\geq$ 1 lepton)	$t\bar{t}$	MG5_aMC@NLO/PYTHIA8	1.76×10^7	NLO	CT10
	$t\bar{t}\gamma$	MG5_aMC@NLO/PYTHIA8	4.18×10^4	NLO	CTEQ6L1

Fake rate

LHC

TABLE III. The main fake processes and the corresponding rates in each sample of non-resonant and $t\bar{t}(\gamma)$ backgrounds. We recall that $P_{j\to\gamma} = 5\times10^{-4}$ and $P_{e\to\gamma} = 2\%/5\%$ in the barrel/endcap calorimeter region. For c_s quarks produced during showering in the $jj\gamma\gamma$ sample, we use $P_{c_s\to b} = 1/8$ as in Ref. [30]. Otherwise the P_T and η dependence of $P_{c\to b}$ is fully considered as explained in the text.

Background(BG)	Process	Fake Process	Fake rate
Non-resonant BG	$b\bar{b}\gamma\gamma$	N/A	N/A
	$c\bar{c}\gamma\gamma$	$c\to b,\ \bar{c}\to\bar{b}$	$(P_{c\to b})^2$
	$jj\gamma\gamma$	$c_s\to b,\ \bar{c_s}\to\bar{b}$	$(P_{c_s\to b})^2$
	$b\bar{b}j\gamma$	$j\to\gamma$	5×10^{-4}
	$c\bar{c}j\gamma$	$c\to b,\ \bar{c}\to\bar{b},\ j\to\gamma$	$(P_{c\to b})^2\cdot(5\times10^{-4})$
	$b\bar{b}jj$	$j\to\gamma,\ j\to\gamma$	$(5\times10^{-4})^2$
	$Z(\to b\bar{b})\gamma\gamma$	N/A	N/A
$t\bar{t}$	Leptonic decay	$e\to\gamma,\ e\to\gamma$	$(0.02)^2/0.02\cdot0.05/(0.05)^2$
	Semi-leptonic decay	$e\to\gamma,\ j\to\gamma$	$(0.02)\cdot5\times10^{-4}/(0.05)\cdot5\times10^{-4}$
$t\bar{t}\gamma$	Leptonic decay	$e\to\gamma$	$0.02/0.05$
	Semi-leptonic	$e\to\gamma$	$0.02/0.05$

Fake rate

100 TeV hadron collider

TABLE IX. The main fake processes and the corresponding faking rates in each sample of non-resonant and $t\bar{t}(\gamma)$ backgrounds. We recall that $P_{j\to\gamma} = 1.35 \times 10^{-3}$, $P_{c\to b} = P_{c_s\to b} = 0.1$ [20] and $P_{e\to\gamma} = 2\%/5\%$ in the barrel/endcap calorimeter region.

Background(BG)	Process	Fake Process	Fake rate
Non-resonant BG	$b\bar{b}\gamma\gamma$	N/A	N/A
	$c\bar{c}\gamma\gamma$	$c\to b,\ \bar{c}\to\bar{b}$	$(0.1)^2$
	$jj\gamma\gamma$	$c_s\to b,\ \bar{c}_s\to\bar{b}$	$(0.1)^2$
	$b\bar{b}j\gamma$	$j\to\gamma$	1.35×10^{-3}
	$c\bar{c}j\gamma$	$c\to b,\ \bar{c}\to\bar{b},\ j\to\gamma$	$(0.1)^2\cdot(1.35\times10^{-3})$
	$b\bar{b}jj$	$j\to\gamma,\ j\to\gamma$	$(1.35\times10^{-3})^2$
	$Z(\to b\bar{b})\gamma\gamma$	N/A	N/A
$t\bar{t}$	Leptonic decay	$e\to\gamma,\ e\to\gamma$	$(0.02)^2/0.02\cdot0.05/(0.05)^2$
	Semi-leptonic decay	$e\to\gamma,\ j\to\gamma$	$(0.02)\cdot1.35\times10^{-3}/(0.05)\cdot1.35\times10^{-3}$
$t\bar{t}\gamma$	Leptonic decay	$e\to\gamma$	$0.02/0.05$
	Semi-leptonic	$e\to\gamma$	$0.02/0.05$